Durham E-Theses

Comparative analyses of rodent and human brain in ageing and disease using novel NMDAR-2B selective probes

Sheahan, Rebecca Louise

Durham
University

Comparative Analyses of Rodent and Human Brain in Ageing and Disease using Novel NMDAR-2B Selective Probes.

Rebecca Louise Sheahan

A Thesis submitted to the University of Durham for the degree of Doctor of Philosophy

Department of Biological and Biomedical Sciences

2007

Supervisor: Dr P.L. Chazot

Abstract

Comparative Analyses of Rodent and Human Brain in Ageing and Disease using novel NMDAR-2B Selective Probes.

The NMDA subtype of excitatory ionotropic glutamate receptors is a hetero-oligomeric ligand-gated ion channel. Molecular cloning techniques have identified three types of NMDA receptor subunits, the NR1, NR2A-D, and NR3A-B. NR2B-containing receptors are the focus of this thesis and are believed to play an important role in learning and memory, as well as being involved in neuronal cell death accompanying cerebral ischeamia, seizures, and degenerative neurological disorders such as Alzheimer's and Parkinson's disease.

The main aim of this thesis was to investigate the comparative abundance and distribution of NR2B receptors in the rodent and human brain using an anti-NR2B selective antibody, and two NMDAR-2B subtype-selective antagonist radioligands, [^{3}H]Ro 25,6981 and [^{3}H] CP-101,606, with a variety of experimental techniques.

This thesis provides new evidence that Ro 25,6981 and CP-101,606 label distinct NMDA NR2B subtype populations in both the rodent and human brain. Ligand autoradiographical and immunohistochemical studies of the mouse and rat brain brain revealed high NR2B receptor expression levels in the CA1 and CA2 hippocampal formation stratum oriens and radiatum, striatum, and outer layers of the frontal and entorhinal cortex in both species, with higher expression levels present in the 3-week compared to 3 month adult rat brain. Radioligand binding studies of native NMDA receptors with a range of NR2B-selective antagonists provided pharmacological evidence for heterogeneity in NR2B-containing receptor populations in the two age groups indicating a developmental switch in early adulthood.

Ligand autoradiography of human control and disease state brain sections revealed an overall *preservation* of NR2B receptors in the 60-92 year age range. Control female cases showed a significantly lower level of NR2B containing receptors compared to age-matched control male cases, in the anterior cingulate cortex (ACC). Interestingly, higher NR2B-containing receptor levels were observed in earlier age cases of AD compared to controls, and a weak correlation overall of increasing NR2B expression with decreasing scores in dementia and psychiatric tests. Overall, this study suggests that the NR2B subtype is *not* the major underlying receptor to explain memory deficits or psychotic symptoms in the common human dementias.

Contents

Chapter 1: Introduction

Chapter 2: Materials and General Methods

Chapter 3: NR2B Subtype Pharmacology in the Rodent Brain: an Ageing Study

3.1: Ligand Autoradiographical comparison of Ro 25,6981 and CP-101,606 in adult mouse brain; Focus on cognitive centres.

3.2 Comparison of Ro 25,6981 and CP-101,606 in young and adult rat: Focus on development

3.2.1 Pharmacological profile of [^{3}H]CP-101,606, an NR2B ligand, binding to rodent NR1/NR2B receptors

3.2.2 Detailed Pharmacological profile of a range of NR2B ligands in P21 and adult rat brain

3.2.3 Ligand Autoradiographical comparison of Ro 25,6981 and CP-101,606 in P21 and adult rat brain; Focus on cognitive centres.

3.2.4 Expression of the NR2B subunit protein in P21 and adult rat brain;

Chapter 4: Ligand Autoradiographical comparison of Ro 25,6981 and CP-101,606 in normal human ageing and dementia with lewy bodies

Figures

Chapter 3.2.3

Chapter 3.2.4

Chapter 4

Appendix One

Tables

Chapter 3.2.2

Chapter 4

Abbreviations

AD	Alzheimer's disease
AMPA	α-amino-3-hydroxy-5-methyl-4-isoxazolepropionic acid
AP5	D-2-amino-5-phosphonovaleric acid
AP7	D-2-amino-7-phosphonoheptanoic acid
APS	Ammonium persulphate
AR	Antigen retrieval
Bmax	Maximum number of receptors per mg protein
BSA	Bovine serum albumin
CA	Central amydala
cDNA	Complementary DNA
CGP 37849	(E)-2-amino-4-methyl-5-phosphono-3-pentenoic acid
CNS	Central nervous system
CO_2	Carbon dioxide
CP-101,606	(1S, 2S)-1-(4-Hydroxyphenyl)-2-(4-phenylpiperidino)-1-propanol
DAB	Diaminobenzadine
D-CPP-ene	D-3-(2-carboxypiperazin-4-yl)-1-propenyl-1-phosphonic acid
DEX	Dexamethasone
dH_2O	Distilled water
DLB	Dementia with lewy bodies
DMEM	Dulbeccos modified eagles medium
DMSO	Dimethyl sulphoxide
DNA	Deoxyribonucleic acid
DPM	Disintigrations per minute
DPX	Synthetic mountant resin (Distyrene, Plasticizer, Xylene)
DRG	Dorsal root ganglion
dsDNA	Double stranded DNA
DTT	Dithiolthreitol
E. *coli*	Escherichia coli
EDTA	Ethylenediaminetetracetic acid
EGTA	Ethylenebis(oxyethylenenitrilo)tetracetic acid

ELISA	Enzyme linked immunoadsorbent assay
FCS	Foetal calf serum
Fm	Femtomoles
GABA	γ-aminobutyric acid
GBX	Kodak fixer or developer
GF/B	Glass fibre filters
GluR	Glutamate receptor subunit
GPCRs	GTP-protein coupled receptors
G-protein	Guanine nucleotide binding regulatory protein
GTP	Guanosine-5'-triphosphate
H_2O_2	Hydrogen peroxide
HB101	Strain of E. coli competent cells
HCL	Hydrochloric acid
HD	Huntingdon's disease
HEK 293	Human embryonic kidney 293 cells
HEPES	N-2-Hydroxyethylpiperazine-N'-2-ethanesulphonic acid
HRP	Horseradish peroxidase
IC_{50}	Concentration of the ligand giving 50% inhibition of specific binding
iGluR	Ionotropic glutamate receptor
IHC	Immunohistochemistry
K_D	Dissociation constant
kDa	Kilodaltons
K_I	Inhibition constant
LA	Lateral amygdala
LB broth	Lurani-Bertani broth
LIVBP	Leucine/isoleucine/valine-binding-protein
LOABP	Lysine/arginine/ornithine-binding protein
LTD	Long term depression
LTP	Long term potentiation
M	Membrane region
M	Molar
mA	Milli amps
MCIDE	Microcomputer Imaging Device Elite

mGluR	Metabotropic glutamate receptor
MK-801	(+)-5-Methyl-10,11-dihydr-5H-dibenzo[a,d]cyclohepten-5,10-imine
ml	Milli-litre
mM	Milli-molar
MPTP	1-methyl-4-phenyl-1,2,3,6-tetrahydropyridine
Mr	Molecular mass
mRNA	Messenger RNA
MSNs	Medium spiny projection neurons
NaCl	Sodium chloride
NaHCO$_3$	Sodium hydrogen carbonate
NaOH	Sodium Hydroxide
NaPO	Sodium phosphate
n$_H$	Hill coefficients
nM	Nano Molar
NMDA	N-methyl-$_D$-aspartate
NR	NMDA receptor subunit
O.D.	Optical density
°C	Degrees centigrade
P21	Postnatal day 21
PAGE	Polyacrylamide gel electrophoresis
PBS	Phosphate buffered saline
PCP	Phencyclidine
PCR	Polymerase chain reaction
PD	Parkinson's disease
pH	Potential of Hydrogen
QIAGEN	Plasmid DNA Maxi Kit
RNA	Ribonucleic acid
Ro 25,6981	R-(R*,S*)-α-(4-hydroxyphenyl)-β-methyl-4-(phenylmethyl)-1-piperidine propanol
RPM	Revolutions per minute
S.D.	Standard deviation
SDS	Sodium dodecyl sulphate
SDS-PAGE	SDS-Polyacrylamide gel electrophoresis

TBS	Tris-buffered saline
TCP	1-[1-(2-thienyl)cyclohexyl]-piperidine
TE buffer	Tris-HCL, EDTA buffer
TEMED	NNN'N'-Tetramethyletylenediamine
Tris	Tris(hydroxymethyl)methylamine
U.V	Ultra-violet
V	Volts
v/v	Volume per volume
w/v	Weight per volume
µg	Microgram

Declaration

I declare that the work within this thesis, submitted for the degree of Doctor of Philosophy, is my own original work, except where stated, and has not been submitted for another degree at this or any other university.

Signed......... *RUSheakar* ....

Date............ *April 2007* ......

Statement of Copyright

Acknowledgements

I wish to express my gratitude to my supervisor Dr. P.L. Chazot for his committed support and guidance throughout this research and to Dr. M.A. Piggott and Dr. C.L. Thompson for their generous technical expertise in the autoradiography and cryostat sectioning carried out during this project. Thanks are due to Dr. D. Burn and M. Johnson from the Institute of Ageing and Health, Newcastle-Upon-Tyne for their valuable assistance with the human study. I would also like to acknowledge the help given to me by other members of the Biological Sciences Department. In particular, Dr. Jane Ives, Dr. Carla Mellough, Dr. Judith Philip, Dr. Victoria Hann, Dr. Helen Payne and to my fellow colleagues from the lab, Fiona Shenton, Sawsan Abuhamdah, Heather Chaffey, Andrea Bradford, Stephanie Burrows.

I would also like to thank Mrs Gafford, who inspired me to pursue biology in the first place, and my family and friends, with special mention to the Paynes, McIlmoyles and Sheahans, for their love, support, prayers and encouragement along the way.

Last but by no means least, I wish to thank my husband Pete, who has given me unconditional love and support, and has been there for me every step of the way, thankyou!

Chapter 1

Introduction

1.1 L-Glutamate as a neurotransmitter

L-Glutamate is the major excitatory neurotransmitter in the central nervous system (CNS) and mediates its actions via activation of both ionotropic and metabotropic receptor families (Kew & Kemp, 2005). In the late 1950's, Curtis and colleagues demonstrated that L-glutamate and L-aspartate, both acidic amino acids, were able to excite all types of central neurons (Curtis *et al.* 1959). Excitatory amino acids participate in both intermediary metabolism and neuronal communication, making it difficult for investigators to demonstrate that these compounds fulfil all criteria for neurotransmitter status. Nonetheless, much research has now shown that L-glutamate fulfils all criteria necessary to define a neurotransmitter, which includes the fact that it is found abundantly in the adult CNS and is synthesised in the brain by different biochemical pathways. Neither glutamate nor aspartate can cross the blood-brain barrier and so must be derived by local synthesis from glucose. Glutamate can be synthesised from 2-oxoglutarate, an intermediate in the Krebs cycle, by transamination or via the enzyme glutamic acid dehydrogenase. Glutamine, most commonly found in the interstitial space, is deaminated in neurons by the enzyme glutaminase to form L-glutamate. L-glutamate, which is found pre-synaptically in specific neurons, is released in vesicles, in a Ca^{2+}-dependant manner after physiological stimulation and mediates many important actions in the CNS. Excitatory neurotransmission and development of the CNS are closely linked, with involvement in the development of long-term potentiation (LTP) and as a result, learning, memory, motor co-ordination and synaptic plasticity. L-glutamate has roles in the pathophysiology of many neurological

disorders, including excitotoxicity mediated after stroke, epilepsy, chronic neurodegenerative disorders (e.g. Alzheimer's disease and Parkinson's disease) and neuropathic pain (Dingledine *et al.* 1999; Dunah *et al.* 1998; Hallet & Standaert, 2004).

1.2 Glutamate Receptors

The many roles of L-glutamate, the major excitatory neurotransmitter in the mammalian CNS, are mediated through a variety of receptors. Our understanding of the glutamatergic field of receptors has greatly increased due to the work of Jeffrey Watkins and colleagues throughout the 1970's and onwards, who identified selective agonists and antagonists that could pharmacologically distinguish between different glutamate receptor subtypes, to further characterise the glutamatergic-induced responses of neurones (Watkins *et al.*, 1990). Four of these agonists, *N*-methyl-D-aspartate (NMDA), amino-3-hydroxy-5-methylisoxazoleproprionic acid (AMPA), kainate and quisqualate, are distinct in the type of receptors to which they bind and have been used extensively to characterise the glutamate receptor family. The work of Watkins and others has led to the general broad classification of two main distinct glutamate receptor families. One is the ionotropic ligand-gated cation channel, and the other is the guanine nucleotide-binding regulatory (G)-protein metabotropic receptor (mGluRs). The ligand-gated ionotropic receptors can be further divided into NMDA and Non-NMDA receptors, depending on whether they bind the selective agonist NMDA (a synthetic analogue of glutamate (Watkins, 1962) from which the receptor derives its name). The Non-NMDA receptor family can again be divided into two groups which bind either the agonist AMPA or kainate (see Figure 1.1).

Ionotropic glutamate receptors are relatively large multisubunit complexes composed of four or five individual proteins that form an ion channel through the cell membrane. These

2

Glutamate

↓

Excitatory Amino Acid Receptors

Ionotropic   **Metabotropic**
(Ion Channels)   (G Protein Coupled)

Ionotropic Glutamate Receptors

NMDA   AMPA   Kainate

NR1   NR2A-D   NR3A-B   GluR1-4   GluR5-7   KA1-2
(a-g)

Metabotropic Glutamate receptors

Group I   Group II   Group III

mGlu1a-d   mGlu2   mGlu4a,b
mGlu5a,b   mGlu3   mGlu6
                                mGlu7a,b
                                m Glu8a,b
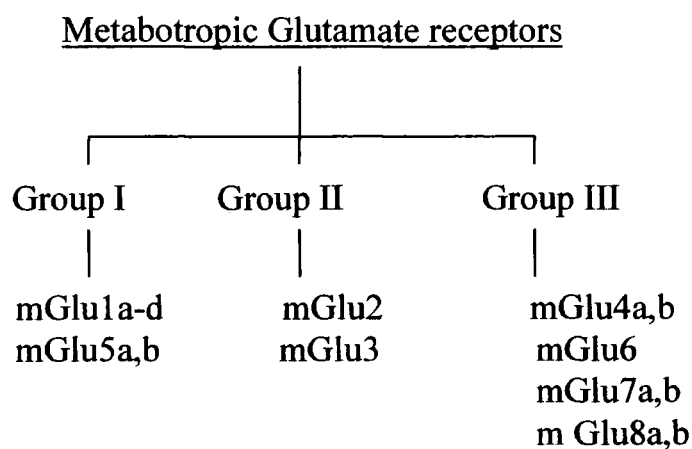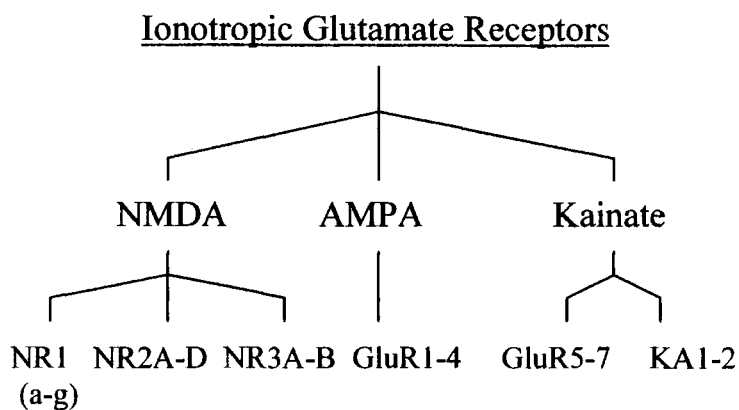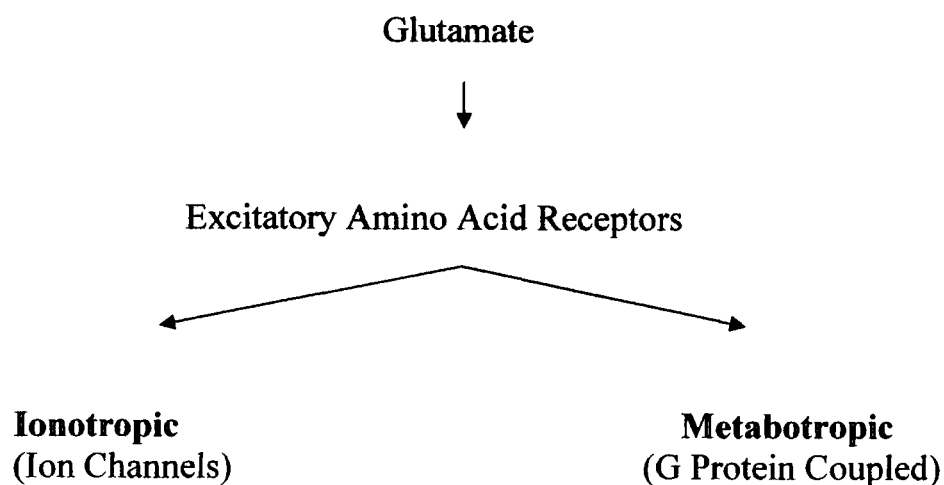
Figure 1.1 Schematic representation of ionotropic and metabotropic
glutamate receptors subtypes, subunits and splice variants.   3

channels remain in a closed state, impermeable to ions, in the absence of an agonist neurotransmitter. Agonist binding, (and also co-agonist binding combined with a depolarisation of the membrane, in the case of NMDA receptors), causes rapid conformational changes that open the ion channel allowing a flow of ions down their electrochemical gradients. Ion flow is terminated when either the transmitter dissociates, or the receptor becomes desensitised. In contrast, metabotropic receptors (G-protein coupled receptors, termed GPCRs) are composed of single polypeptides which bind to and activate GTP-proteins which elicit a series of enzymatic steps required to produce a response. This response is of slower onset and longer duration to that of the ionotropic receptors.

1.3 The NMDA Receptor

The N-methyl-D-aspartate (NMDA) receptor, a subtype of the ionotropic glutamate receptor family, is a hetero-oligomeric ligand-gated ion channel that interacts with multiple intracellular proteins by way of different subunits (McBain & Mayer, 1994) (see Figure 1.2). The exact number of subunits comprising the receptor is unknown but there is evidence for a tetrameric structure (Laube et $al.$ 1998) and for a pentameric structure (Dingledine et $al.$ 1999; Hawkins et al, 1999). Activation of the receptor, which results in the opening of the ion channel, requires the binding of glutamate and the co-agonist, glycine, together with a depolarisation of the membrane. The voltage-dependant Mg^{2+} ion block is then removed from the channel, and this allows the passage of Na^{2+}, K^+ and Ca^{2+} ions through the channel. These receptors are sensitive to modulation by various ligands, including not only their co-agonists glutamate and glycine, but also Mg^{2+}, polyamines, redox reagents and protons (Mutel et al, 1998).

Functional NMDA receptors are composed of a multimeric association of subunits that belong to two families: a single gene product, NR1, with eight splice variants due to differential splicing of three inserts and NR2A, B, C, and D, which are products of different genes that have high homologies (Hollmann & Heinemann, 1994). A third family, the NR3, have recently been classified and are reported to have a regulatory role. The pharmacological properties of NMDA receptors and their sensitivity to modulators depend on the type of NR1 splice variant and NR2 subtype that are associated in the receptor. The receptor subunits show distinct distribution patterns in adult brain and during development (Kutsuwada *et al.*, 1992; Laurie & Seeburg, 1994a; Monyer *et al.*, 1994; Mori & Mishina, 1995).

1.4 Molecular Biology of NMDA Receptors

As described in section 1.3, NMDA receptors are heteromeric ligand-gated ion channel complexes assembled from NR1, NR2 and NR3 subunits, usually in a tetrameric or pentameric formation. The NR1 subunit is ubiquitously expressed throughout the central nervous system and contains the glycine binding site, it is the product of a single alternatively spliced gene, and must be present to allow the receptor to be functional. The NR2 subunit contains the glutamate binding site and exists as four different isoforms encoded by different genes NR2A-NR2D (McBain & Mayer, 1994). NMDA receptor diversity arises from the presence of different NR2 subunits within the complex, and there is compelling evidence that some native NMDARs contain more than one type of NR2 subunit (Chazot & Stephenson, 1997b). The identity of the NR2 subunit (NR2A,-B,-C,-D) is critical in determining many of the functional properties of the receptor, such as channel conductance and deactivation time (Brickley *et al*, 2003).
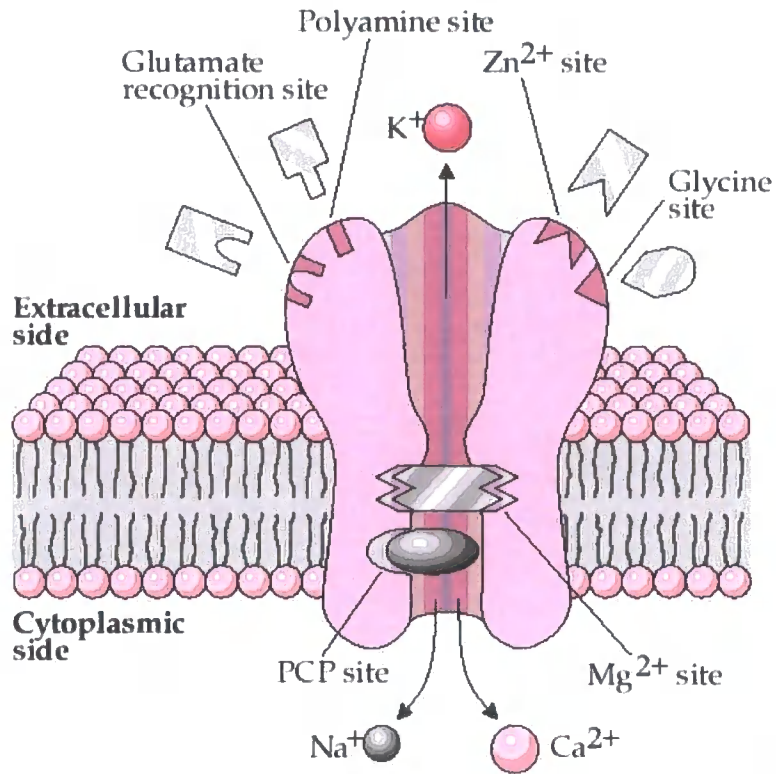
Figure 1.2 Schematic representation of the NMDA (N-Methyl-D-Aspartate) receptor complex. (www.chemistry.emory.edu)
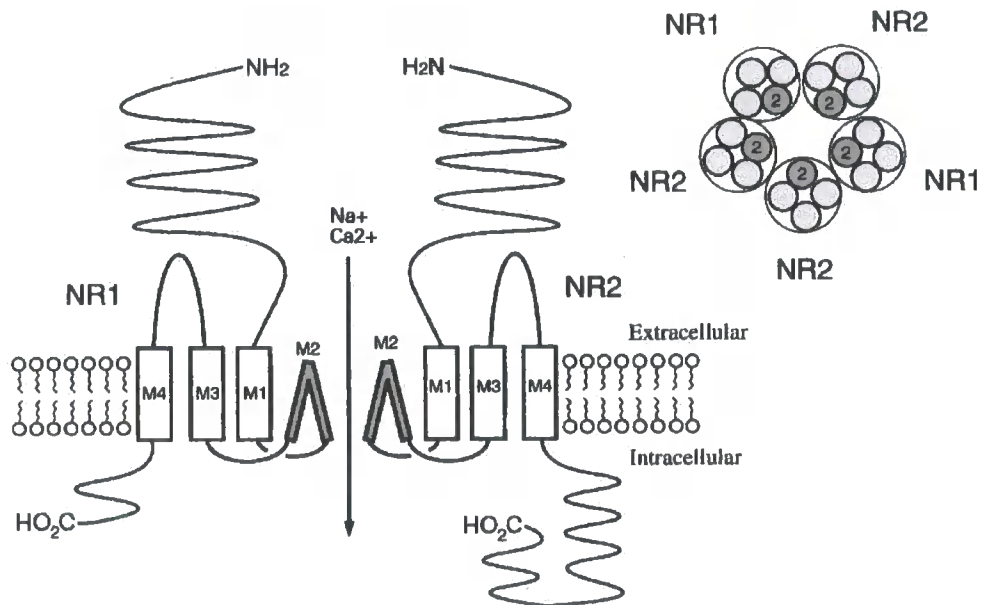
Figure 1.3 Hypothetical structure of NMDA receptors

Biochemical Journal (1998) Volume 325, (www.biochemj.org)

1.4.1 The NR1 Subunit

The NR1 subunit is encoded for by a single gene and comprises 938 amino acids with a calculated molecular mass (Mr) of 105 Kilodaltons (kDa). It was the first NMDA receptor subunit to be isolated and cloned. In 1991, Moriyoshi and colleagues reported that, using expression cloning techniques in xenopus oocytes, a complementary DNA encoding the rat NMDA receptor had been cloned and characterized. The single protein encoded by the cDNA formed a receptor-channel complex that had electrophysiological and pharmacological properties characteristic of the NMDA receptor. This protein had a significant sequence similarity to the AMPA/kainate receptors and contained four putative transmembrane segments following a large extracellular domain. The NMDA receptor messenger RNA was expressed in neuronal cells throughout the brain regions, particularly in the hippocampus, cerebral cortex and cerebellum (Moriyoshi et al., 1991). All NMDA receptors contain at least one NR1 subunit and as a result, NR1 is found ubiquitously in the brain. The cloning of NR1 subunit splice variants of the gene was reported by many groups including Durand et al., 1992; Sugihara et al., 1992 and Nakanishi et al., 1992. The NR1 subunit gene has a total of 22 exons, the alternative splicing occurs at three different locations, exons 5, 21 and 22, to give rise to eight splice forms, ranging from NR1-1a to NR1-4b (Moriyoshi et al., 1991; Cull-Candy et al., 2001; Thompson et al., 2002).

1.4.2 The NR2 Subunit

The NR2B subunit is composed of 1456 amino acids with an approximate molecular mass of 170 – 180 kDa. Hydropathy analysis of amino acid sequences predicted from the cDNA for the NR2B subunit suggests the presence of an extracellular NH_2-terminal signal peptide and four putative transmembrane domains (M1 – M4) (Kutsuwada et al, 1992). M2 forms a

7

re-entrant loop that lines the channel. Although the NR2 subunits have the same basic structure as NR1 and other glutamate-gated ion channels (Hollmann & Heinemann, 1994), they differ in that they possess large intracellular C-terminal domains, in excess of 600 amino acids and containing scattered regions of conserved sequences. The size of these C-termini is larger than the extracellular NH2-terminal segment preceding the first transmembrane region (Monyer et al, 1992).

The primary structures of the NMDA NR2 subunits were revealed for both mouse (Kutsuwada et al, 1992) and rat (Monyer et al, 1992) using independent cloning strategies. The predicted amino acid sequences for the ε2 (mouse terminology) and NR2B subunits show a sequence of 45 amino acids, specifically residues 1362 – 1406, which differ between the mouse and rat homologues (McBain & Mayer, 1994). The four NR2 subunits share considerable homology.

The NR1 and NR2 subunits possess an asparagine residue (amino acid residue 589 for NR2B) in the second transmembrane region. This domain is the putative pore-forming region for the NMDA receptor subunits. Thus, the asparagine residue may play a role in the high Ca^{2+} permeability of the channel (Loftis et al, 2003).

1.4.3 The NR3 Subunit

A third NMDA receptor family has more recently been characterised. The NR3 subunit family comprises NR3A and NR3B which are encoded for by separate genes. They are inhibitory subunits and have a regulatory role, affecting the electrophysiology of the receptor. (Cull-Candy et al, 1998, Nishi et al, 2001, Das et al, 1998). Both Ciabarra et al., (1995) and Sucher et al., (1995) independently isolated the NMDAR-L (χ1) clone, which was described as an NMDA receptor-like subunit and is now known as the NR3A subunit.

The NR3A polypeptide is predicted to be made up of 1115 amino acids with a calculated Mr of 125 KDa, and shows ~24% sequence homology with non-NMDA receptor subunits (Sucher et al., 1995).

1.5 Stoichiometry of the NMDA Receptor Complex

The structure of native NMDA receptors is still not fully known, although much work has been done to elucidate their stoichiometry (see Figure 1.3). *In situ* hybridisation and Immunochemical techniques suggest that native NMDA receptors are hetero-oligomeric complexes. Blahos & Wenthold (1996), suggest the receptor is assembled from one NR1 subunit, expressed in eight splice variants, and four NR2 subunits (NR2A-D), and that the pharmacological and physiological properties of the receptor are determined by the combination of subunits and splice variants. Other biochemical studies also provide evidence that functional NMDA receptors in rat brain and transfected cell lines are formed from oligomeric complexes of NR1 and NR2 subunits (Sheng *et al.*, 1994; Chazot *et al.*, 1994). Chazot & Stephenson (1997b) directly demonstrated using immunopurification studies, that native receptors can be heterogeneous with respect to either the NR1 or the NR2 subtype. These results support previous observations identifying more than one NR1 splice variant in the same receptor complex, and at least two different NR2 subunits co-associated with an NR1 subunit (Sheng *et al.*, 1994; Blahos & Wenthold, 1996 and Luo *et al.*, 1997). Subunit co-expression studies in *Xenopus* oocytes comparing native to recombinant NMDA receptors indicated that the NR1-1a could assemble with more than one type of NR2 subunit (Wafford *et al.*, 1993).

Co-expression of wild-type and mutant forms of either the NR1 or NR2 subunits has recently revealed the exact copy number of NR1 and NR2 subunits per oligomer. The

receptors produced displayed properties of either wild-type, mutant or a wild-type/mutant hybrid, the relative proportions of which changed with variations to the ratio of wild-type to mutant subunits. Analysis of the dose-response curves revealed three independent components of glycine and glutamate sensitivity. Binomial analysis of these data indicates the presence of two glycine and two glutamate binding subunits in the functional receptor, data consistent with NMDA receptors being tetrameric proteins composed of four homologues subunits (Laube *et al.*, 1998; Premkumar & Auerbach, 1997; Behe *et al.*, 1995). Mutagenesis studies have localised the glutamate and glycine binding sites to the NR2 and NR1 subunits respectively (Kuryatov *et al.*, 1994; Hirai *et al.*, 1996), and the binding of both these molecules is required for activation of the receptor. Studies indicate that two glutamate and two glycine molecules must bind to the receptor for its activation (Benveniste & Mayer, 1991; Clements & Westbrook, 1991). These functional studies support the biochemical studies, therefore suggesting the structure to be at least a tetramer. Work carried out by MacKinnon (1995) also supports the NMDA receptor tetramer structure theory. MacKinnon observed that receptors with re-entrant loop domains, such as voltage-gated K^+ channels, are of tetrameric structure and are analogous to the NMDA receptor.

In 1993, Brose *et al* used chemical cross-linking and size exclusion chromatography to estimate the size of the native NMDA receptor to be ~730kDa. Knowing that the NR1 recombinant receptor protein is ~116kDa, and the NR2 is ~160-180kDa, these results would suggest a pentameric stoichiometry. A pentameric structure for the NMDA receptor has been suggested by Premkumar & Auerbach, who in 1997 used a similar technique to Laube *et al* (1998). They described the receptor as three NR1 and two NR2 subunits. The work of Hawkins *et al* (1999) is in agreement with the pentameric receptor stoichiometry, although they put forward the suggestion that two NR1 and three NR2 subunits is the likely

receptor formation. The research carried out to date provides various theories as to the structure of NMDA receptors. Despite a large increase in the understanding of the function and pharmacological properties, the precise stoichiometry remains ambiguous.

1.6 NMDA Receptor Transgenic Mice

NMDA Receptor

NMDAR1
NR1 Global Knockouts
NR1 Conditional Knockout
NR1 N598 Mutants

NMDAR2

NMDAR3
NR3A Global Knockout

NMDAR2A
NR2A Global Knockout

NMDAR2B
NR2B Global Knockout
NR2B C-terminal Deletion Mutants
NR2B Global Knock-in

NMDAR2C
NR2C Global Knockout

NMDAR2D
NR2D Global Knockout
NR2D Global Knock-in
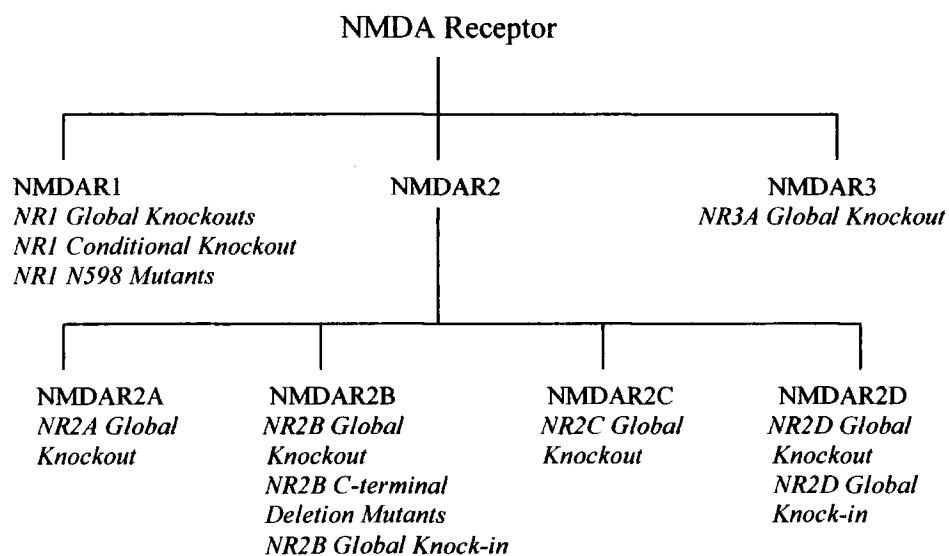
Figure 1.4. NMDA Receptor Transgenic Mice

Transgenic mice have altered levels of NMDA receptor subunit expression compared to wild-type mice. There are various types of transgenic alterations, the majority of which are global knockouts. This is where the expression of a functional product of the gene of interest has been abolished throughout the brain. Conditional knockout mice models have the deletion of the subunit expression located at specific brain regions. There are also knock-in mouse strains, where a subunit has been over-expressed.

1.6.1 NMDAR1 Subunit Transgenic Mice

NR1 global knockout models have been generated by homologous recombination in embryonic stem cells. As well as NR1 expression loss throughout the brain, there is a reduction of NR2B expression and a complete loss of the NMDA-induced rise in intracellular calcium. The mutation is however lethal and results in the mutant mice dying within a day of birth (Li *et al.*, 1994). The NR1 subunit has been suggested to have a neuroprotective role immediately after birth when selected cell death occurs, and the loss of the NR1 subunit results in a large increase in apoptosis. These studies demonstrate that the NR1 subunit is essential to NMDA receptor function (Forrest *et al.*, 1994).

NR1 conditional knockout mice can have the NR1 deletion in either the hippocampal CA1 region, the hippocampal CA3 region or cortical regions. Each of these transgenic models is generated by the *cre-loxP* recombination method, and the loss of NR1 expression is restricted to the specific regions described above. These mice are viable and develop normally although have non-lethal minor defects such as deficiencies in spatial memory.

1.6.2 NMDAR2 Subunit Transgenic Mice

The expression of all four NMDA receptor subunits NR2A-D have been modified. Global knockout models for NR2A, NR2B, NR2C and NR2D were all viable (Ebralidze *et al.*, 1996). The NR2A subunit knockout mice performed poorly in the Morris water maze test, showing deficits in spatial learning and associative learning tasks. Long term potentiation (LTP) was reduced but not abolished (Sakimura *et al.*, 1995). NR2C and NR2D global knockout models display a normal overall neuroanatomy and have no motor impairments (Ebralidze *et al.*, 1996; Ikeda *et al.*, 1992). Kutsuwada *et al.*, 1996 have suggested that the NR2B subunit plays an important role in synaptic plasticity and neuronal formation using

NR2B global knockout mice model. These mutant mice show a complete loss of NMDA receptor-mediated responses in the hippocampus, and LTP and the formation of trigeminal nucleus neuronal networks are also affected.

NR2B knock-in models show better long term visual recognition memory, enhanced ability to dissociate fear responses from contextual cues, and faster spatial learning in Morris water maze tests. These behavioural studies using mice over-expressing the NR2B subunit show enhanced ability to retain information leading to better long-term memory (White *et al.*, 2004), again supporting the theory that NR2B is involved with LTP, learning and memory formation. Tang & colleagues (1999) has also shown over-expression of NR2B in the forebrains of transgenic mice leads to enhanced activation of NMDA receptors, facilitating synaptic potentiation in response to stimulation. These mice exhibit superior ability in learning and memory in various behavioural tasks, showing that NR2B is critical in gating the age-dependant threshold for plasticity and memory formation.

1.6.3 NMDAR3 Subunit Transgenic Mice

The NMDAR3 (NR3A and NR3B) subunits have only recently been characterised, and only little is known about their function. The NR3A subunit is expressed mainly during brain development and it would appear from NR2A knockout studies, to have a regulatory role in dendritic spine development. (Das *et al.*, 1998).

1.7 Distribution of NMDA receptor subunits in the CNS

NMDA receptor subunit protein levels and their distribution patterns in the rat brain can vary between subunits. Regional distribution studies of the NMDA receptor subunits NR2A, 2B, 2C and 2D in adult rat brain were carried out by Wenzel *et al.* (1995). Using

histo-blot techniques, they showed NR2A immunoreactivity in almost all regions of the brain, NR2B was restricted to the forebrain, NR2C was confined to cerebellum, thalamus and olfactory bulb, with NR2D staining in the spinal cord, striatum, thalamic regions and brain stem structures (Dunah *et al.*, 1998). NMDA receptors containing the NR2A subtype are therefore likely to represent a subtype predominant throughout the brain, with the other NR2 subtypes displaying more regional specificity. The regionally overlapping distribution of certain subunits points to the existence of receptors containing multiple NR2 subunits (see 1.5) (Wenzel *et al.*, 1995). Similar immunoblotting work by Laurie *et al.* (1997) using rat and human brain, showed the NR2B subunit protein to be predominantly expressed in forebrain structures, such as the cortex, hippocampus, striatum, thalamus and olfactory bulbs. Moderate NR2B levels were found in the midbrain, with low expression occurring in the cerebellum and spinal cord. In 1995, Wang *et al.* reported similar findings in adult rat brain. They demonstrated high levels of NR2B subunit expression in the olfactory bulbs, hippocampus and cerebral cortex. Regional subunit expression differences have been reported between rats and mice, since prominent NR2B immunoreactivity is found in Purkinje cell bodies and dendrites in the mouse cerebellum, but NR2B is low in the rat cerebellum (Thompson *et al.*, 2000; Laurie *et al.*, 1997). Thompson *et al.* (2002) described the anatomical distribution of NR1, 2A, 2B, 2C and 2D in the adult murine hippocampal formation. NR1 was localised to cell bodies of the pyramidal neurons, granule and hilar cells in the dentate gyrus, with co-localisation of the 2A, 2B and 2D, but not 2C. The NR2B subunit appears to be widely distributed throughout the hypothalamus and thalamus, supporting its participation in a variety of regulatory functions (Loftis & Janowsky, 2003).

1.7.1 Distribution of NMDA receptor subunit mRNA in the CNS

Individual mRNAs for NMDA receptor subunits show overlap in many brain regions but are specialised in others. In the rat CNS, cloned NR1 mRNA is the most abundantly expressed and is ubiquitously distributed. Its co-expression is necessary for functional expression of all other cloned receptor subunits (Brose *et al.*, 1993). Standaert *et al.* (1994) report regional variations for each of the NR1 splice variants in both the developing and adult CNS. *In situ* hybridization by Law *et al* (2003) has shown the distribution and relative abundance of NR1, NR2A and NR2B subunit mRNA in the hippocampal formation and adjacent cortex of the human brain at five stages of life. At all ages, the three mRNAs were expressed in all subfields, predominantly by pyramidal neurons, granule and hilar cells, however their abundance varied with ontogeny. In the dentate gyrus, subiculum and parahippocampal gyrus, NR2B mRNA levels were higher in the neonate than in the older age groups. They have concluded that NMDA receptor subunit mRNAs are differentially expressed during postnatal development of the human hippocampus, with a similar pattern to that seen in the rodent. Changes in subunit composition may contribute to maturational differences in human hippocampal NMDA receptor function, and role in schizophrenia and other neurodevelopmental disorders. Goebal & Poosch (1999) studied the rat CNS and detected NR2B mRNA in the following regions, in rank order, Cortex > olfactory bulbs > hippocampus > striatum >brain stem > cerebellum. Sun *et al.* (2000) continued this work further, demonstrating the NR2B subunit transcript to be highly expressed in motor cortex and less so in periform cortex.

1.8 NMDA mRNA and Subunit Expression during Brain Development

The expression of the various NMDA receptor genes is a dynamic process, under developmental control. Recent evidence suggests that NMDA receptors are critical for neuronal migration and synaptogenesis during brain development (Loftis & Janowsky., 2003). In situ study of mRNAs encoding NMDA receptor subunits in the developing rat CNS revealed that, at all stages, the NR1 gene is expressed in virtually all neurons, whereas the four NR2 transcripts show distinct expression patterns. NR2B and NR2D mRNAs occur prenatally, whereas NR2A and NR2C mRNAs are first detected near birth. All transcripts except NR2D peak around p20. NR2D mRNA peaks at about p7 and then declines to adult levels (Monyer *et al.*, 1994). Zhong *et al.* (1995) described developmental changes in mRNA levels, showing pronounced increases in the levels of mRNAs encoding NR1 and NR2A in the cerebral cortex, hippocampus, and cerebellum between postnatal days 7 and 20. In cortex and hippocampus, the expression of NR2B mRNA was high in neonatal rats and remained relatively constant over time. In contrast, in cerebellum, the level of NR2B mRNA was highest at postnatal day 1 and declined to undetectable levels by postnatal day 28. NR2C mRNA was not detectable in cerebellum before postnatal day 11, after which it increased to reach adult levels by postnatal day 28. mRNA for the NR2B subunit is significantly decreased between the ages of 3 and 30 months in most cerebral cortical regions and in dentate gyrus granule cells (Magnusson, 2000).

NMDA protein expression, as with gene expression, is developmentally regulated. Studies in adult animals demonstrate good agreement between gene and protein expression. Analyses of neonatal rat brains by Laurie *et al.* (1997) revealed the NR2B subunit to be strongly expressed at birth, unlike the NR2A subunit, and increases until postnatal day 6 to 20 before a decline, most markedly in the cerebellum to the adult level. Similarly, rat

16

cerebellum at postnatal day 2 shows undetectable levels of NR2A, but abundant levels of NR2B protein. With increasing age, NR2A levels increase, while NR2B levels decrease and are no longer detectable by postnatal day 22 (Wang *et al.*, 1995). The NMDA receptor channel epsilon 1 subunit mRNA is expressed postnatally throughout the mouse brain, epsilon 2 subunit mRNA is found throughout the entire embryonic brain, however, becomes restricted to forebrain regions at postnatal stages. Epsilon 3 subunit mRNA appears postnatally and primarily in the cerebellum (Watanabe *et al.* 1992). Immunochemical analysis of the developing rat brain by Takai *et al* (2003b) showed the intensity of each subunit expression changed with the developmental age, while the distribution remained constant irrespective of age. Low levels of NR1 were expressed in the cerebral cortex and hippocampus in foetal brain, although widely expressed throughout the whole neonatal brain. NR2A and NR2C distribution showed temporal and spatial similarities to that of NR1, while NR2B expression is thought to be abundant throughout the brain during early development, with expression restricted to forebrain in adulthood. Changes in subunit expression are likely to underlie some of the changes in the functional and pharmacological properties of NMDA receptors that occur during development.

1.9 Pharmacological Properties of NMDA Receptors

The pharmacological properties of the NMDA receptor are closely linked to its electrophysiological properties, for example, the magnesium block of the receptor. NMDA receptors are pharmacologically complex as they contain many distinct binding sites, and have a diverse range of subunit compositions, each displaying different pharmacological and functional profiles (Moriyoshi *et al.*, 1991).

1.9.1 NMDA/Glutamate Binding site

The glutamate binding site on the NMDA receptor is localised on the NR2 subunit (Hawkins *et al.*, 1999). The site is believed to be a "venus fly-trap" model. The ligand – binding domain, S1S2, can be expressed and studied in isolation. It consists of two lobes that form a cleft, which is open at rest. When it binds agonist, the cleft closes around the ligand through a conformational change involving the formation of hydrogen bonds between the agonist and S1S2. This change results in the opening of the ion channel and allows Ca^{2+} to flow into the cell. The mechanism of closure involves an open↔closed equilibrium for the ligand-binding domain. The balance of equilibrium shifts from the open to the closed state when it interacts with agonist (Madden D, 2002a). Shortly after the ligand binds to the receptor, the receptor becomes desensitised to the depolarisation of the cell and the ion channel becomes impermeable to Ca^{2+} again.

Watkins & colleagues (1962) distinguished the NMDA receptor from other ionotropic glutamate receptors following the synthesis of its selective agonist NMDA. Unsurprisingly, most of the available selective NMDA receptor agonists are based on this diagnostic ligand, NMDA. Although this compound acts selectively at NMDA receptors, it cannot discriminate between receptor subtypes. However, a conformationally constrained analogue of glutamate, homoquinolinic acid, shows higher affinity for NMDA receptors containing NR2B and is the first NMDA receptor agonist to display sub-type selectivity. The search for selective excitatory amino acid receptor antagonists, again pioneered by Watkins & colleagues, led to the development of D-2-amino-5-phosphonovaleric acid (AP5) and D-2-amino-7-phosonoheptanic acid (AP7) (Davies *et al.*, 1981). Cyclic derivatives of both long chain phosphonate analogues AP5 and AP7, have since been described and exhibit improved ligand affinity and selectivity. These compounds include D-3-(2-

carboxypiperazin-4-yl)-1-propenyl-1-phosphonic acid (D-CPP-ene) and (E)-2-amino-4-methyl-5-phosphono-3-pentenoic acid (CGP 37849).

1.9.2 Co-Agonist Glycine Binding Site

The NMDA receptor requires the binding of a co-agonist glycine, as well as an agonist, for the opening of the ion channel. The glycine binding site on the NMDA receptor is localised on the NR1 subunit. Work carried out by Johnson & Ascher in 1987, demonstrated that the magnitude of the electrophysiological responses of cultured neurons, to applied NMDA were potentiated in the presence of sub-micromolar concentrations of glycine (Johnson & Ascher, 1987). Later in 1988, Kleckner & Dingledine reported that glycine is an absolute requirement for the activation of NMDA receptors; hence the name co-agonist was given to the glycine binding site. The agonist D-serine, acting at the glycine binding site was identified by Hashimoto et al., 1993.

There have been a number of glycine binding antagonists developed which are derivatives of kynurenic acid, for example, 5,7-dichlorokynurenic acid (5,7-DCKA) and 7-chlorokynurenic acid (7-CLKA). More recent glycine binding site antagonists have been generated using the older compounds as templates, including L-689,560, L-701,324 and substituted indole-2-carboxylates for example, GV150, 526A and GV196,771A. They all displace [^{3}H]-glycine binding with affinities below 10nM, however, none display sub-type selectivity in their actions. This is most likely due to the glycine binding site being located on the NR1 subunit while the glutamate binding site is on the NR2 subunits.

1.9.3 Polyamine Modulatory Binding Site

Polyamines are polycationic substances that stabilize intracellular conformations of negatively charged nucleic acids. Polyamines modulate NMDA receptor function. An example of this is spermine, which stimulates the receptor and increases its affinity for glycine. It may also decrease the affinity of the receptor for glutamate and generate a voltage dependent inhibition of the channel. The effects of polyamine site antagonists are specific for channels containing the NR2B subunit, making them useful tools as NR2B selective ligands. Modulators of the polyamine binding site include polyamine analogues Spermidine, Ifenprodil, Ro 25,6981, CP-101,606 and Haloperidol.

1.9.4 Ion Channel Binding Sites

Some compounds act as NMDA receptor channel blockers. They act by binding to the open pore of the NMDA receptor channel and so are termed non-competitive antagonists, for example the dissociative anaesthetics ketamine and phencyclidine (PCP). Anis & colleagues in 1983 demonstrated that ketamine and PCP, selectively reduce excitation of central mammalian neurons by N-methyl-D-aspartate (Anis *et al.*, 1983). The binding of these compounds depends upon the receptor being in its correct open state configuration, therefore requiring the presence of both agonist and co-agonist. More recently the structure of PCP has been exploited to develop a range of open channel blockers which include 1-(1-2-thienyl)-cyclohexyl-piperidine (TCP) and (+)-5-methyl-10,11-dihyro-5H-dibenzo[a.d]cyclohepten-5,10-imine (MK-801). The highest affinity compound to date is MK-801 with a binding affinity of 18nM. Both mementine and ketamine are lower affinity antagonists. These compounds have proved very effective NMDA receptor antagonists and

MK-801 has been used in a radiolabelled form to label NMDA receptor populations in brain slices, although so far, there are no compounds which show a subunit selectivity.

1.9.5 Divalent Cation Binding Site: Mg^{2+} Block of the NMDA Receptor

NMDA receptors are unique from other ligand-gated cationic channels, in that as well as the requirement for the binding of both co-agonists glutamate and glycine, and its high permeability to Na^{2+}, K^+ and Ca^{2+}, its ion channel is blocked by extracellular Mg^{2+} in a voltage-dependent manner. At resting membrane potential, NMDA receptors are permeable to K^+, Na^{2+} but not Ca^{2+} ions. This is due to a hydrated Mg^{2+} ion complexing to amino acid side chains located within the ion channel opening, forming what is known as a "magnesium block". This narrows the ion channel sufficiently to block the entry of the comparatively larger Ca^{2+} hydrated ion, whilst still allowing the passage of Na^{2+} and K^+ ions through the pore (Dingledine, 1983: Nowak *et al.*, 1984:, Mayer *et al.*, 1984). This block is removed when the membrane experiences depolarisation caused by a decrease in the ion concentration gradient across the cell membrane. The Mg^{2+} ion unbinds from the pore and allows the flow of Ca^{2+} ions through the channel.

NMDA receptor channel subunits are classified into the epsilon and zeta families according to the amino-acid sequence homology. Mori & colleagues (1992) have reported that replacement by glutamine of asparagine 598 in putative transmembrane segment M2 of the zeta 1 subunit strongly reduces the sensitivity of the heteromeric epsilon 2/zeta 1 NMDA receptor channel to Mg^{2+} block. The corresponding mutation of the epsilon 2 subunit has a similar effect. Furthermore, the heteromeric epsilon 2/zeta 1 NMDA receptor channel with the mutation on both subunits shows greatly reduced sensitivity to MK-801, a channel blocker of the NMDA receptor channel, but is still susceptible to inhibition by Zn^{2+}. These

findings suggest that the conserved asparagine residue in segment M2 constitutes a Mg^{2+}-block site of the NMDA receptor channel, and that the MK-801 site overlaps the Mg^{2+} site. These mutagenesis studies have identified these residues as playing a key role in ion modulation of channel activity and magnesium block in the NMDA receptor (Mori *et al.*, 1992). Differences between NMDA receptors with different NR2 subunit composition cause differences in extent of magnesium block, for example, NR2A or NR2B subunits are more sensitive to magnesium block than NR2C or NR2D subunits (Monyer *et al.*, 1992, Wyllie *et al.*, 1996). These characteristics are believed to play an essential role via the NMDA receptor channel, to mediate the induction of long-term potentiation of synaptic efficacy, a form of activity-dependent synaptic plasticity thought to underlie memory, learning and development.

1.10 Physiological Role of NMDA receptors

1.10.1 Synaptic Plasticity and Transmission

The NMDA receptor mediates the excitatory synaptic transmission in the central nervous system (CNS), the primary neurotransmitters being glutamate and NMDA. The channels are characterized by a voltage-dependent regulation of activity and a high Ca^{2+} permeability. As previously described, they are involved with important functions of the CNS such as synaptic plasticity in the hippocampus and synapse formation during the developing period (Wenzel *et al.*, 1997). Recent work in the hippocampus indicates that NMDAR activation can lead to induction of LTP as well as other distinct forms of synaptic plasticity, including short-term potentiation or LTD, and that this can confer increased flexibility to neuronal circuits involved in information processing and storage (Malenka &

Nicoll, 1993). NMDARs with different synaptic locations and subunit compositions are involved in various forms of synaptic plasticity in adult rat cortex (Massey *et al.*, 2004). Synaptic plasticity in the dentate gyrus is dependent on activation of the NMDA receptors. Williams *et al* (2003) have shown that synaptic plasticity in turn regulates NMDARs, since subunits of the NMDAR complex are bi-directionally and independently regulated in the dentate gyrus following activation of perforant synapses in awake animals. 48 hours after low-frequency stimulation, producing mild synaptic depression, there was a decrease in NR1 and NR2 subunits. 48 hours after high-frequency stimulation, producing long-term potentiation, there was an increase of NR1 and NR2 subunits. The increased levels of NR1 and NR2 after 48h were found to be associated with synaptic membranes, increased NMDAR-associated proteins, post-synaptic density protein 95, neuronal nitric oxide synthase and Ca^{2+}/calmodulin-dependent protein kinase II, α subunit. These findings suggest that the persistence of LTP is associated with an increase in the number of NMDAR complexes (Williams *et al* 2003).

In rat visual cortex, NMDAR properties depend primarily on NR2A and NR2B subunits, and the NR2 subunit composition changes with age and visual experience. Yoshimura *et al* (2003) examined the roles of NR2 subunits in activity-dependent long-term modification of synaptic responses, in rat visual cortex. Experiments using NR2B selective and NR2 non-selective antagonists demonstrated that NR2A- and NR2B-containing NMDARs contribute selectively to inhibitory LTD-field-LTP and excitatory LTP, respectively. It was also found that the developmental decline in the NR2B component was paralleled by the decline in the incidence of excitatory LTP. These results implicate NR2 subunit composition in the regulation of neocortical plasticity and demonstrate differential subunit regulation at inhibitory and excitatory connections (Yoshimura *et al* 2003). Philpot *et al* (2001) showed that transgenic over-expression of NR2B in rat visual cortex did not alter NMDAR kinetics

23

or synaptic plasticity in vitro, despite previous findings that visual experience can bi-directionally regulate the composition and function of the NMDA receptor (Philpot *et al.*, 2001).

Fujisawa *et al* (2003) investigated the role of *in vivo* synaptic activity upon the trafficking of the NMDAR subunit NR2B, at mature synapses by electron microscopic immunocytochemistry. *In vivo* blockade of the NMDARs was achieved by applying the NMDAR antagonist D-APV onto the cortical surface of one hemisphere of anesthetized adult rats. Inactive L-APV was applied to the contralateral hemisphere for within-animal control and to assess basal level of NR2B subunits at synapses. A decrease of NR2B labelling was detected, with significant reductions seen at post-synaptic densities as well as within the cytoplasm of spines and axon terminals. The data demonstrate that blockade of NMDARs induces rapid trafficking of NR2B subunits out of synaptic membranes, spines and terminals. This is in contrast to previous observations that NR2A subunits move into spines and axon terminals following *in vivo* blockade with D-APV.

Experimental results are beginning to clarify the mechanistic relationships between synaptic plasticity, LTP, LTD and the processes involved in learning and memory, although much remains unknown.

1.10.2 Long-Term Potentiation (LTP)

The phenomenon of long-term potentiation was first discovered by Lømo and was published as an abstract in 1966 (Lømo, 1966). Subsequent papers brought out in 1973 by Bliss & Gardener-Medwin first described LTP in detail (Bliss & Lømo, 1973; Bliss & Gardener-Medwin, 1973). The phenomenon can be defined as "a persistent increase in synaptic strength (as measured by the amplitude of the EPSP in a follower neuron) that can

be induced rapidly by a brief burst of spike activity in the presynaptic afferents, and can last from seconds to hours". In LTP, the strength of synapses between neurons in the central nervous system is potentiated for prolonged periods following brief but intense synaptic activity. To quote Bliss & Lynch (1988): "No matter how often one has witnessed the phenomenon, it is impossible not to retain a sense of amazement that such modest stimulation can produce so immediate, so profound, and so persistent an effect". The discovery of the critical role of the NMDA receptor in the induction of LTP came in 1983 by Collingridge & colleagues (Collingridge et al. 1983). By the end of the 1970's, synapses in the CA1 hippocampal neurones were identified as sites for the generation of LTP (Douglas & Goddard, 1975; Schwartzkroin & Wester, 1975). Previously, in 1957, Scoville & Milner reported that "the anterior hippocampus and hippocampal gyrus, either separately or together, are critically concerned in the retention of current experience". In the early 1960's, the hippocampus was beginning to be thought of as the main site in the brain for the processing of recent memories, a theory supported by the work of Kandel et al (1961) and Andersen et al (1963). They demonstrated intracellular recordings of synaptic transmission in the hippocampus. The importance of hippocampal LTP for spatial learning was reported by Morris (2003). The phenomenon is not restricted to synapses in the hippocampus. Racine et al. (1983) carried out a systemic study of the distribution of synapses which possess the ability to undergo LTP in the limbic system. They concluded that "With few exceptions, LTP could be produced throughout the limbic forebrain". LTP has been shown to be a cooperative process, requiring a large number of axons (McNaughton et al., 1978), and is termed "associative LTP". Associative LTP is blocked by NMDA antagonists (Collingridge et al, 1983; Harris et al, 1984; Reymann et al, 1989) and requires postsynaptic calcium increase (Lynch et al., 1983). Induction of associative-LTP requires a threshold depolarisation, the NMDA receptor to be occupied by glutamate

and an increase in post-synaptic calcium, as well as the removal of the Mg^{2+} block (Nowak *et al.*, 1984). The work of Nowak *et al.* (1984) provided a complete explanation for both the voltage-dependent properties of the NMDA receptor as well as for the criteria that had to be met for the induction of associative LTP (Bennett, 2000). The maintenance of associative-LTP involves increases in protein synthesis (Duffy *et al.*, 1981), increases in the size of dendritic spines (Fifkova *et al.* 1977), an increase in the amount of transmitter released (Dolphin *et al.* 1982) and an increase in the density of glutamate receptors (Lynch *et al.* 1982).

1.10.3 Long term depression (LTD)

LTD, like LTP is initiated by the activation of NMDA receptors and is a persistent modification of synaptic strength associated with learning, memory and neuronal development. Antagonists with higher affinities for the NR2A/B subunits relative to NR2C/D subunits show more potent inhibition of LTP than of LTD (Hrabetova *et al.*, 2000). It appears that LTD, like LTP, is not a single uniform phenomenon but rather must be considered a generic term that is used to describe any long-lasting decrease in synaptic strength (Malenka, 1993). Linden & Connor (1993), describe cerebellar long-term depression as "a persistent, input-specific attenuation of the parallel fibre-purkinje neuron synapse induced by co-activation of parallel fibres and climbing fibres". Recent studies have provided evidence that LTD induction requires both Ca^{2+} influx via voltage-gated channels, and stimulation of protein kinase C via metabotropic receptor activation. Two other mechanisms, Na^{2+} influx via AMPA receptors, and stimulation of a nitric oxide/cGMP cascade may also be involved (Linden & Connor, 1993). Linden *et al.* (1991), provided evidence to support the model of LTD induction described above. Linden showed

both specific mGluR and AMPA receptor antagonists completely block the generation of LTD. It is proposed that the physiological importance of LTD is to provide a cellular mechanism in the function of cerebellar purkinje cells that modulate sensory information that in turn control voluntary movements and reflexes.

LTD can be readily induced in adult rat cortex following inhibition of glutamate uptake, by the activation of NMDA receptors, although activation of synaptic NMDARs is not necessary for LTD induction, suggesting LTD is initiated primarily by extrasynaptic NMDA receptors (Massey *et al.*, 2004). Liu *et al* (2004) used rat hippocampal slice preparations to show that selectively blocking NR2B-containing NMDARs completely eliminates the induction of LTD but not LTP.

Both LTP and LTD are important in the formation and function of neuronal synaptic plasticity and transmission and storage of information in the brain. They need to be highly regulated in order to maintain the balance of receptor activity, since over-activation of excitatory receptors can lead to neuronal death.

1.11 Normal Aging of the Cerebral Cortex

The cerebral cortex, the grey matter outer layer of the cerebrum, is known to be responsible for primary sensory functions, motor co-ordination and control, and the "higher-order" functions of language and thinking. The cerebral cortex undergoes significant structural and neurochemical changes with increasing age, showing both regional and temporal specificity.

27

1.11.1 Structural Changes

The most significant change occurring in ageing brains is the reduction of both size and weight resulting from "shrinkage" (Brody. 1955, Dekaban. 1978, Matsumae *et al.* 1996). This has been proved by the use of accurate non-invasive magnetic resonance imaging (MRI). This age-related shrinkage is region specific. Haug *et al.* in 1983 showed that the parietal and occipital cortex displayed no shrinkage in aged brains, while the extrapyramidal and orbital cortex displayed greater than 15 percent atrophy.

Age-related atrophy was said to be caused by vast neuronal loss throughout the brain, and it has been hypothesised by Meier-Ruge *et al.* (1978) that 100,100 neurons in the human brain disappear daily, this is a 19.7 percent reduction in cell number by the age of 80 years. However, further research has since suggested that cell density actually increases as brain volume decreases with age, therefore weakening this theory (Haug *et al*, 1991). The most important factor in causing age-related brain shrinkage is now thought to be loss of white matter, possibly caused by damage of myelinated fibres. Loss of white matter was more marked than with grey matter in the cerebral cortex according to work carried out by Guttmann & colleagues (Guttmann *et al.*, 1998). Peters *et al.*, 2000 obtained similar findings and went on to show that white matter loss in aged monkey neocortex correlated closely with their age-related cognitive decline. Scheibel & colleagues in 1975 were the first to report a significant age-related loss of dendrites in the cerebral cortex, which has since been reported to include shortening and fewer dendritic branches (Jacobs *et al.*, 1993). This significant loss of dendritic structures may limit the availability of postsynaptic substrate in aged brains for synaptic connections (Wong. 2002).

Synapses, the structures linking neurons via neurotransmitters in the brain, have been shown to decline with age in both animals and humans (Adams & Jones. 1982,

Huttenlocher. 1979). It has also been reported that age-related modifications of the synapses occur, involving the loss of intracellular structures, for example, mitochondria and synaptic vesicles. This may affect metabolism and function of the synapses in the aged brain (Wong. 2002).

1.11.2 Neurochemical Changes

As well as significant structural loss of dendrites and synapses in the cerebral cortex with age, there are also age-related neurotransmitter system modifications. The present theory suggests that there is an imbalance between the functioning of different neurotransmitter systems, rather than an overall reduction in neurotransmission. Glutamate is the major excitatory synaptic neurotransmitter in the cerebral cortex as well as playing an important role in cellular metabolism. Studying changes in glutamatergic synaptic function with age has proved difficult and produced widely varying results, although studies in the loss of glutamate receptors themselves have shown consistency. Significant decreases in the mRNA level of glutamate receptors were found in the aged cerebral cortex (Carpenter et al, 1992). NMDA receptors appear to be altered to a greater extent than other glutamate receptors. Binding studies performed with homogenized cerebral cortex revealed significant decreases in NMDA but not AMPA and kainate receptors (Tamaru et al., 1991). NMDA binding in the parietal and occipital cortex in monkey has been shown to decrease (Wenk et al., 1991), and NMDA receptors have been shown to decrease with age in rodents (Kito et al., 1990). NMDA receptor subunits also show an age-related change in the cerebral cortex. For example, Magnusson (2000), showed decreases in mRNA levels of the NR1 and NR2B subunits, but no age-related change in the NR2A subunit. If subunit expression is altered with age, it would therefore alter the NMDA receptor composition. The subunit

composition of the receptor regulates single channel properties, ligand binding affinities, the voltage dependant block by Mg^{2+} and the sensitivity to Zn^{2+}. Clayton *et al.* (2001) have therefore hypothesized that age-related changes in the expression of specific NMDAR subunits may lead to the age-related changes in hippocampal function and behaviour.

1.11.3 Functional Changes

Senescence is a phenomenon universal to all living organisms and with this process brings a decrease in the functional capacity of the central nervous system. In humans, the most common neural deficits occurring with age are modifications in gait control, sleeping cycle, and learning and memory (Timiras *et al.* 1973). The use of functional magnetic resonance imaging (fMRI) has revealed a positive correlation between the reduction in cortical activation and cognitive performance. For instance, decreases in cortical activities in aged humans have been matched with the decline in working memory formation (Rypma & D'Esposito, 2000). The NMDA receptor has been implicated in the induction of LTP at hippocampal synapses, and has been proposed to play a significant role in the involvement of the hippocampus with learning and memory. Synaptic function is modified specifically in the hippocampus with age, where a reduced ability in the formation of LTP is seen. Aged rats are known to have deficits in LTP, learning and memory (Clayton *et al.*, 2001). Clayton & colleagues have shown that aged rats have significantly lower levels of NR2B mRNA and protein compared to young rats, which is complements recent findings that mice over-expressing NR2B show improved learning and memory. NR2A subunit mRNA and protein levels however, showed no change with age.

The plasticity of the brain may also decline with age, and there is evidence that the aged brain cannot recover as well after lesion or negative influence. Lowy *et al.*, 1995, have

shown that stress induced increase in glutamate release is five times higher than the level found in younger animals. The aged brain could therefore be subject to damage by the increased extracellular levels of excitatory neurotransmitters. Lesions studies of the cerebral cortex after hypoxic insults were more severe in older rats than in younger controls, correlating with a decline in plasticity (Hoyer & Krier, 1986). The ability of the cerebral cortex to cope with insult may be affected by both structural and functional modifications that occur with age.

1.12 The Ageing process: learning and memory.

If the hippocampus is involved in the consolidation of new memories and this involves the mechanism of LTP, then it is natural to enquire as to whether any changes occur in LTP with ageing, as clearly memory deteriorates with longevity (Bennett, 2000). A large number of synaptic connections are lost with senescence due to loss of dendritic spines and eventual loss of the dendrites themselves. Barnes (1979) studied changes in LTP using high-frequency stimulation experiments on mature and senescent rats. She showed that the amount of synaptic enhancement during LTP was statistically correlated with the ability to perform in memory tasks, thus, the correlation between LTP and senescence based on the idea that spatial memory depends on LTP in the hippocampus was realised. Morris *et al.* (1986) made the first attempt to link LTP with the learning process. They used APV (a recently discovered NMDA receptor blocker and therefore LTP blocker) to show a selective impairment of place learning, a process thought to be dependent on the hippocampus (O'Keefe & Conway, 1978). They saw no impairment in visual discrimination tests on rats, an LTP-independent process, which suggested a link between LTP and learning. Castellano *et al* (2001) reported evidence of memory impairments when

31

NMDA antagonists (in particular AP5) were injected into different rat brain structures, including amygdale and hippocampus.

Donald Hebb, the author of "The Organization of Behaviour" (1949), was a Canadian neuropsychologist who famously stated the following "rule" as a cellular mechanism for learning: "When an axon of cell A is near enough to excite cell B and repeatedly or persistently takes part in firing it, some growth process or metabolic change takes place in one or both cells such that A's efficiency, as one of the cells firing B, is increased". This is often paraphrased as, "Neurons that fire together wire together". This is now a well accepted idea and has formed the basis for much research over the years.

Aged humans and rodents demonstrate deficits in numerous cognitive functions. Both aged animals and ageing humans exhibit declines in working and reference memory. Changes in NMDA receptor composition during aging could have a great impact on memory performance. The over-expression of NR2B in the forebrain of transgenic mice produces animals with superior performance in a variety of learning and memory tasks (Tang et al., 1999; Tang et al., 2001; White & Youngentob 2004). Aged rats are known to have deficits in LTP, learning and memory. The work of Clayton & Browning (2001) supports the hypothesis that age-related changes in the expression of the NR2B subunit might underlie these deficits in LTP, learning and memory in aged animals. Kuehl-Kovarik et al (2003) have developed a novel technique for successfully isolating healthy neurons from aged, as well as young, mouse cortex. Their technique has enabled them to determine if functional age differences in the NMDA NR2B subunit were detectable at the level of individual cortical neurons. Their findings showed little down-regulation of NR2B during aging. In the hippocampus, the NR2B subunit has been shown to decrease with aging in the rat. A decrease in the NR2B protein with age correlates with deficits in spatial learning and antisense knockdown of the NR2B subunit blocks NMDA-dependent LTP.

With increasing age, there is a decrease in spatial memory ability for humans and non-human primates, as well as rodents. Bai *et al* (2004) have used in situ hybridisation techniques on tissue sections from three different ages of rhesus monkeys, in order to determine whether primates show changes during aging in the mRNA expression of NR2B. There was a significant decrease in the NR2B mRNA expression overall in the prefrontal cortex and in the caudate nucleus between young and old monkeys. NR2B expression showed no significant changes in the hippocampus or the parahippocampal gyrus. The results in the prefrontal cortex, caudate and hippocampus were similar to those seen previously in C57BL/6 mice during aging. This suggests that mice may be a model for primates to further examine the age-related changes in the expression of NR2B in important regions of the brain (Bai *et al* 2004).

1.13 Modulation of NMDA Receptors: NR2B Selective Compounds

Manipulation of the NMDA receptor by various pharmacological agents has revealed much information regarding the regulation of NR2B. This section outlines some of the compounds which act at NR2B-containing NMDA receptors with varying degrees of selectivity and potency.

The best characterised subtype-selective antagonist is ifenprodil. Studies in the 1980s showed that ifenprodil is an NMDA receptor antagonist with a novel pharmacological profile (Carter *et al.*, 1988; Reynolds & Miller, 1989; Chenard & Menniti, 1999). Ifenprodil and its related compound eliprodil were found to be neuroprotective but lack the motor and behavioural side-effects associated with other classes of NMDA antagonists. Eliprodil is an analogue of ifenprodil and acts at the ifenprodil binding site on NMDA receptors (Grimwood *et al.*, 2000; Pabel *et al.*, 2000). Ifenprodil inhibits channel opening

(Coughenour & Barr, 2001) and increases NMDA receptor affinity for glutamate-site agonists (Zhang & Shi, 2001). A new generation of NR2B subtype-selective antagonist congeners, based on the basic structure of ifenprodil and eliprodil have now been developed. It is hoped that these NR2B subtype-specific antagonists will show superior therapeutic implications again.

CP-101,606, a Pfizer compound, has been shown to be a potent neuroprotectant selective for forebrain neurons. Autoradiography indicates the CP-101,606 binding site is located in forebrain, most notably in hippocampus and the outer layers of cortex (Menniti et al., 1997) and acts to inhibit NMDA receptor channel activity by potentiating proton inhibition (Mott et al, 1998). Recent evidence suggests CP-101,606 displays a distinct pharmacological profile compared to other ifenprodil congeners. For example, work carried out by Chazot et al (2002a) has provided evidence for two distinct classes of NR2B-directed NMDA receptor antagonists, one which binds with high affinity irrespective whether another NR2 subunit type is present (Ro 25,6981), and a second class which is affected significantly by the presence of another NR2 subunit type within the receptor complex, exemplified by CP-101,606.

Ro 25,6981, a Roche compound, is an NR2B-selective antagonist, which binds to the ifenprodil binding site (Grimwood et al., 2000; Mutel et al., 1998, Lynch et al., 2001). Fischer et al. (1997) studied the characteristics of the interaction between Ro 25,6981 and NMDA receptors in a variety of different tests in vitro. They demonstrated that Ro 25,6981 is a highly selective, activity dependant blocker of NMDA receptors that contain the NR2B subunit, with potent neuroprotective effects in vitro. Mutel et al (1998) studied the in vitro binding properties of [^{3}H]Ro 25,6981 in rat brain using autoradiography. They detected a high density of binding sites in several layers of the cerebral cortex, in the hippocampus, dentate gyrus, caudate putamen, medium densities in the globus pallidus, thalamus, spinal

cord dorsal horn and motorneurons, whereas the cerebellum, pons and medulla were poorly labelled. Previous studies by Hawkins *et al.* (1999) have shown that Ro 25,6981 binds both NR1/NR2B and NR1/NR2A/NR2B receptors with similar high affinities, suggesting that Ro 25,6981 is an NR2B-selective compound, irrespective whether complexed with other NR2 subunit types.

MK-801 is an NMDA receptor non-competitive antagonist, which acts as a channel-site ligand. Binding assays to examine the ligand preferences of recombinant NMDA receptors were carried out by Lauire & Seeburg (1994b). These revealed that [^{3}H]MK 801 showed the affinity ranking NR1-NR2A = NR1-NR2B >> NR1 > NR1-NR2C = NR1-NR2D, therefore showing that the ligand binding affinities of recombinant NMDA receptors are dependent on their subunit composition.

Haloperidol, a dopaminergic antagonist, is a common antipsychotic used to alleviate the symptoms of schizophrenia, such as delusions and hallucinations. It has an eight- to ten-fold higher affinity for NR2B-containing receptors, showing the same subunit specificity as ifenprodil, polyamines and magnesium (Gallagher *et al.*, 1998). Results by Lee & Rajakumar (2003) indicated that NR2B-containing receptors are mainly involved in mediating haloperidol-induced c-fos expression in the limbic striatum. This is important as it may have implications in the treatment of schizophrenia. Co-administration of a NR2B selective blocker may reduce severity of haloperidol induced extrapyramidal motor symptoms without affecting its therapeutic potential.

Williams (1995) studied the modulatory effects of spermine, histamine, and ifenprodil on recombinant N-methyl-D-aspartate (NMDA) receptors expressed from the NR1A and epsilon 4 (NR2D) subunits by voltage-clamp recording in Xenopus oocytes. His results showed that NR1A/epsilon 4 receptors were insensitive to potentiation by histamine and to blockade by ifenprodil. Histamine may be able to modulate the activity of NR2B-

glutamate
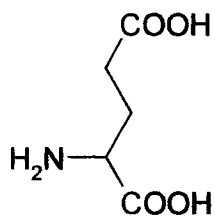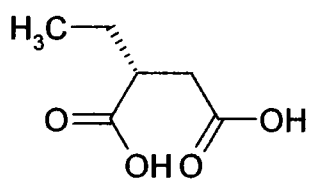
NMDA
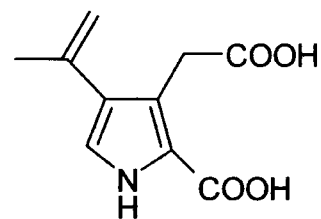
kainate
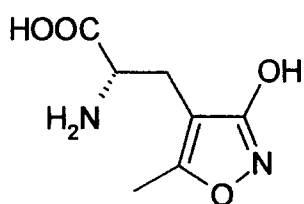
ampa
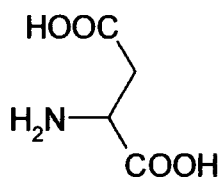
aspartate

Figure 1.5 Ionotropic Glutamate Receptor Agonists
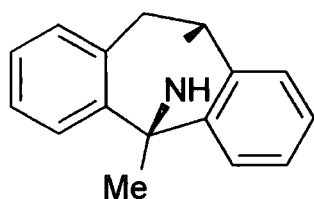
MK-801
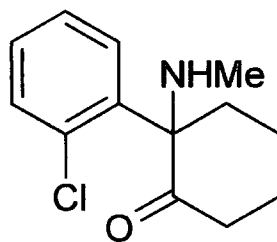
Ketamine
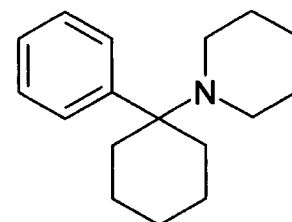
PCP
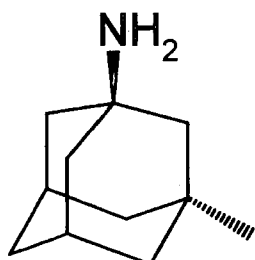
Memantine

Figure 1.6 Channel-blocking antagonists for NMDA receptors
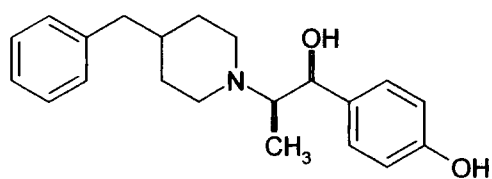
Ifenprodil
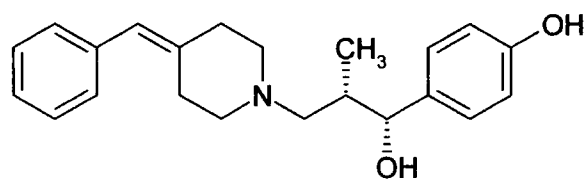
Ro 25,6981
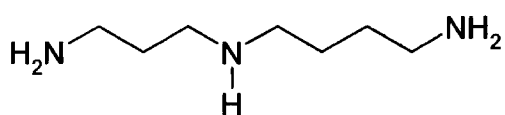
Spermidine
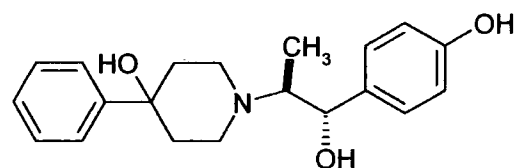
CP-101,606
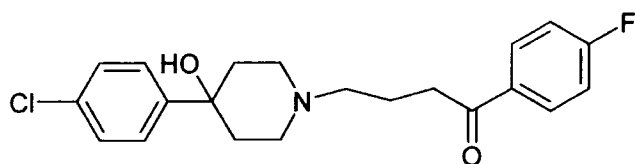
Haloperidol
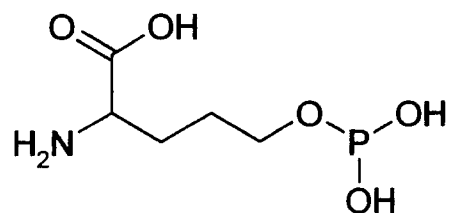
APV
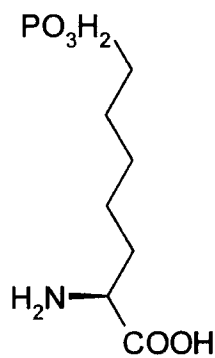
D-AP7
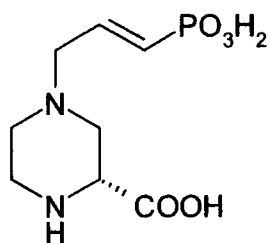
D-CPP-ene
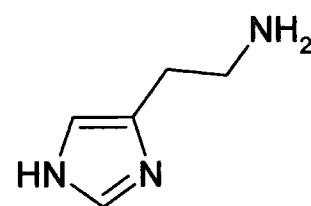
Histamine

Figure 1.7 Antagonists for NMDA receptors

containing receptors and therefore was chosen for use in the radioligand binding studies in this project.

1.14 Neuroprotective role of NMDA Receptors: Therapeutic Implications

NMDA receptors have long been associated with synaptic transmission and neural plasticity, and are considered valid CNS therapeutic targets. Their modulation has implications in a wide range of clinical states, including acute and chronic pain, stroke, head trauma and neurodegenerative diseases such as PD, AD and DLB. Aberrant NMDA receptor activity is believed to play a causal role in the neuronal loss associated with major human chronic conditions including AD and PD (Chazot, 2003). A variety of compounds have been shown to limit or prevent excitotoxicity by blocking NMDA receptor-mediated neurotransmission. However, many first-generation NMDA antagonists did not live up to clinical expectations in trials of acute brain injury because of the multiple side-effects (Albensi et al., 2004a). These non-selective inhibitors were developed when little was known about the high degree of heterogeneity within the receptor family, and this may explain why adverse side-effects, which included cardiotoxicity, were seen with their use. Drug concentrations high enough to be neuroprotective typically block glutamate receptors in healthy brain tissue, which makes it very difficult to achieve a satisfactory side effect profile (Dingledine et al., 1999). However, NMDA receptor antagonists continued to be the focus of much interest in terms of therapeutic targets for neurodegenerative diseases. Newer drugs block excititoxicity via alternative mechanisms; for example, there is compelling evidence that the NR2B subunit is an important subunit to focus upon in respect to dementias associated with a wide range of neurodegenerative diseases including DLB, PD and AD (Chazot, 2003). Several substances selective for NR2B NMDA receptor

subtypes such as eliprodil, CP-101,606 and Ro 25,6981 have claimed to have good neuroprotective profiles. Glutamate receptors have been proposed to mediate the apoptotic actions of glucocorticoids in hippocampal cells. Lu et al (2003) have studied the role of NMDARs in this process, by pre-treating primary hippocampal cells from neonatal (postnatal day 4) rats with antagonists to ionotropic glutamate receptors (iGluR) before exposure to the specific glucocorticoid receptor agonist dexamethasone (DEX). MK801, a general NMDA antagonist, and ifenprodil, a NR2B selective NMDA antagonist, were used to block iGluR. This blockade resulted in a significant attenuation of DEX-induced cell death; the finding that ifenprodil exerted a similar potency to MK801 demonstrates the involvement of NR2B receptors in glucocorticoid-induced cell death (Lu et al, 2003).

Ifenprodil was shown to be a selective antagonist for a subset of NMDA receptors containing the NR2B subunit. There is now a wide range of potential therapeutic targets for NMDA antagonists and it is hoped that NR2B selective agents in particular might possess an improved clinical safety profile compared to non-selective compounds (Chenard & Menniti, 1999). There are several reasons for this. In animal models, NR2B subunit expression decreases with age, correlating well with reduced long term potentiation (LTP) and inferior cognitive performance (Clayton et al., 2002). NMDA receptors with pharmacological properties indicative of the NR1/NR2B subtype decrease, in comparison to other subtypes, in the frontal cortex of aged humans (Piggott et al., 1992). Transgenic mice over-expressing the forebrain NR2B subunit show much enhanced cognitive performance (Tang et al., 1999). Increased synaptic strength via tetanic-induced LTP elicits a selective increase in NR2Btyr phosphorylation (Nakazawa et al., 2001). These data together would suggest that manipulation of the NR2B subunit, that is its controlled potentiation, may offer a strategy for treating cognitive abnormalities.

Cerebral Ischaemia represented the first therapeutic indication for the non-selective NMDA receptor antagonists and, more recently, the NR2B-selective compounds. Many NR1/NR2B antagonists, including ifenprodil, eliprodil and the selective and potent congeners, Ro-25,6981 and CP-101,606, offer promise in preclinical models of ischaemia.

1.15 Parkinson's Disease

Parkinson's disease (PD) was first described in 1817 by James Parkinson in a paper entitled "An Essay on the Shaking Palsy". It is a common neurological disorder which affects 1-2 per 1000 of the population and its incidence rises after the age of 50, affecting 1-2% of the elderly in the UK. The disease is due to the striatal deficiency of dopamine following neuronal degeneration within the substantia nigra (Nicholls, 2003). PD is characterised by an insidious onset with slowing of emotional and voluntary movement, muscular rigidity, postural abnormality and tremor.

1.15.1 Clinical and Pathological Diagnosis

The diagnosis of PD is usually a clinical one. The most common clinical features include tremor, stiffness, or clumsiness, difficulty in walking, fatigue, depression, and is usually asymmetrical at presentation. Typical signs include a blank facial expression, a reduction in the spontaneous blink rate, and a soft monotonous voice. The gait becomes stooped and walking becomes slow and shuffled. Cognitive dysfunction and dementia can occur later in the disease. Modern imaging techniques may play a role in the future in the pre-clinical diagnosis of the disease. For example, the use of fluoro-dopa PET imaging clearly shows the impairment of fluoro-dopa uptake in the region of the caudate and putamen in the Parkinsonian patient.

1.15.2 Neuropathology of PD

The predominant lesion in PD is cell degeneration and loss of pigmented neurones in the pars compacta of the substantia nigra. Other neurones contain cytoplasmic inclusion bodies called Lewy bodies. Their precise origin is unknown, but they contain accumulations of normal neurofilament and stain positively with ubiquitin, a protein involved with protyolisis. Lewy bodies are also found in other brain regions including the spinal cord, the locus coeruleus and the cerebral cortex. They are believed to be highly sensitive markers for PD although they are not fully specific for example, diffuse cortical (Lewy-Body) disease with dementia. Approximately 60% of nigral neurones have to be lost, with an 80 % depletion of striatal dopamine, before the symptoms of PD develop (Nicholl, 2003).

1.15.3 Management and Treatment

Drug treatments remain the pre-dominant form of PD management although these need to be in association with other vital aspects such as nursing, physiotherapy, and dieticians. Drugs used today include anticholinergics, which exert antiparkinsonian effects to control tremor, but have a range of side effects including visual hallucinations, poor concentration and memory and blurred vision. Some drugs, for example, Levadopa, will induce dyskinesias.

The use of long–term levadopa therapy in Parkinson's disease has been linked to the development of motor complications, including dyskinesias. Calon *et al* (2003) have used autoradiographical techniques to study the glutamate receptors in the brains of controls and PD patients. [^{3}H]Ro 25-6981 binding to the NR1/NR2B NMDAR was increased in the putamen of PD patients experiencing motor complications compared to those who did not (+53%) and compared to controls (+18%) whereas binding remained unchanged in the

caudate nucleus. Calon *et al* (2003) suggest the putamen may play a role in the development of motor complications following long-term levadopa therapy, due to its glutamate receptor super-sensitivity.

NR2B selective N-methyl-d-aspartate receptor antagonists have been shown to reduce levadopa-induced dyskinesias in parkinsonian monkeys, indicating that those compounds may be useful agents for the treatment of Parkinson's Disease (Blanchet *et al.*, 1999). Mutant hamsters (dt^{sz}) are a model of paroxysmal dyskinesias in which dystonic episodes occur in response to stress. Previous work has shown enhanced levels of spermine which stimulates NMDA receptors, particularly those containing the NR2B subunit, in these mutant brains. Richter (2003) has shown that Ro 25,6981, a highly selective non-competitive NR2B-subunit NMDA receptor antagonist, fails to exert antidystonic effects, even causing moderate aggravation at higher doses (12.5mg/kg), indicating that over stimulation by polyamines, of receptors containing the NR2B subunit, is not involved in the dystonic syndrome.

NMDAR antagonists have antidyskinetic effects in animal models of Parkinson's disease (PD). Undesired side effects such as ataxia and psychosis however exist due to the non-selective nature of the inhibition of NMDARs throughout the CNS. Therefore more selective drugs are being sought as possible treatments for PD. Animal behavioural studies carried out recently by Loschmann *et al* (2004) use the NMDAR NR2B selective antagonist Ro 25-6981. Their work has shown that Ro 25-6981 induced contraversive rotations in (6OHDA)-lesioned rats without stimulating locomotion in normal rats and reversed parkinsonian symptoms in (MPTP)-treated common marmosets. Ro 25-6981 potentiated the action of levadopa in both species and attenuated the maximal levadopa response in 6-OHDA-lesioned rats chronically treated with levadopa without reducing the overall response. Ro 25-6981 also potentiated the action of the dopamine receptor agonist

apomorphine, A68930 and quinpirole in 6-OHDA-lesioned rats. These observations suggest a therapeutic potential of NR2B-selective NMDA receptor antagonists in the management of PD (Loschmann *et al*, 2004).

1.16 Dementia with Lewy Bodies

Dementia with lewy bodies (DLB) is a primary, neurodegenerative dementia sharing clinical and pathological characteristics with both Parkinson's disease (PD) and Alzheimer's disease (AD) (McKeith *et al.*, 2003). However, DLB shows subtle differences from both of these disease states in the nature of the symptoms and in the damage found in the brain after death. DLB is the second most common form of dementia in the UK, making up about a fifth of all dementia cases, and affects 130,000 people nationwide. As yet, there is no specific treatment available for DLB patients. DLB has only recently been accepted as a separate disease in its own right, largely due to the fact that there is no non-invasive diagnostic test for DLB, highlighting the importance of information relating to this disorder which has been gathered by autopsy examinations.

The disease is caused by degeneration and death of nerve cells in the higher parts of the brain, and its name is derived from the tiny deposits (Lewy bodies) which are found in certain regions of the brain after death. DLB may occur late in the course of Parkinson's disease for some patients and around 75% of DLB patients will go on to develop signs and symptoms of Parkinson's, the two are closely linked.

1.16.1 Clinical and Pathological Diagnosis

Consensus clinical diagnostic criteria characterize DLB as a progressive disorder in which episodic memory impairment is often minimal in the early stages, whereas attentional and

visuospatial deficits may be disproportionately prominent (Gelb, 1999). The presence of two or more of the three core clinical features (fluctuating attention, recurrent visual hallucinations, parkinsonism), together with the variable presence of several supportive features (that is, those seen in other disorders), indicates "probable" DLB (McKeith *et al.*, 2003). Memory loss or disorientation can be associated with extrapyramidal signs (EPS) such as resting tremor, rigidity, stooped posture, shuffling gait, coming under the heading of parkinsonism previously mentioned. Supportive features can include such symptoms as repeated falls, brief periods of loss of consciousness, delusions, sleep disturbances and sensitivity to neuroleptics. The dementia associated with DLB affects concentration, memory, language, the ability to recognise faces and objects, the ability to carry out simple tasks and to reason.

The pathological diagnosis for DLB is made during post-mortem examinations where different brain regions are examined for the presence of Lewy bodies. Both PD and DLB involve the accumulation of Lewy bodies, in DLB this occurs in the brainstem and cortical areas of the cerebral hemispheres, whereas only the brainstem is significantly affected in PD. DLB is also commonly associated with pathological changes that characterize Alzheimer's disease. These include the formation of amyloid plaques, seen frequently in DLB cases, and neurofibrillary tangles, less commonly seen in DLB. High cortical senile plaque counts are found in the majority of DLB cases although the plaque composition is different to those found in AD cases. Gelb (1999) has described a semi-quantitative LB scoring system where brain regions are given a score of either one, where LB's are present in a given area, or a score of two, where there are more than five LB's in the area. Three possible categories are then generated from the resulting grouped scores, brainstem predominant, limbic, and neocortical DLB.

1.16.2 Neuropathology: Lewy Bodies

Lewy bodies (LB's) are so called because they were first identified in 1913 by Dr. Freiderich Lewy, a German neurologist. They are tiny spherical protein deposits which are seen in damaged nerve cells. Their presence in the brain disrupts the brain's normal functioning, including the action of chemical messengers, for example, acetylcholine and dopamine. These intracytoplasmic neuronal inclusions have a core of filamentous and granular material surrounded by radially oriented filaments 10-20nm in diameter. LB's in pigmented brainstem nuclei, and the substantia nigra in particular, coupled with neuronal loss and gliosis, make up the characteristic pathological findings in PD (McKeith *et al.*, 2003). In the late 1980's antiubiquitin immunocytochemical staining methods allowed LB detection, and ubiquitin antibodies identified lewy neurites in the hippocampus of DLB patients. More recently, antibodies to the presynaptic protein α-synuclein have been shown to label greater numbers of cortical and hippocampal LB's. α-synuclein is a natively unfolded protein, thought to be important in the production of synaptic vesicles, prone to filament formation and self-aggregation. McKeith *et al.*, 2003 have suggested that these α-synuclein aggregates trap other cytoskeletal proteins and degradation products. The resulting aggregates may exert neurotoxic effects within the neurones and it is possible that LB formation is a protective response by the neurones to sequester toxic species in a less active form.

1.16.3 Cognitive Impairment and Psychosis

The assessment of the cognitive status of patients is vital to identify early changes in physiological status, ability to learn and evaluating responses to treatment. In older patients, cognitive function is especially likely to decline during illness or injury. The Mini Mental

State Examination (MMSE), validated and widely used since its creation in 1975, is an effective tool to assess cognitive impairment. It is an eleven question test covering five areas of cognitive function: orientation, registration, attention/calculation, recall and language. A score of 23 or below, from a possible 30, indicates cognitive impairment. The test is effective but does have limitations, for example, patients that are hearing and visually impaired or who have low English literacy, or with communication disorders may perform poorly even when cognitively intact (Folstein *et al.*, 1975). DLB patients perform poorly compared to age-matched controls on neuropsychological tasks, especially on visual perception and learning tasks. Performance on recognition tasks is consistently more impaired than in AD, although a better performance is seen in verbal memory and orientation tasks than AD.

At least 80% of DLB patients also experience some form of neuropschiatric symptoms, particularly visual and auditory hallucinations, delusions, delusional misidentification, apathy, anxiety and depression (McKeith *et al.*, 1996).

1.16.4 Management and Treatment

To date there are no cures for DLB and the drugs used only produce modest benefits. First a diagnosis must be reached from a detailed clinical history, usually a summary of cognitive, psychiatric and motor disabilities. In the absence of safe and effective drugs, clinical management so far involves educating patients and carers about the nature of the symptoms and how best to cope with them. DLB patients with parkinsonian symptoms respond to the dopamine replacement drugs used to treat PD, but the response it generally not as good as with true PD patients. Treatment for psychosis and cognitive impairment can be complex since treatment for one symptom can often exacerbate other symptoms. DLB patients

experiencing rigidity and stiffness may benefit form anti-Parkinson's disease drugs although these can make hallucinations and confusion worse. Of particular importance is the need to avoid certain neuroleptics (tranquillisers) since they can induce Parkinson-like side-effects and may even cause sudden death. Recent research suggests that cholinesterase inhibitor drugs used to treat Alzheimer's may also be useful, drugs such as donezepil hypochloride (trade name Aricept), rivastigime (Exelon) and galantamine (Reminyl).

1.17 Alzheimer's Disease

Alzheimer's disease (AD) is the most common form of dementia among older people and affects the parts of the brain that control thought, memory and language. Onset of the disease is usually after age 60 years and the risk increases with age. Approximately 5 percent of men and woman aged 65 to 74 have AD, and almost half of those aged 85 and older have AD. The disease is named after the German doctor who first described the condition in 1906, Dr. Alois Alzheimer. Whilst studying the brain tissue of a woman who had died of an unusual mental illness, he noticed abnormal clumps, now called amyloid plaques, and tangled bundles of fibres, now called neurofibrillary tangles. Today, AD is characterised by the presence of plaques and tangles in the brain, and by the loss of specific cell populations within selective subregions of the hippocampus. The disease is a progressive neurodegeneration and is not a normal phenomenon in aging. It begins with mild forgetfulness and ends with severe brain damage.

1.17.1 Clinical and Pathological Diagnosis

It is not yet fully understood what causes AD. It is likely to be a combination of factors, affecting individuals differently. The most important risk factor is age, with disease cases

doubling in number every 5 years after the age of 65. Education, diet and environment all have a role in the development of the disease as well as the possibility of a genetic factor. A gene has been identified which makes the protein apolipoprotein (ApoE), this helps carry cholesterol in the blood and has been suggested to increase the risk of AD. Early on-set familial AD is a rare form of AD that usually occurs between the ages of 30-60 years and is inherited.

Diagnosis of AD can only be carried out with certainty at autopsy, where the presence of amyloid plaques and neurofibrillary tangles confirm the disease. Therefore, a "probable" diagnosis is made based on clinical analysis. Experimental evidence has shown that a clear, direct relationship exists between pathological change, as measured by the number of senile plaques, and the severity of dementia (Wilcock & Esiri 1982; Mountjoy 1986). A clinical assessment looks at the observable cognitive and behavioural symptoms. This involves tests of memory, problem solving, attention and language as well as medical examinations and brain scans. Patients with AD may have problems remembering familiar people, and can no longer think clearly or carry out simple routine tasks. In later stages of the disease patients can show aggressive or anxious behaviour or wander away from home.

1.17.2 Neuropathology of AD

Alzheimer's disease is caused by widespread neurodegeneration throughout the association cortex and limbic system; the areas that control memory and retention of learned information. Recent studies have shown that neurodegeneration begins with disconnection of the perforant pathway, which involves the hippocampus and plays a major role in short term memory. Eventually, the neurodegenerative process spreads to all pathways involved in learning and memory, also affecting circuitries which play major roles in higher

cognitive functions, including language, orientation, and judgement (Masliah, 1998). Research strongly supports the hypothesis that neurofibrillary tangles, along with associated neuropil threads, are at least partly responsible for nerve cell degeneration in the cerebral cortex and hippocampus. Both tangles and threads are intracellular abnormalities, with tangles found in cell bodies and apical dendrites, and threads found in distal dendrites. Tangles and threads are characterized by the precipitation of insoluble, abnormal fibrous material, now known as paired-helical fragments (PHF). These fibrillary appendages develop first at the dendrites, then through a series of cross-linkages and twists spread throughout the nerve cell soma (Braak & Braak 1998). There is increasing evidence for the involvement of glutamate-mediated neurotoxicity in the pathogenesis of AD (Danysz & Parsons, 2003). Research by Danysz & colleagues suggests that in AD, NMDA receptors are tonically overactivated, which leads to neuronal damage and impairment of synaptic plasticity. The Mg^{2+} block under normal resting conditions is thought to be disrupted in the continuous mild activation state. Overactivation of NMDA receptors using direct agonists produced deficits in synaptic plasticity, and interestingly, they found that synaptic plasticity was restored using therapeutically-relevant concentrations of memantine, an un-competitive NMDA receptor antagonist. Memantine improves both cognitive symptoms and slows the progression of the disease because it takes over the physiological function of Mg^{2+}.

Excitotoxicity, mediated via ionotropic glutamate receptors, may play a crucial role in this selective neuronal vulnerability. Biochemical and in situ hybridization techniques have been used by Mishizen-Eberz et al (2004) to investigate whether alterations in NMDA receptor subunits occurred during the progression of AD. Their data showed that with increasing AD neuropathology, protein levels and mRNA expression for NR1/2B subunits were significantly reduced, while the NR2A subunit mRNA expression and protein levels were unchanged. Their work supports the hypothesis that alterations occur in the expression

of specific NMDAR subunits with increasing AD pathology severity, which is hypothesized to contribute to the vulnerability of these neurons.

1.17.3 Management and Treatment

AD is a slow disease and it cannot yet be stopped by treatment, therefore drugs used are to help prevent existing symptoms from becoming worse for a limited time. The drugs tacrine (Cognex), donepezil (Aricept), rivastigmine (Exelon, or galantamine (Reminyl) are all used to treat AD. Memantine (Namenda) has been approved to treat moderate to severe AD although its effects are limited. Some drugs may also help control behavioural symptoms such as sleeplessness, agitation, anxiety and depression.

1.18 Aims of the Study

The focus of this research project is to address five major hypotheses:

1: The NR2B subtype population is distinct in 3 week-old and adult rat brain

2: Distinct ifenprodil-like compounds can distinguish between NR2B subtype populations

3: NR2B subtypes decline in aged human striatal and cortical brain regions

4: NR2B subtypes change in normal human ageing

5: The Levels of NR2B subtypes correlate with MMSE in human dementias

Radioligand binding techniques will be used to define the pharmacological profiles of CP-101,606, Ro 25,6981, Haloperidol, Ifenprodil, Spermidine and Histamine binding in both P21 and adult rat brain. Immunohistochemistry, using in house generated and purified antibodies, will also be used to determine the expression of both the NR2B and NR2D subunit proteins in P21 and adult rat brain, focusing on primary cognitive centres. Ligand

autoradiography will be used to assess any differences in the NR2B-containing subtypes in the P21 and adult rat brains using [^{3}H] CP-101,606 and [^{3}H] Ro 25,6981, two NR2B radioligands previously suggested to bind distinct populations (Chazot *et al.,* 2002).

A detailed quantitative ligand autoradiographical study will be performed using [^{3}H] CP-101,606 and [^{3}H] Ro 25,6981 in normal human ageing and Dementia with Lewy bodies (DLB), Alzheimer's disease (AD) and Parkinson's Disease dementia (PDD). NMDA NR2B receptors are known to play a role in synaptic transmission and neural plasticity and aberrant receptor activity is believed to play a causal role in the neuronal loss associated with major human chronic conditions including AD and PD (Chazot, 2003). Since the NR2B subunit has been implicated in having a role in learning and memory, and is involved in synaptic plasticity of the developing brain, it is therefore predicted that as memory and cognitive ability decrease with age, so too would the expression of the NR2B subtype(s) within the brain.

Chapter 2

Materials and General Methods

2.1 Source of Materials

2.1.1 Sigma-Aldrich Chemical Company (Poole, Dorset, UK)

Kodak D-19 Developer

Kodak Unifix

Ampicillin

LB Broth

Agar

Dulbeccos modified Eagles medium/F12

Sodium Bicarbonate

Sodium Hydroxide

Trypsin EDTA

DAB (Diaminobenzidine tablets)

DTT (Dithiothreitol)

EDTA (Ethylenediaminetetracetic acid)

EGTA (Ethylenbis(oxyethylenenitrilo)tetracetic acid)

Foetal calf serum.

Folin-ciocalteau phenol reagent.

Hydrogen peroxide (30% v/v)

Luminol.

N-2-Hydroxyethylpiperazine-N'-2-ethanesulphonic acid (HEPES)

p-coumaric acid.

Pre-stained molecular weight markers (molecular weight range 205-31.5kDa)

SDS (Sodium dodecyl sulphate)

Sodium azide

Sodium hydroxide.

Sodium phosphate

Tris

Tween-20.

B-actin

B-mercaptoethanol

Ro 25,6981

Histamine

Haloperidol

Ifenprodil

Spermidine

Ketamine

2.1.2 BDH Laboratory Supplies (Leicestershire, UK)

TEMED (N,N,N′,N′-Tetramethylethylenediamine)

Acrylamide

Ammonium persulphate

Methanol

Glycerol

Isobutanol

Ethanol

DMSO (Dimethyl sulphoxide)

Sodium hydrogen carbonate

Potassium phosphate

HCL (Hydrochloric acid)

Sodium chloride

DPX mountant

Potassium chloride

2.1.3 Promega Ltd (Southampton, UK)

VECTASTAIN® ABC Kit

DNA molecular weight markers

HB101 Competent *E.coli* cells.

2.1.4 Amersham Biosciences (Aylesbury, Bucks, UK)

Glass fibre filter paper for binding

Blotting paper

Nitrocellulose

Hyperfilm

HRP linked secondary antibody-Rabbit

HRP linked secondary antibody –Mouse

2.1.5 QIAGEN Ltd (Dorking, Surry, UK)

QIAGEN® plasmid maxi kit.

2.1.6 Miscellaneous

[^{3}H] CP,101-606 was a gift from Dr F. Menniti (Pfizer, Groton, USA)

[^{3}H] Ro 25,6981 was a gift from Dr J. Kemp and colleagues (Hoffmann LaRoche, Switzerland)

CP-101,606 unlabelled, Pfizer

[^{3}H] MK-801

2.2 Instruments and Equipment

Spectrophotometry: Jenway Genova spectrophotometer

Centrifuges: Bench-top refridgerated Biofuge fresco Heraeus, Beckmann J2 series

Incubators: Shel lab

Orbital shaker: Stuart Scientific

Heating Block: Grant

Magnetic Stirrer: Bibby Sterilin, Heated stirrer FALC.

Water bath: Nüve

pH meter: Mettler Toledo

Balances: Fine balance Mettler Toledo, balance Scout Pro Ohaus

Electrophoresis equipment: Pharmacia, Amersham Biosciences

Radioligand Binding equipment: Brandell Cell Harvestor

Microscopes: Nikon elipse E400 microscope

Photography: Dage 72 MTI CCD72S video camera, Nikon coolpix 950 digital camera

Other equipment: Scanner for films, Power packs Amersham Biosciences. Vortxer Scientific Laboratory Supplies

Glassware, plastics and disposables: Bibby Sterilin, Greiner bio-one Cellstar, Sarstedt

2.3 Preparation of Standard Solutions

2.3.1 Lowry Reagent A:

2% (w/v) Sodium carbonate, 0.1M sodium hydroxide and 0.5% (w/v) SDS.

2.3.2 Lowry Reagent B:

2% (w/v) Sodium potassium tartrate.

2.3.3 Lowry Reagent C:

1% (w/v) Copper sulphate.

2.3.4 Stacking gel buffer:

0.5M Tris-glycine, pH 6.8, containing 8mM EDTA and 0.4% (w/v) SDS.

2.3.5 Resolving gel buffer:

50mM Tris, 384mM glycine, 1.8mM EDTA and 0.1% (w/v) SDS, pH 8.8.

2.3.6 Stock acrylamide:

30% (v/v) Acrylamide and N.N'-methylenebisacrylamide.

2.3.7 Electrode buffer:

50mM Tris, 384mM glycine, 1.8mM EDTA and 0.1% (w/v) SDS, pH 8.8.

2.3.8 Sample buffer:

30mM Sodium hydrogen phosphate, 30% (v/v) glycerol, 0.05% (v/v) bromophenol blue and 7.5% (w/v) SDS, pH 7.0. (DTT added later)

2.3.9 Pre-stained molecular weight markers:

Pre-stained standards (protein molecular weight range 205-31.5 kDa, Sigma) stored in sample buffer, see above.

2.3.10 Transfer buffer:

25mM Tris, 192mM glycine and 20% (v/v) methanol, pH 8.4.

2.3.11 Phosphate buffered saline (PBS):

4mM Sodium hydrogen phosphate, 1.7mM potassium hydrogen phosphate, 137mM sodium chloride, 107mM potassium chloride, pH 7.4.

2.3.12 Tris buffered saline (TBS):

50mM Tris-HCL, 0.9% sodium chloride, pH 7.4.

2.3.13 Radioligand binding Tris buffer:

50mM Tris-HCL pH 7.4 containing 5mM EDTA and 5mM EGTA

2.3.14 Radioligand binding wash buffer:

10mM sodium phosphate pH 7.4

2.3.15 Autoradiography pre-incubation buffer:

50mM Tris-HCL pH 7.4 containing 10mM EDTA

2.3.16 Autoradiography incubation buffer:

50mM Tris-HCL pH 7.4 containing 10mM EDTA

2.3.17 Autoradiography wash buffer:

50mM Tris-HCL pH 7.4

2.3.18 TE Buffer:

10mM Tris pH 8.0 containing 1mM EDTA

2.3.19 HBS buffer (Hepes buffered saline):

280mM Sodium chloride and 1M sodium hydrogen phosphate pH 7.12.

2.3.20 TEE buffer:

50mM Tris-citrate pH 7.1, containing 5mM EDTA and 5mM EGTA.

2.3.21 Homogenisation Buffer:

50mM Tris-HCL pH 7.4 containing 5mM EDTA, 5mM EGTA and 320mM sucrose.

2.3.22 LB Broth:

0.47% (w/v) LB broth in dH_2O containing 1.5% (w/v) solid agar and ampicillin (50µg/ml)

2.4 General Methods

2.4.1 Adult and P21 Membrane Preparation

Either adult (~200g) or P21 Sprague-Dawley male rats were stunned and decapitated. The brain tissue was dissected and kept cool on ice. The tissue was then homogenised in ice-cold homogenisation buffer (50mM Tris-HCL pH 7.4 containing 5mM EDTA and 5mM EGTA, and 320mM Sucrose) using a dounce glass/glass homogeniser. The homogenate was centrifuged at 2200rpm, $4^{\circ}C$ for 10 minutes in a JA20 rotor. The supernatant was removed and kept on ice and the pellet was resuspended in ice-cold buffer. The homogenate was centrifuged as before. The supernatants were then pooled and centrifuged at 15,000rpm, $4^{\circ}C$ for 30 minutes. The supernatant was discarded and the pellet was resuspended in homogenisation buffer (5ml buffer for every 1g initial brain tissue). Aliquots of 1ml were prepared and stored at $-20^{\circ}C$.

2.4.2 Determination of protein concentration of the membrane preparation

The protein concentration was determined using the method of Lowry *et al.*, (1951) using BSA (bovine serum albumin) as the standard protein. A stock solution of BSA (1mg/ml) was serially diluted in water, to give a range of standard BSA concentrations from 0 to 100μg/ml. Lowry reagent A (section 2.3.1), Lowry reagent B (section 2.3.2), and Lowry reagent C (section 2.3.3) were mixed in a volume ratio of A(100): B(1): C(1). To both the BSA standards and the protein samples (5μl protein + 95μl dH_2O, and 10μl protein + 90μl dH_2O) 0.5 ml of the mixture of reagent A, B, and C was added, each sample was vortexed and incubated at room temperature for 10 minutes. All samples were assayed in triplicate. On the addition of 50μl of Folin-Ciocalteau phenol reagent (1M, 1:1 mix of Folin reagent and water) each sample was vortexed and incubated at room temperature for 30 minutes.

The reaction was terminated by adding 0.5ml of water to each tube. The O.D. at λ=750 nm was determined for each sample using a Jenway Genova spectrophotometer. A calibration curve was plotted of O.D. at λ=750 nm for the BSA samples. This was then used to determine the unknown protein concentrations.

2.4.3 SDS-Polyacrylamide Gel Electrophoresis

Immunoblotting was carried out essentially as described by Duggan *et al.*, (1991), using SDS-PAGE in 7.5% polyacrylamide mini-slab gels under reducing conditions.

2.4.4 Preparation of the Resolving Gel

The resolving gel (7.5%) was prepared by mixing 6ml distilled water with 3ml resolving gel buffer (section 2.3.5), 3ml stock acrylamide (section 2.3.6), 60μl APS (10% w/v ammonium persulphate) and 6μl TEMED. The polyacrylamide solution was immediately poured into a Biotech gel caster holding 2 gels, using gel plates of 10 x 8 cm and spacers of 1mm width. Saturated water/butanol solution (100μl) was added over the top of each gel to prevent drying out. The gels were covered with parafilm and were allowed to polymerise for 60 minutes at room temperature. Gels were individually wrapped in tissue and stored in electrode buffer (section 2.3.7) at 4°C until use.

2.4.5 Preparation of Protein Samples for SDS-PAGE

Samples were made up using approximately 20μg protein per tube in a total volume of 15μl. 5μl protein were added to 5μl sample buffer (1x) (section2.3.8), 3μl distilled water and 2μl DTT (added just before loading). Pre-stained standards (protein molecular weight

range of 32.6-205 kDa) were made up of 5μl pre-stained standard protein (section 2.3.9), 8μl distilled water and 2μl DTT. All samples were boiled in a water bath for 5 minutes and then centrifuged at 18,000 x g for 30 seconds at room temperature before analysis by SDS-PAGE.

2.4.6 SDS-Polyacrylamide Gel Elecrophoresis

The resolving mini-slab gel was clamped into a Hoefer Mighty Small II vertical slab SE250 unit. The stacking gel was prepared by mixing 2.3ml distilled water, 1ml stacking gel buffer (section 2.3.4), 650μl stock acrylamide (section 2.3.6), 80μl APS (10% w/v ammonium persulphate) and 5μl TEMED. The stacking gel solution was immediately poured into the mini-slab gel above the resolving gel. A welled comb was inserted into the stacking gel. The gel was allowed to polymerise for 30 minutes after which the comb was carefully removed and the wells were washed with distilled water. Electrode buffer (section 2.3.7) was poured into the wells and into the base of the electrophoresis unit. Protein samples (15μl) and pre-stained standards (protein molecular weight range 31.5-205kDa) (15μl) were loaded into the wells of the stacking gel using a Hamilton syringe. Electrophoresis was carried out at a current of 10mA for 30 minutes followed by 15mA for approximately 2 hours, until the appropriate pre-stained molecular weight marker (31.5 kDa) was at the bottom of the gel.

2.4.7 Immunoblotting

After SDS-PAGE (section 2.4.6), the proteins from the gel were transferred to nitrocellulose membranes. A transfer cassette sandwich was constructed with the following

order of components each of which had been pre-equilibrated in transfer buffer (section 2.3.10), sponge, two sheets of blotting paper, nitrocellulose membrane, the SDS-PAGE gel, two further sheets of blotting paper and a final piece of sponge. On addition of each component to the transfer cassette air bubbles were carefully removed by pressing each layer flat with a test tube. Proteins were transferred at a constant voltage of 50 V for 2.5 hours using a Hoefer TE series transfer tank containing transfer buffer (section 2.3.10) at room temperature.

Following the transfer of the proteins, the nitrocellulose membrane was briefly rinsed with TBS (section 2.3.12) and incubated with blocking buffer (TBS pH 7.4 containing 5% (w/v) dried milk, 0.02% (v/v) Tween-20 and 50μl NaOH) 15ml for 1 hour at room temperature with gentle shaking. After blocking of the non-specific antibody sites the nitrocellulose membranes were washed with ~10ml of TBS. The appropriate affinity-purified primary antibodies (section 3.4.2.1) were diluted in incubation buffer (TBS pH 7.4 containing 2.5% (w/v) dried milk) to working concentrations (0.25-5μg/ml). The nitrocellulose membranes were incubated with the diluted primary antibody solution (10ml) for 1 hour at room temperature or over night at 4°C with gentle shaking.

After incubation in primary antibody, the nitrocellulose membranes were washed four times in wash buffer (TBS pH 7.4 containing 2.5% (w/v) dried milk and 0.2% (v/v) Tween-20) 10ml at 10 minute intervals with gentle shaking at room temperature. Nitrocellulose membranes were then incubated with horseradish peroxidase (HRP) labelled secondary antibody, either anti-rabbit or anti-mouse depending on what the primary antibody was raised in, at a dilution of 1/2000 in incubation buffer (10ml). The membrane was incubated for 1 hour with gentle shaking at room temperature. The unbound secondary antibody was removed by washing the membrane as described above. The nitrocellulose membrane was

drained of excess wash buffer and briefly rinsed in TBS. Immunoreactive bands on the

nitrocellulose membranes were developed by processing in a solution containing 68mM p-

coumaric acid (100µl), 1.25mM luminal (10ml) and 30% H_2O_2 (6µl) for 1 minute at room

temperature. After removal of the reagents the immunoblot was wrapped in cling film and

placed in a film cassette. The immunblot was exposed to Hyperfilm™ for various lengths

of time (1-5 minutes). The film was then developed in Kodak D-19 developer until the

immunoreactive bands were visible and then fixed in Kodak Unifix for 5 minutes at room

temperature.

Chapter 3

NR2B Subtype Pharmacology in the Rodent Brain: an Ageing Study

Section 3.1

Ligand Autoradiographical comparison of Ro 25,6981 and CP-101,606 in adult mouse brain: Focus on cognitive centres.

3.1.1 Introduction

Experimental observations by Niepce de St. Victor in 1867, and those by Bequerel in 1869, birthed the discovery of autoradiography. The first biological experiment involving autoradiography was carried out in 1924, although it wasn't until some years later, in 1946, that the resolution of these autoradiographs was sufficiently improved, thus forming a technique that would become the basis for modern autoradiography. The presence of radioactive isotopes is detected by covering tissue sections with photographic emulsion. At sites of radioactive material, the radioactive emission acts on the silver halide in the emulsion. Subsequent development and fixation of the film turn radiated silver halide into black grains, providing a visible photographic image. Autoradiography and Immunohistochemistry (IHC, described in chapter 3.2.4) are both useful techniques to demonstrate the distribution of receptor subunits within tissue sections. IHC is a method of detecting the subunit protein using specific antibodies. The subunit protein is not necessarily required to be complexed with other subunits in the formation of a functional receptor. The labelled subunit may be unaccompanied by other subunits and could possibly

be in transition from the nucleus to the cell membrane for use. The antibody will theoretically bind to all the NR2B subunits present in the tissue, both on their own and those incorporated into functional receptors. This is distinct from the labelling which can be seen from autoradiographical studies. In these experiments, the radioligand will only bind to functional receptors in the tissue, since the receptor complex is essential for the binding of the ligand to occur. The radioligand will not bind to individual subunits on their own; therefore any areas on the developed autoradiographical film showing binding will be only indicating the presence and distribution of the NR2B subunit found within functional receptor complexes.

The distribution of the NR2B subunit in the mouse brain is not widely covered in the literature, although immunohistochemical studies on adult mouse brain by Thompson *et al* (2002) have shown that the NR2B subunit is detected in the cell bodies of pyramidal neurons, granule cells, apical dendrites of the CA subfields and hilar cells of the dentate gyrus. Anti-NR2B subunit-specific immunostaining was also prominent in purkinje cell bodies and dendrites of the cerebellum but absent from the granule cell layer, although this does not detect functional NR2B receptors. (Thompson *et al* 2000). There are however, data relating to the effects of the ageing process on the NMDA subunit expression, despite the inconsistencies that arise, especially with regard to the hippocampus. Magnusson *et al* (2006) analyzed male C57BL/6 mouse brain sections for [^{3}H]glutamate binding to NMDA receptors using receptor autoradiography and for mRNA of NR1, NR2A, and NR2B subunits of the NMDA receptor using *in situ* hybridization. Their results suggested that the ageing process affects NMDA receptors more in the intermediate hippocampus than the dorsal. Magnusson (2000) suggested that changes during ageing in the expression of different subunits of the NMDA receptor may account for the differential effects of ageing on agonist versus antagonist binding to the NMDA binding site. *In situ* hybridization and

63

autoradiography were performed on sections from C57Bl/6 mice representing three different age groups (3, 10, and 30 months of age). Results revealed a significant overall decrease between 3 and 30 month olds in the density of mRNA for the zeta1 subunit in the cortex and hippocampus and mRNA for the epsilon2 subunit was significantly decreased in a majority of cortical regions and in the dentate granule cells. Age-related changes in mRNA density correlated with changes in NMDA binding. Areas which exhibited the greatest decline in NMDA binding sites with age include the majority of cortical and hippocampal brain regions from the C57Bl and BALB/c strains of mice. The NMDA receptor appears to be selectively vulnerable to the aging process throughout much of the cerebral cortex and hippocampus (Magnusson & Cotman 1993a).

Chazot *et al.* (2002a) previously reported that Ro 25,6981 and CP-101,606 label distinct subtypes of recombinant mouse NR2B receptors. The Ro 25,6981 ligand bound to rodent forebrain with high affinity irrespective whether another NR2 subunit type was present, whereas CP-101,606 binding was affected significantly by the presence of another NR2 subunit type within the receptor complex. The subtype selectivity's of both ligands were determined using defined recombinant NMDA receptor subunits expressed in HEK 293 cells. [^{3}H]CP-101,606 bound to adult rodent forebrain and NR1/NR2B receptors expressed in HEK 293 cells with $K_D = 4.2$ nM and 6.0 nM, respectively. In contrast, no high affinity specific binding was detected to NR1, NR2A, NR2B subunits expressed alone or NR1/NR2A receptors. Immunoblotting studies using HEK 293 cells transfected with NR1, NR2A and NR2B receptor subunits and complexes comprising all three subunits were carried out. Subunit-selective antibodies were used to probe the material isolated by anti-NR2A immunoaffinity chromatography. The immunopurified material contained all three NMDA receptor subunit polypeptides. However, in contrast to parallel studies in which high affinity [^{3}H]Ro-25,6981 binding activity was observed, no high affinity [^{3}H]CP-

101,606 binding sites were detected to the immunopurified material (Chazot *et al.* 2002). The previous studies using cloned mouse receptor complexes have shown both Ro 25,6981 and CP-101,606 bind distinct subtypes of NR2B receptors. The work in this section is a continuation of the study using these two ligands, looking at their binding to native NR2B containing receptors expressed in mouse brain sections. The aim of this study was to autoradiographically show the distribution of ligand binding within the tissue sections, and to reveal any differences in specific ligand binding levels not only between different brain regions, but also between the two ligands themselves. The hypothesis is that both CP-101,606 and Ro 25,6981 used in this study will label similar brain areas since both ligands are NMDAR2B selective, however there may be differences in the intensity of labelling seen between the two ligands due to there respective sub-population binding selectivities.

The method used in this study was that essentially described by Mutel *et al.* (1998), with some modifications made, and is described in (3.1.2.2). Autoradiography was carried out on slide-mounted mouse sections, prepared as described in (3.1.2.1) using the radiolabelled ligands **[^{3}H]CP-101,606** [(1S,2S)-(4-[^{3}H]hydroxyphenyl)-2-(4-hydroxy-4-phenylpiperidino)-1-propanol], and **[^{3}H]Ro 25,6981** (R-(R*,S*)-α-(4-[^{3}H]hydroxyphenyl)-β-methyl-4-(phenylmethyl)-1-piperidine propanol]. This provided a high resolution image of localised receptor binding, showing neuroanatomical detail between brain regions. Spermidine, was used to define specific binding of the radioligand (Hawkins *et al.* 1999).

3.1.2 Methods

3.1.2.1 Perfusion and Sectioning of Mouse Brain

The perfusion was performed by Dr C.L. Thompson. An adult wild-type mouse was deeply anaesthetised using Pentobarbitol, and assessed by failed nictating reflex and pressure-induced retraction of hind limb. The anaesthetised rodent was then pinned out with its ventral surface uppermost. The ribcage was exposed and retracted, and a 25 gauge microlance was inserted into the left ventricle through which ice-cold 0.1M sodium phosphate buffer pH 7.4 containing 0.1% (w/v) sodium nitrate was perfused via a peristaltic pump, and the right atrium was cut. The rodent was exsanguinated in this manner for 5 minutes. The perfusate was then exchanged for freshly prepared, ice-cold 0.1M NaPO buffer, pH 7.4 for 20 minutes, after which the brains were dissected out and immediately frozen in isopentane over liquid nitrogen for 1 minute at $-70°C$. The brains were then horizontally sectioned ($16\mu m$) on a cryostat ($-24°C$). The sections were thaw-mounted onto poly-D-lysine coated microscope slides and stored at $-20°C$ until use.

3.1.2.2 NMDA R2B receptor autoradiography

The autoradiographical method used was that essentially described by Mutel et $al.$ (1998), with some modifications made. Tissue sections were brought to room temperature (30 minutes) and incubated in pre-incubation buffer (section 2.3.15) for 2 x 10 minutes at room temperature (10 slides per coplin jar, 30ml buffer). The volume of buffer used for pre-incubations, radioligand incubations and washes were all 30ml, the maximum capacity of the coplin jars used when holding 10 slides back to back. Sections were then incubated in buffer containing 10nM [³H]CP-101,606 (specific activity = 29.6Ci/mmol, stored at $-20°C$) from Dr. Menniti (Pfizer, Groton, USA), or 10 nM [³H]Ro 25,6981 (specific activity = 25.6

66

Ci/mmol, stored at -20°C) from Dr. J. Kemp and colleagues (Hoffmann LaRoche, Switzerland) for 90 minutes at 4°C, until equilibrium is reached. 10 slides per coplin jar, containing 30ml radiolabelled buffer. Non-specific binding was determined in the presence of 10mM unlabelled spermidine (an endogenous polyamine) as used by Chazot *et al.* (2002) rather than 10μM Ro 04, 5595. The reaction was terminated by three washes at 4°C (2 x 5 minutes and 1 x 15 minutes) in 50mM Tris-HCL buffer containing 5mM EDTA pH 7.4. This was the optimal rinse time to produce the maximal relative specific binding. After the three buffer washes, slides were briefly dipped in ice-cold distilled water (2 seconds) and then dried in a stream of cold air. Slides were left to thoroughly air dry overnight. The sections were then transferred to X-ray cassettes, each including tritium autoradiographic microscales as calibration standards, and exposed against tritium-sensitive Hyperfilm for 6 weeks at room temperature. The exposed films were then developed in GBX developer (Kodak) for 5 minutes at room temperature, rinsed in distilled water, fixed for 5 minutes in GBX fixer (Kodak), washed under running tap water for 2 minutes and dried.

3.1.2.3 [^{3}H]Ro 25,6981 and [^{3}H]CP-101,606

The radioligand concentrations used were altered from those stated by Mutel *et al.* (1998). Preliminary unpublished studies by M. Lake (2002) were carried out using a range of radioligand concentrations. The concentrations of the radioligands used were chosen so they were the affinity (K_D) of their specific binding to ensure that each autoradiography run measured an acceptable number of receptor binding sites. The K_D of CP-101,606 and Ro 25,6981 is approximately 10nM (Chazot *et al.*, 2002a, chapter 3.2.2.3), therefore a 10nM concentration was used for direct comparison. Before starting the experiment, the concentration of the incubation buffer containing the radioligand was checked by taking a

20µl aliquot into a scintillation vial with 1ml scintillation fluid (Packard Ultima Gold) and measuring the dpm value in a Packard tri-carb 1900CA scintillation counter.

3.1.2.4 Image analysis

The resulting brain images on the films were scanned into the computer using a Dell All-in-one scanner and were quantitatively analysed using the densitometry software package Image J to measure ligand binding levels in specific brain regions. The radioactive tritium standards were used to calculate a standard curve for each autoradiogram, which allowed the conversion from optical density values to units of concentration (nci/mg of tissue protein), for each brain region analysed. The non-specific tissue sections were present on the same film as each of the corresponding total binding tissue sections. Specific binding was determined by subtracting mean non-specific binding from mean total binding. Inter-assay variability was eliminated by using radioligand from the same batch for each autoradiographical run, and by standardising each film using calibration microscales.

3.1.2.5 Statistical Analysis

Statistical analysis performed involved students unpaired t-test, indicated with the use of Microsoft Excel to analyse individual regions of the brain. Statistical significance was set at $p<0.05$ level for the t-tests analysis, with a minimum n value of 10 determinations.

Olfactory Bulbs

Frontal Cortex Inner

Striatum

Frontal cortex Outer

Thalamus

Hippocampal Formation

Cerebellum

Entorhinal cortex

0   2.5mm

The Hippocampal Formation

CA2

Pyramidal Cells

CA3

CA1

SO   SR

Polymorph Layer

Granule Layer

Dentate Gyrus

SO = Stratum Oriens
SR = Stratum Radiatum
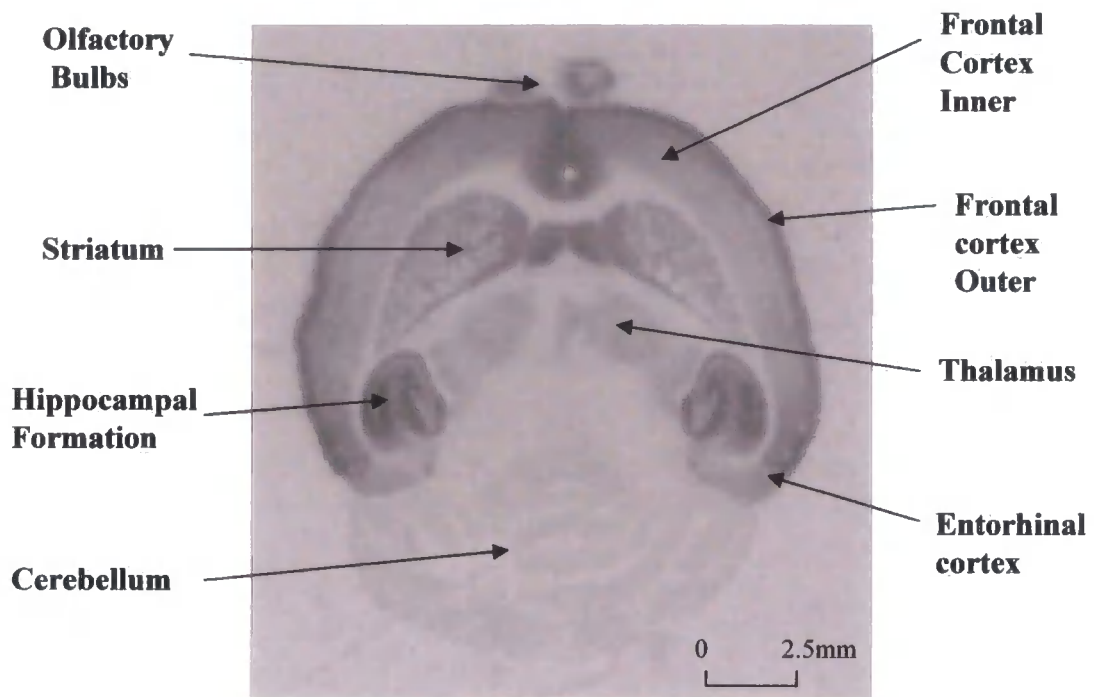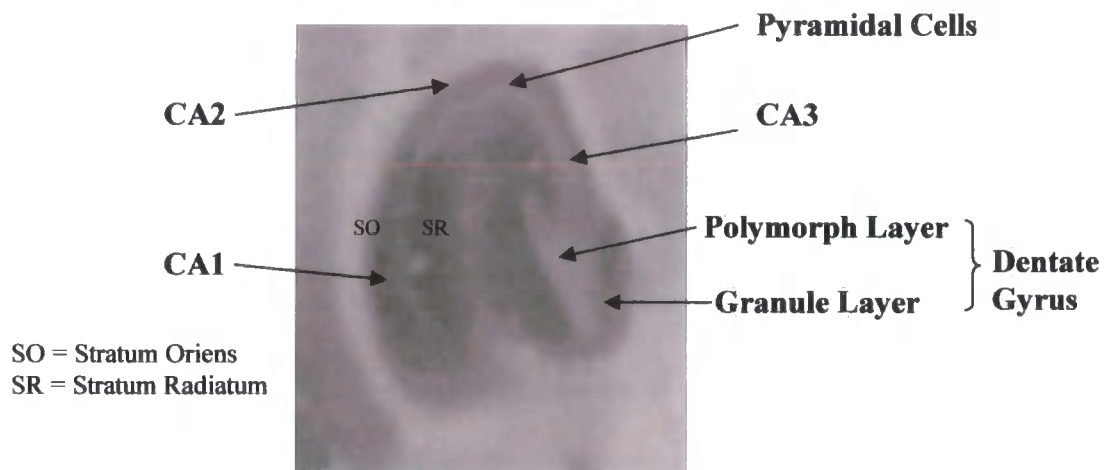
Figure 3.1.1 Example of an Adult Mouse brain section. NR1/NR2B-containing receptors labelled by [^{3}H]Ro 25,698. Specific binding defined using 10mM spermidine. Areas analysed were CA1 SO, CA1 SR, CA2 SO, CA2 SR, CA3 SO, CA3 S Lucidum, DG Poly (Dentate Gyrus Polymorph layer), DG gran (Dentate Gyrus granule layer), PC (CA2 Stratum Pyramidale cells), Ent cx (Entorhinal cortex), In F cx (Inner frontal cortex), Out F cx (Outer Frontal cortex), Thal (Thalamus), Stria (Striatum) and Cereb (Cerebellum).

A   **B**

0   2.5mm

Total **D**

C
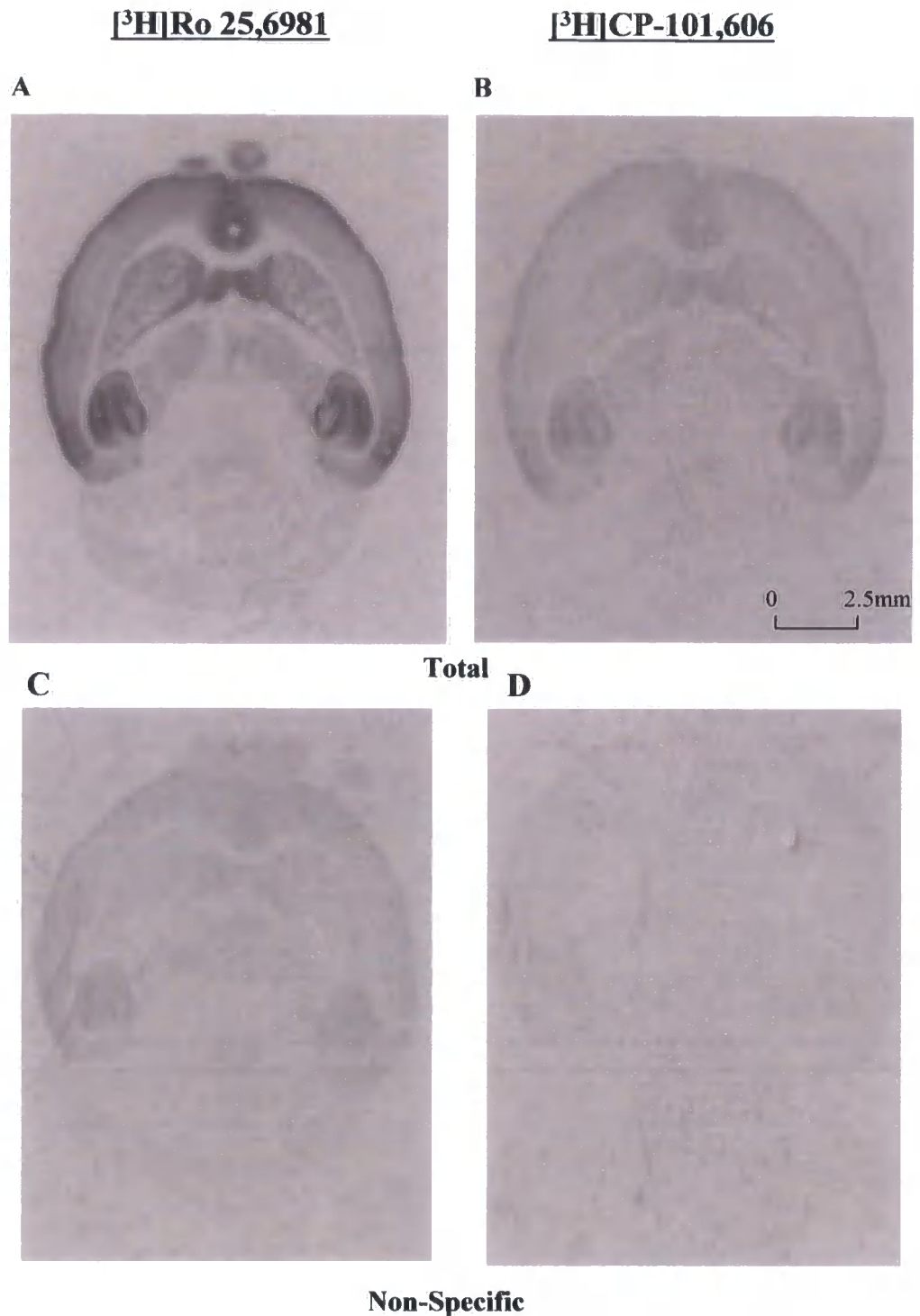
Non-Specific

Figure 3.1.1 (a) Autoradiography of Adult Mouse brain slices. (A,B) Total binding for $[^3H]$Ro 25,6981 and $[^3H]$CP-101,606 respectively and (C,D) Non-specific binding for $[^3H]$Ro 25,6981 and $[^3H]$CP-101,606 respectively. Specific binding defined using 10mM spermidine.
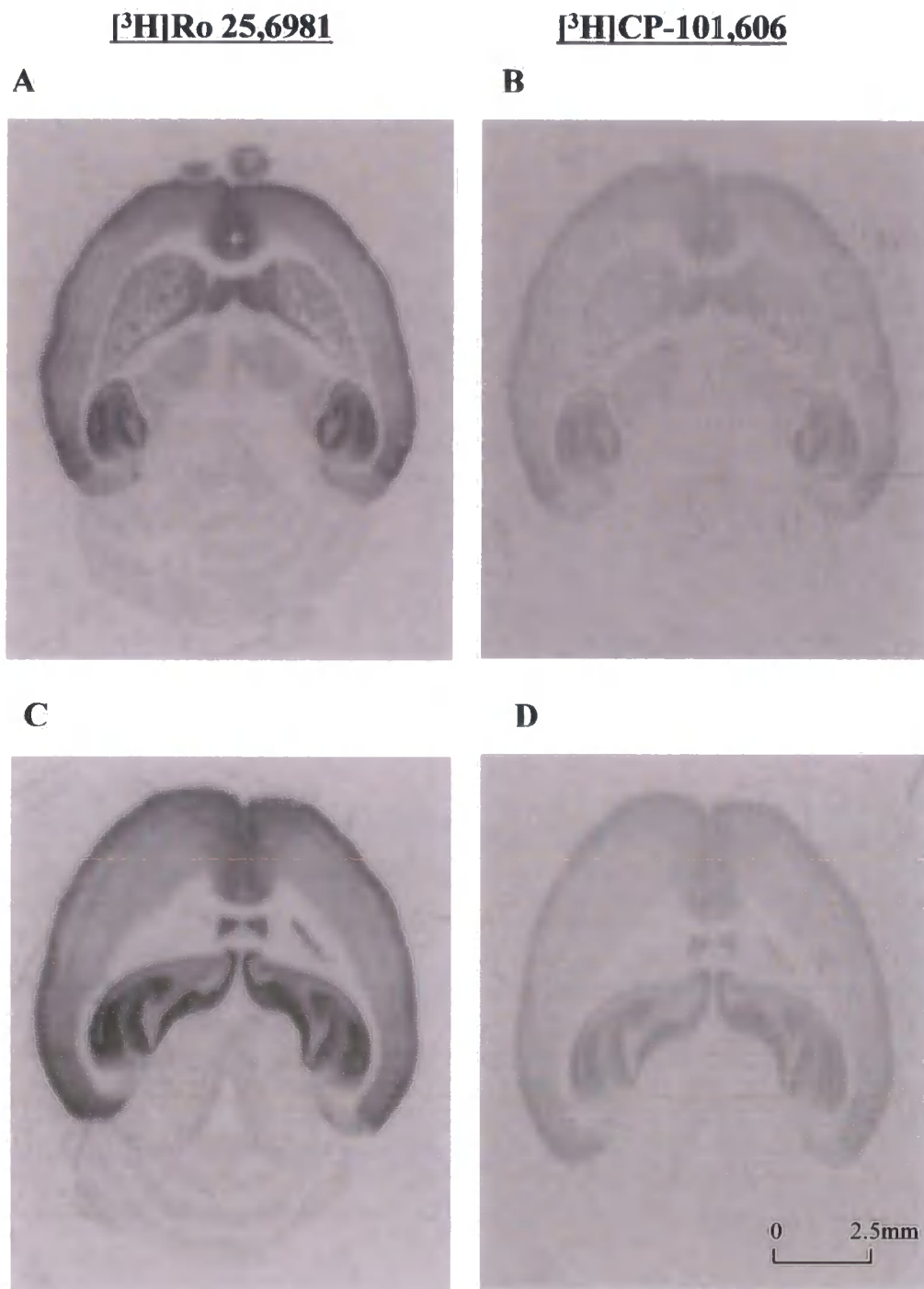
Figure 3.1.2 Autoradiography of Adult Mouse brain slices. (A,C) [³H]Ro 25,6981 labelled receptors and (B,D) [³H]CP-101,606 labelled receptors. Specific binding defined using 10mM spermidine.

3.1.3 Results

3.1.3.1 Results (Figure 3.1.1-3.1.2)

The first three figures in this section (Figure 3.1.1-2) are scanned images of the resulting films showing a qualitative analysis of the binding data. These are followed in Figures 3.1.3-4 by a quantitative analysis of the binding levels in each tissue. Figure 3.1.1 is a representative example of an adult mouse brain section showing the typical pattern of radioligand binding seen in the brain areas analysed, in this case [^{3}H]Ro 25,6981 has been used. The darker areas indicate those which have been labelled by the radioligand, the greater the intensity, the higher the binding density in that tissue. The mouse brain sections are cut horizontally as described in 3.1.2.1 with the areas labelled being identified using "The Mouse Brain in Stereotaxic Coordinates" by G. Paxinos and K. Franklin, Academic Press, 2nd Edition (2001). There is clear labelling seen in the hippocampal formation, which has been divided into the following sections for analysis, CA1 SO (stratum oriens), CA1 SR (stratum radiatum), CA2 SO, CA2 SR, CA3 SO, CA3 SR (Lucidum), DG Poly (Dentate Gyrus Polymorph layer), DG gran (Dentate Gyrus granule layer), PC (CA2 striatum pyramidale cells). The pyramidal cell bodies and polymorph layer of the dentate gyrus show low levels of binding, suggesting the receptors containing the NR2B subunits are located on the neuronal projections which are seen labelled in the SO, SR and granule layer. The frontal cortex is also well labelled, and has been divided into two. The outer frontal cortex in many of the sections clearly shows a higher binding level than that seen in the inner frontal cortex. The entorhinal cortex, striatum and thalamus are also well labelled. The cerebellum shows very low binding levels. Figure 3.1.1(a) shows representative examples of adult mouse sections showing total and non-specific binding levels, clearly showing the very low binding in the non-specific sections. Figure 3.1.2 shows scanned

images of the resulting films giving representative examples of both [^{3}H]Ro 25,6981 (left hand side) and [^{3}H]CP-101,606 (right hand side) binding in adult mouse brain sections. There were considerably higher binding level of [^{3}H]Ro 25,6981 overall than the [^{3}H]CP-101,606 ligand binding levels. In each of the examples shown, ligand binding was seen in the frontal and entorhinal cortex, striatum, thalamus, hipppocampal formation and appeared to be marginally above background in the cerebellum. Non-specific binding was defined using 10mM spermidine. As described in section 3.1.2.4, the non-specific value is calculated by subtracting mean non-specific binding from mean total binding.

3.1.3.2 Results (Figure 3.1.3 -3.1.4). Refer to legends below each figure.

3.1.3.3 Results (Figure 3.1.5 (A-O)).

The standard curves generated from each autoradiogram tritium standard scale were used to convert optical density values (dots per inch (dpi)) units to concentration of radioligand bound to the tissue (nci/mg of tissue protein). The same data as previously described (see figures 3.1.3-4) were further analysed to show mean specific binding levels (± SD for n = 10 determinations) for both [^{3}H]Ro 25,6981 and [^{3}H]CP-101,606 in adult mouse brain sections in each brain region defined. When comparing binding levels of the [^{3}H]Ro 25,6981 and [^{3}H]CP-101,606 in the mouse tissue, there were significantly higher levels of [^{3}H]Ro 25,6981 binding in all the regions analysed (p<0.01), with the exception of the hippocampal pyramidal cells (p= 0.29), the F CX Inner (p= 0.09) and the cerebellum (p= 0.99).
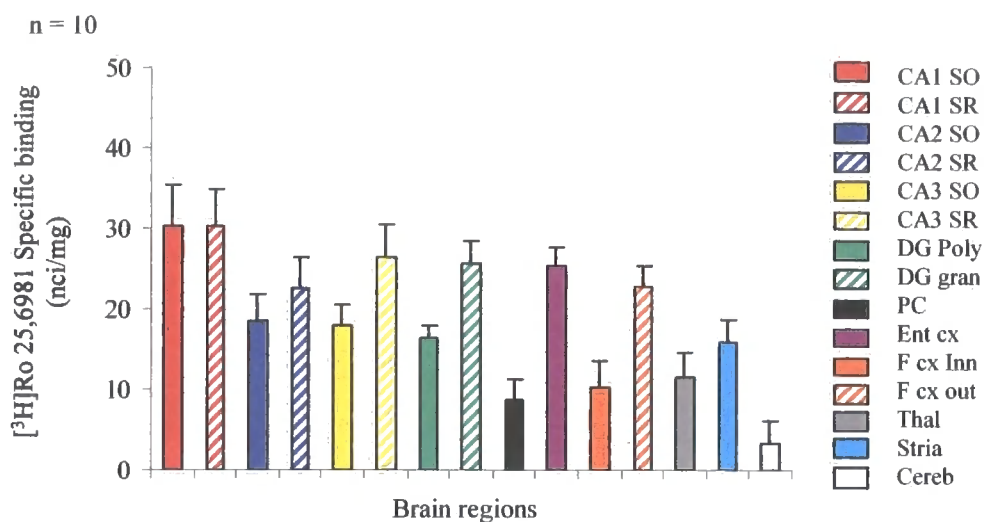
Figure 3.1.3 Graph showing the differences in [³H]Ro 25,6981 specific binding (nci/mg) densities (mean ± SD for n = 10 determinations) for Adult mouse brain.

Adult mouse brain sections prepared as described in section 3.1.2.1 were assayed for radiolabelled Ro 25,6981 binding by autoradiography (3.1.2.2). As shown in figure 3.1.3, there were higher levels of [³H]Ro 25,6981binding in the CA1 SO, CA1 SR, CA2 SR, CA3 SR, DG Gran, Ent CX and F CX Outer, than in all other regions analysed, except the CA2 SO, which showed similar binding levels when compared to CA2 SR. The lower levels of binding were seen in the regions CA3 SO,DG Poly, F CX Inner, thalamus, striatum and minimal binding was seen in the pyramidal cell layer and cerebellum. There is a clear variation in the levels of binding seen between the different brain regions analysed, ranging from the highest level in the CA1 SO to the lowest in the cerebellum.
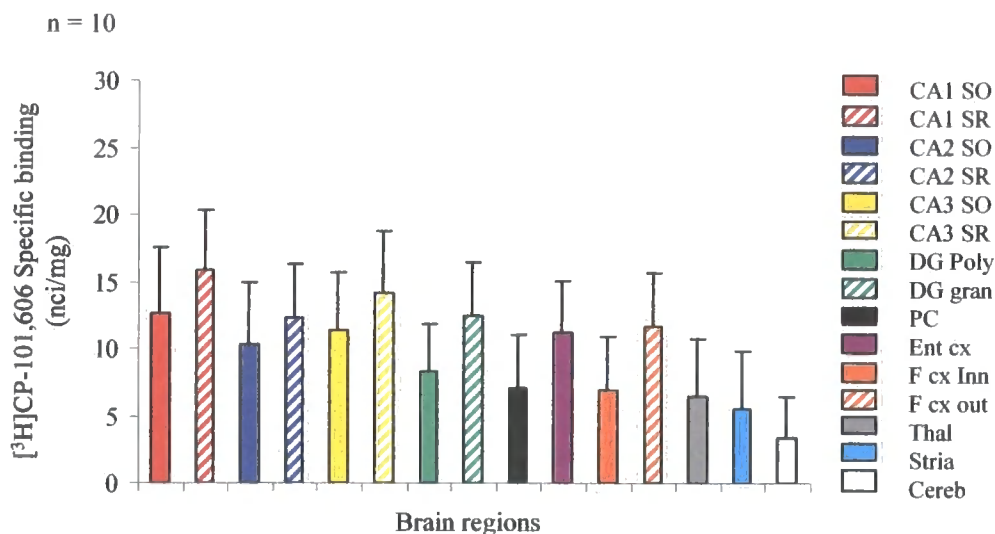
Figure 3.1.4 Graph showing the differences in [³H]CP-101,606 specific binding (nci/mg) densities (mean ± SD for n = 10 determinations) for Adult mouse brain.

Adult mouse brain sections prepared as described in section 3.1.2.1 were assayed for radiolabelled CP 101,606 binding by autoradiography (3.1.2.2). As shown in figure 3.1.4, there were higher levels of [³H]CP-101,606 binding in the CA1 SR than in the regions DG Poly, PC, FCX Inner, thalamus, striatum and cerebellum. All other regions showed lower levels of binding compared to the CA1 SR. The lowest levels of binding were seen in the regions DG Poly, PC, F CX Inner, thalamus, striatum and minimal binding in the cerebellum which is consistent with levels seen with the [³H]Ro 25,6981 ligand. There is also variation in the levels of binding seen between the different brain regions analysed, as there was with the [³H]Ro 25,6981 ligand. In this case, binding levels ranged from the highest level in the CA1 SR to the lowest in the cerebellum.
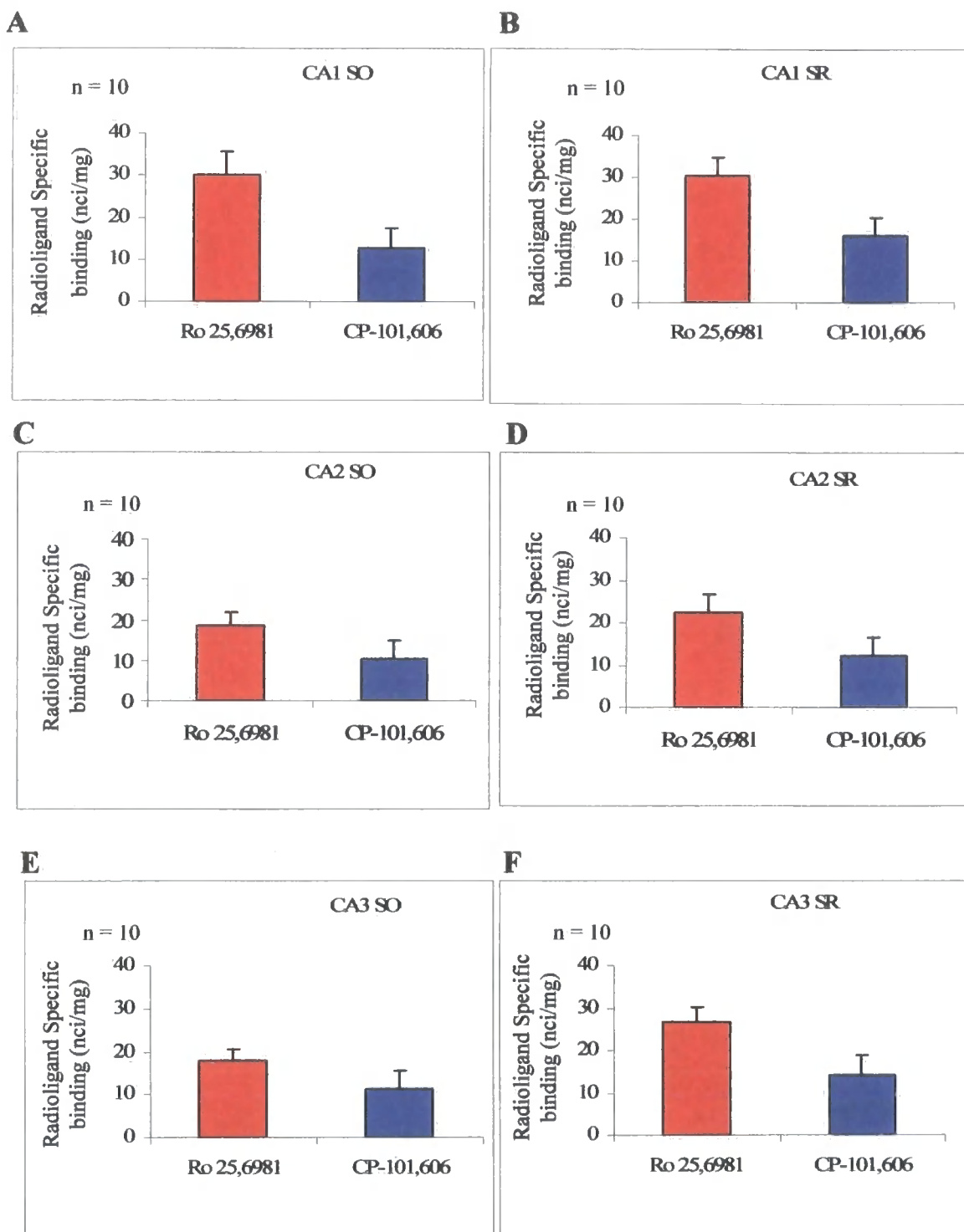
Figure 3.1.5 (A-F) Mean average specific binding (nci/mg) ± SD of [³H]Ro 25,6981 and [³H]CP-101,606 for Adult Mouse in Hippocampal regions (A) CA1 SO (B) CA1 SR (C) CA2 SO (D) CA2 SR (E) CA3 SO and (F) CA3 SR. (SO = stratum oriens, SR = stratum radiatum).
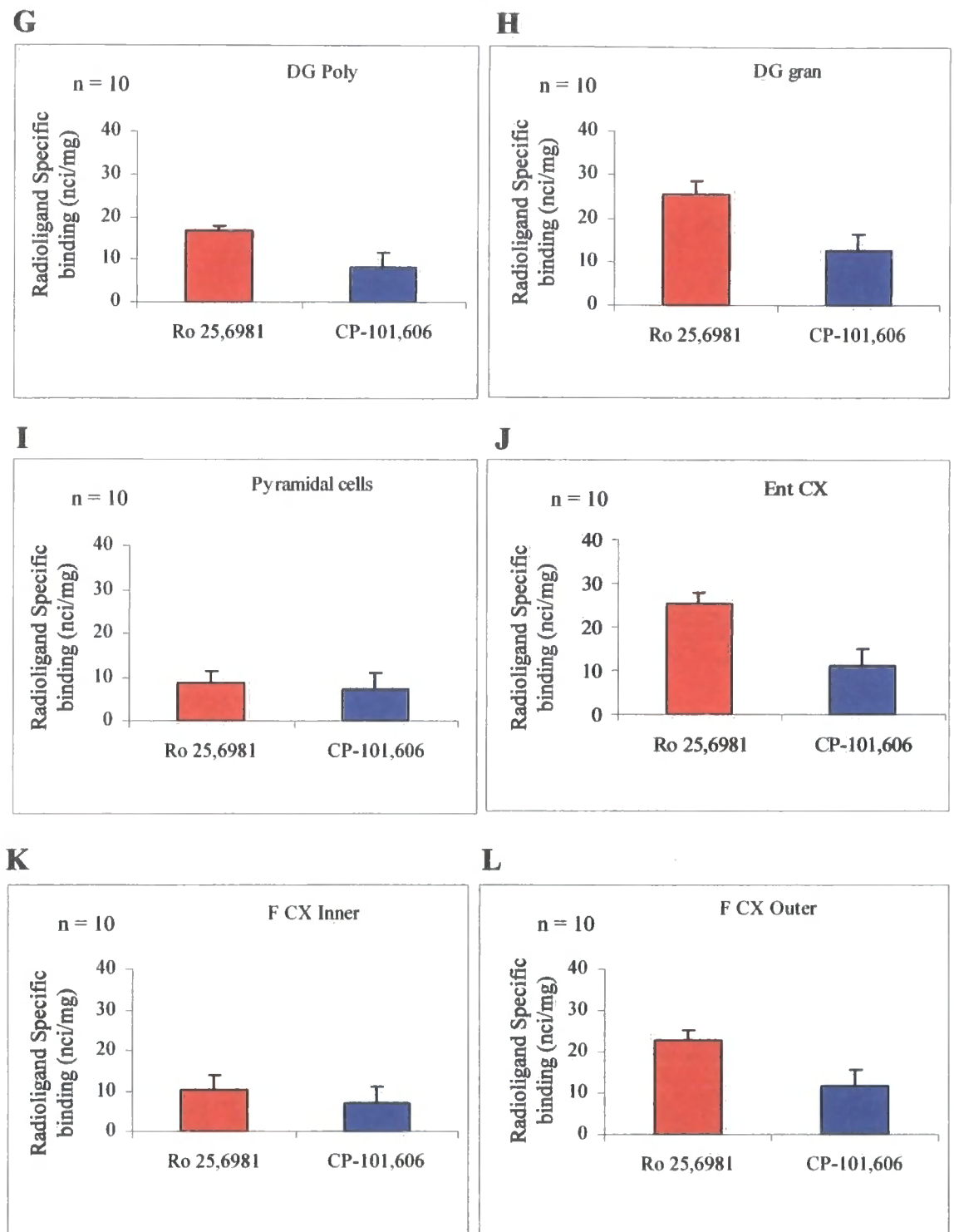
Figure 3.1.5 (G-L) Mean average specific binding (nci/mg) ± SD of [³H]Ro 25,6981 and [³H]CP-101,606 for Adult Mouse in (G) DG Polymorph (H) DG Granule (I) Pyramidal cells (J) Entorhinal cortex (K) Frontal cortex inner and (L) Frontal cortex outer. (DG = dentate gyrus layers).
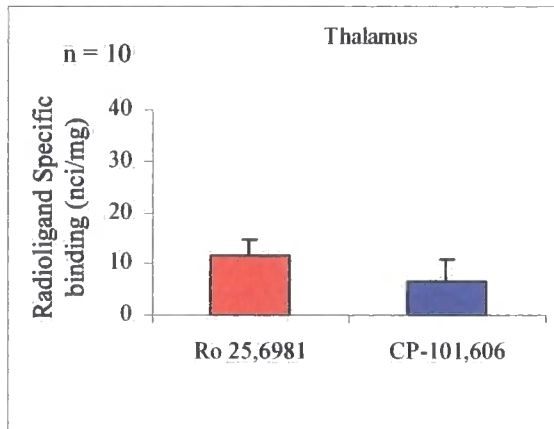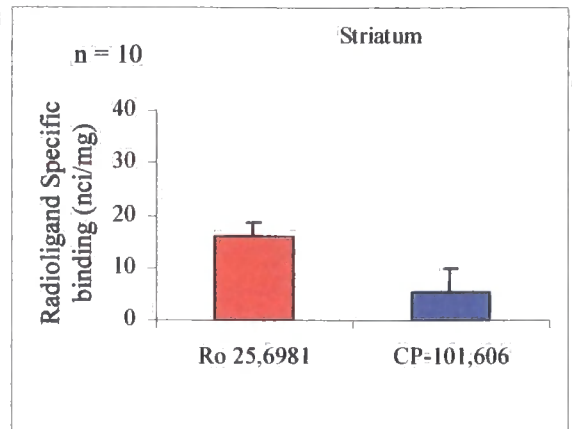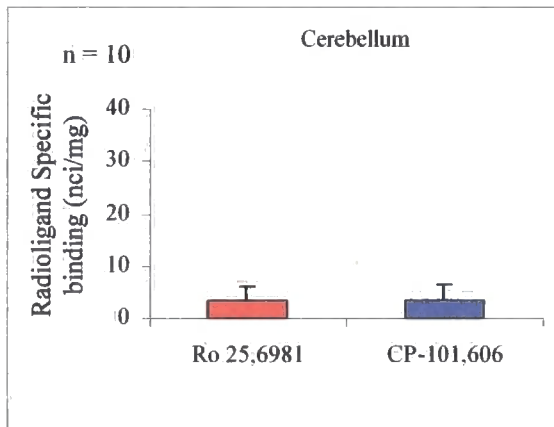
Figure 3.1.5 (M-O) Mean average specific binding (nci/mg) ± SD of [³H]Ro 25,6981 and [³H]CP-101,606 for Adult Mouse in (M) Thalamus (N) Striatum (O) Cerebellum.

3.1.4 Discussion

In this section the mouse brain has been analysed using two NR2B-selective NMDA receptor antagonists. Previous studies have revealed their subtype selectivites and affinities for binding to recombinant mouse NR2B receptors as well as native NR2B rodent receptors (Chazot et al. 2002b; Menniti et al. 1997: Mutel et al, 1998). The two aspects to consider with the data from this section are the distribution pattern of binding for the two ligands in the mouse brain, and the difference between the binding levels of the two ligands. In Figure 3.1.3-4 both Ro 25,6981 and CP-101,606 showed high binding levels in the CA1, CA3, granule layer of the dentate gyrus, entorhinal cortex and outer layers of the frontal cortex. Similarly, the lowest binding levels were seen in the cerebellum, thalamus, inner layers of the frontal cortex and pyramidal cell layer of the hippocampus for both ligands analysed. Menniti et al. (1997) used autoradiography to indicate that the CP-101,606 binding site is found most abundantly in the forebrain, hippocampus and the outer layers of the cortex. It was expected that both CP-101,606 and Ro 25,6981 used in this study would label similar areas to those in the Menniti et al.,(1997) study since both ligands are NMDAR2B selective. Figure 3.1.2 clearly shows the similar distribution pattern in the mouse brain section, comparing the two ligands. The interesting observation is that there is a difference in the levels of binding when comparing the two ligands. The differences in the intensity of labelling seen between the two ligands may be due to there predicted sub-population binding selectivities. As previously discussed, the CP-101,606 ligand is suggested to bind to a sub-population of NR2B-containing receptors, those which contain only the NR2B subunit combined with NR1. If the Ro 25,6981 ligand binds to all receptors containing the NR2B subunit, then we would expect to see a difference in the level of binding in brain tissue, since different receptor populations are labelled by each ligand. Our results would

support this theory as Ro 25,6981 binding levels are significantly higher than the CP-101,606 binding in nearly all the brain regions analysed, see figure 3.1.5. The only exceptions to this were the hippocampal pyramidal cell layer and the inner frontal cortex, where there was no significant difference between the two levels. There is only a minimal level of binding seen in the cerebellum for both ligands. The lower binding levels of CP-101,606 would suggest that the ligand is indeed selectively labelling a smaller group of NMDA receptors, those which contain only the NR2B subunit. The Ro 25,6981 data (see figure 3.1.3) shows that the CA1 region of the hippocampus has a higher binding level than the CA2, CA3 and dentate gyrus regions of the hippocampus. However, the CP-101,606 data (see figure 3.1.4) shows a similar level of binding in the CA1, CA2, CA3 and dentate gyrus regions. Previous studies have shown the presence of NR2B receptors in the CA1 sub-field of the human, rat and macaque monkey hippocampus. Electron microscopic immunogold studies demonstrated that both NR2A and NR2B are often present in asymmetric synapses in CA1, commonly colocalized with NR1 (Janssen *et al.* 2005). The hippocampal formation includes the dentate gyrus and the sub fields CA1, CA2 and CA3, with the main output pathways of the hippocampus arising from the CA1 field and the subiculum. The hippocampus has been implicated in the normal operation of learning and memory in humans (Scoville & Milner, 1957) as well as in animal models (Jarrard, 1978; McNaughton *et al.*, 1989 and Morris *et al.*, 1982).

The forebrain NR2B subunit is known to be important in the process of memory formation, and transgenic over-expression of this subunit in the mouse brain results in mice which demonstrate superior memory in a number of behavioural tasks, including object recognition (Tang *et al.* 1999). White & Youngentob (2004) continued this work and found that transgenic mice with NR2B over-expression had a clear memory advantage in an NMDA-dependant odour memory paradigm. Further studies, using young and mature mice

would need to be carried out in order to determine if the NR2B subunit distribution and abundance was affected by age. Studies have already suggested that alteration in subunit expression exist with increasing age. Magnusson *et al.* (2002) carried out western blot experiments to determine the effects of aging on the protein expression of the NR1 and NR2B subunits of the NMDA receptor. C57Bl/6 mice showed decreased expression of the mRNA for the NR2B and NR1 subunits in subregions of the cerebral cortex and hippocampus with increased age. These results demonstrated that changes in the protein expression of the NR1 and NR2B subunits occur during the ageing process and, in some cases, were greater than changes seen previously in mRNA expression. These subunit alterations may explain some of the changes that are seen in NMDA receptor functions during ageing.

In summary, the NR2B distribution shown by these results is in support of the published literature and provides further evidence for two distinct classes of NMDA-R2B antagonists, represented by Ro 25,6981 and CP-101,606. Section 3.2.3.of chapter 3 continues the work from this section, and covers the autoradiography of the rat brain in a similar way to the mouse brain. Cloned mouse NR2B receptors have been previously used to study the binding affinities of Ro 25,6981 and CP-101,606. The binding levels and distribution patterns in the mouse have been covered in this section. Taking this study further, we shall use these two ligands to assess the rat brain. An autoradiographical study will demonstrate the distribution of ligand binding within both the P21 and adult rat brain. Unlike the mouse data, where only adult sections have been used, this study will address the issue of age and its affect on NR2B distribution and abundance in the rat brain. This will reveal not only which brain areas express NR2B-containing receptors for both ages analysed, but will also show any differences in binding levels in these areas between the young and adult rat brain.

Chapter 3: Section 3.2

Comparison of Ro 25,6981 and CP-101,606 in young and adult rat: Focus on development

Section 3.2.1

Pharmacological profile of [^{3}H]CP-101,606, an NR2B ligand, binding to rodent NR1/NR2B receptors

3.2.1.1 Introduction

The assembly of recombinant populations of NMDA receptors results in receptors with multiple pharmacological properties dependent on subunit combinations. Since the absolute polypeptide compositions of native NMDA receptors are unknown, a convenient model system in which to study the properties of defined cloned NMDA receptor subtypes and thus to compare them with their *in vivo* counterparts is their expression in mammalian cells. This permits the pharmacological, functional and biochemical characterization of either a single type of NMDA receptor subunit or co-expression of combinations of NR1 and NR2 subunit genes. Chazot *et al* (1999) demonstrated transient expression of functional NMDA receptors in mammalian cells. A study by Chazot *et al* (2002a) involved heterologous expression of NMDA receptors. The subtype-selectivity of racemic [^{3}H]CP-101,606, a novel high-affinity NMDA receptor radioligand was determined using defined recombinant NMDA receptor subunits expressed in Human embryonic kidney (HEK) 293 cells. [^{3}H]CP-101,606 bound to adult rodent forebrain and NR1/NR2B receptors expressed in HEK 293 cells with K_D=4.2 nM and 6.0 nM, respectively. Chazot *et al* (1994) showed that three

NMDA receptor subunit types (NR1, R2A and R2C) can co-assemble following their co-expression in mammalian cells with a pharmacological profile that is similar to that found for native adult mouse cerebellar NMDA receptors. The NMDA R1, R2A, and R2C subunits were expressed transiently in double or triple combinations in human embryonic kidney (HEK) 293 cells, and the biochemical and pharmacological properties of the cloned receptors were compared with those of adult mouse forebrain and cerebellum. Hawkins *et al* (1999) transfected HEK 293 cells with the NR1-1a and NR2A NMDA receptor subunits to deduce the subunit stoichiometry and quaternary structure of wild-type and mutant cloned NMDA receptors. The study employed a biochemical approach to determine the number of NMDA R2 (NR2) subunits/receptor together with the NMDA R1 (NR1)/NR2 subunit ratio of both cloned and native NMDA receptors. Grimwood *et al* (2000) studied recombinant human NR1a/NR2B receptors with native receptors in rodent brain membranes. Laurie & Seeburg (1994b) assessed recombinant NR1 homomeric and NR1-NR2 heteromeric NMDA receptors by homogenate binding assays. The binding affinities for the majority of NMDA ligands used in the study were similar to those reported for native NMDA receptors. Thus the ligand binding affinities of recombinant NMDA receptors were found to be dependent on their subunit composition. Studies using recombinant NMDA receptors have also been carried out by Sharma & Reynolds (1999).

In this study, recombinant NR1/NR2B NMDA receptors were generated by transfection into HEK 293 cells. HEK 293 cells expressing the NR1/NR2B receptor subtype were produced and used in radioligand binding studies to assess the pharmacological binding profile of $[^3H]$CP-101,606, an NR2B–selective ligand.

Competitive binding experiments measure equilibrium binding of a single concentration of radioligand at various concentrations of an unlabelled competitor. This determines the affinity of the receptor for the competitor. In addition to binding to the receptors of

physiological interest, radioligands bind to non-receptor sites. Therefore, both total and non-specific binding are measured, with specific (receptor) binding as the difference. The aim of this study was to transiently express the NMDA NR1/NR2B receptor in the HEK 293 clonal cell line, in order to investigate the pharmacological properties of an NR2B ligand, using the radiolabelled NR2B receptor antagonist [^{3}H]CP-101,606 (kindly supplied by Dr. Menniti (Pfizer, Groton, USA)).

3.2.1.2 Methods

3.2.1.2.1 Transformation of Competent *E. coli* Cells

This method was performed as essentially described by Dagert & Ehrlick (1979). For the transformation of competent *E. coli* cells, a frozen aliquot (100μl) of HB101 competent cells were removed from -80°C and thawed on ice for 5 minutes. The appropriate plasmid DNA (20ng/μl) was added to the competent cells (100μl) and mixed gently. The cell mixture was then incubated on ice for 30 minutes and heat-shocked by placing in a water bath at 42°C for 60 seconds. After 2 minutes incubation on ice, LB broth (section 2.3.22) (900μl) was added to the transformed cells. Following a one hour incubation in an orbital shaker at 250xg at 37°C, the cell suspension (100μl) was plated onto culture plates prepared with 1.5% (w/v) agar in LB broth containing ampicillin (50μg/ml). The culture plates were incubated at 37°C for 18-20 hours in an inverted position.

3.2.1.2.2 Glycerol Stocks of Transformed Competent *E. coli* Cells

Transformed competent E. *coli* cell stocks were prepared by mixing 500μl of LB broth supplemented with 50% (v/v) sterile glycerol and 50μg/ml ampicillin with 500μl of the small overnight culture (section 3.2.1.2.4). The cell culture mixture was immediately added to a cryogenic vial and stored at -80°C until use.

3.2.1.2.3 Amplification and Preparation of Plasmid DNA

3.2.1.2.4 Preparation of Small-Scale Culture of Plasmid DNA

LB broth (10ml) containing ampicillin (50μg/ml) was added to a sterile 50ml falcon tube and inoculated with one isolated colony from the culture plate (section 3.2.1.2.1) using a

sterile loop. The small culture was incubated for 18-20 hours in an orbital shaker at 250xg at 37°C.

3.2.1.2.5 Preparation of Large-Scale Culture of Plasmid DNA

LB broth (500ml) containing ampicillin (50µg/ml) was inoculated with 3ml of the small overnight culture (section 3.2.1.2.4) in a sterile 500ml flask. The large culture was incubated for 18-20 hours in an orbital shaker at 250xg at 37°C.

3.2.1.2.6 Harvesting the Large-Scale Culture and Purification of Plasmid DNA Using QIAGEN™ Plasmid Maxi-Kit

E. coli cells were harvested by transferring the large overnight culture (section 3.2.1.2.5) into two ice-cold centrifuge tubes, and centrifuging at 6500xg for 10 minutes at 4°C. The supernatant was discarded and the remaining pellet was resuspended in ice-cold P1 buffer (10ml). Bacteria containing the plasmid were then lysed by the addition of P2 buffer (10ml), mixed by gentle inversion, and incubated at room temperature for 5 minutes. The mixture was then neutralised with chilled P3 buffer (10ml), mixed by gentle inversion and incubated on ice for 20 minutes. The solution was then centrifuged at 14,000xg for 30 minutes at 4°C and the clear lysate was removed into a fresh tube.

A QIAGEN™ 500 tip was equilibrated with QBT buffer (10ml). The lysate was gently poured onto the column and allowed to pass through the column under gravity flow. The column was washed twice with QC buffer (30ml), then QF buffer (15ml) was added to the column to elute the plasmid DNA. Ice-cold isopropanol (0.7%vol) (10.5ml) was added to the eluted DNA and the solution was centrifuged at 14,000xg for 30 minutes at 4°C. The remaining pellet was carefully washed with ice-cold ethanol (1ml) and air-dried for

approximately 30 minutes. The purified DNA was dissolved in TE buffer (section 2.3.18) (500μl) and stored at 4°C until the purity and yield of the DNA was calculated.

3.2.1.2.7 Quantification and determination of Purity of the DNA yield

The purity and concentration of plasmid DNA was determined by measuring the OD at λ = 260nm and at λ = 280nm (Sambrook *et al.*, 1989). The ratio of the optical densities at λ = 260nm and λ = 280nm (OD_λ = 260nm / OD_λ = 280nm) should be within the range 1.8 – 2.0. For plasmid DNA concentration at λ = 260nm, and OD = 1 corresponds to ~50μg/ml for double stranded DNA (dsDNA). The DNA was then diluted to a final concentration of 1μg/ml in TE buffer and stored in 100μl aliquots at -20°C until use. Once thawed, DNA was stored at 4°C.

3.2.1.2.8 Preparation of Mammalian Cell Culture Media

3.2.1.2.9 Preparation of DMEM/F12 Media + L-Glutamate

All procedures were performed under sterile conditions. Liquid Dulbeccos Modified Eagle Medium/F12 (DMEM/F12) (500ml) containing L-glutamate (0.0365 g/L) and 15mM N-2-hydroxyethylpoiperazine-N'-2-ethane sulphonic acid (HEPES) was supplemented with 10% (v/v) foetal calf serum (FCS), 40ml of 7.5% (w/v) $NaHCO_3$ (final 3g/L) and penicillin (500 IU/ml)/ streptomycin (500μg/ml) solution (20ml). The final volume was made up to 1 litre with sterile water and adjusted to pH 7.6 using NaOH (2M). The media was then filter-sterilised using a 0.2μm Sartorius Sartolab-V150 filter unit and stored at 4°C until use.

3.2.1.2.10 Preparation of DMEM/F12 Media - L-Glutamate

All procedures were performed under sterile conditions. Liquid DMEM/F12 1:1 containing 15mM (HEPES) (500ml) was mixed with 50ml of 10% (v/v) FCS, 20ml of 7.5% (w/v)

$NaHCO_3$ (3g/L) and penicillin (500 IU/ml)/ streptomycin (500μg/ml) solution (10ml). The final volume was adjusted to pH 7.6 using NaOH (2M). The media was then filter-sterilised using a 0.2μm Sartorius Sartolab-V150 filter unit and stored at 4°C until use.

3.2.1.2.11 Subculturing of HEK 293 cells

HEK 293 cells were grown in 250ml Greiner culture flasks at 37°C in 5% CO_2 in DMEM/F12 media containing L-glutamate in a Shel lab incubator. Every two to three days the cells were subcultured by removal of the old media and then washed with ~5ml pre-warmed PBS (section 2.3.11). Following a one minute incubation in 2ml pre-warmed trypsin-EDTA at 37°C, 10ml DMEM/F12 media containing L-glutamate was added to the cells. The cells were then separated by gentle pipetting. Finally, 2ml of the cell suspension were added to a fresh flask and a further 10ml of DMEM/F12 media containing L-glutamate were added. This was then incubated at 37°C in 5% CO_2.

3.2.1.2.12 Preparation of New Stocks of HEK 293 Cells

HEK 293 cell stocks were prepared by removing the old media and washing the culturing cells with pre-warmed PBS, before adding 4ml trypsin-EDTA for 1 minute at 37°C, and then adding 20ml of pre-warmed DMEM/F12 media containing L-glutamate. The cells were pelleted by centrifugation at 200xg for 5 minutes at 4°C. The pellet was resuspended in 4.8ml DMEM/F12 media containing L-glutamate, supplemented with 0.6ml 10% (v/v) foetal calf serum (FCS) and 0.6ml dimethyl sulphoxide (DMSO). The cell suspension was immediately divided into three cryogenic vials and stored at -80°C for 34 hours and then transferred to liquid nitrogen. For the preparation of a new culture, a single cryogenic vial of frozen HEK 293 cells was thawed at 37°C. Cells were pelleted by centrifugation at 200xg for 5 minutes at 4°C and resuspended in 15ml DMEM/F12 media containing L-

glutamate. The cells were added to a tissue culture flask, which was incubated at 37°C in 5% CO_2 and cultured.

3.2.1.2.13 Calcium Phosphate Precipitation-Mediated Transfection of HEK 293 cells

HEK 293 cells were transfected by the calcium phosphate precipitation method (Gorman *et al.*, 1990). Cells were subcultured 24 hours prior to the transfection to a density of ~4x10^6 cells (30-40% confluent) per flask. On the day of the procedure the medium was removed 3 hours prior to the transfection and replaced with 10ml of DMEM/F12 medium lacking L-glutamine. The cells were incubated at 37°C in 7.5 % CO_2.

For the transfection of the cells, two tubes were prepared. These were Tube A containing 440µl 1:10 TE buffer (section 2.3.18), 10µl DNA (1µg/µl) (2.5µl NR1/7.5µl NR2B) and Tube B containing, 500µl of 2x HBS buffer (section 2.3.19). Calcium chloride (2.5M) (50µl) was heated to 37°C and was slowly added to Tube A and mixed well. The contents of Tube A were added to Tube B at a rate of 1 drop per 5 seconds and the mixture was pipetted up and down until the solution appeared cloudy. The contents of Tube B were added slowly to the medium over HEK 293 cells and the medium was swirled to distribute the precipitate evenly. Following a 3 hour incubation at 37°C at 7.5% CO_2, the medium from the cells was aspirated. 15% (v/v) glycerol in PBS (section 2.3.11) was gently spread over the cells and incubated for 30 seconds at room temperature. The Glycerol solution was removed and the cells were rinsed with DMEM/F12 medium lacking L-glutamine (~5ml). Fresh L-glutamine-free DMEM/F12 medium (10ml) + Ketamine (10mM) was added, 1ml/flask. Finally the cells were incubated at 37°C for 48 hours with a CO_2 level of 5% and were harvested as described in section 3.2.1.2.14.

3.2.1.2.14 Harvesting and Membrane Preparation of HEK 293 cells

Transfected HEK 293 cells were harvested 48 hours post transfection. The media was drained from the small petri-dishes and replaced with 1.5ml cold homogenisation buffer (section 2.3.21). Cells were scraped into the culture media using Greiner cell scrapers and placed into an ice-cold dounce glass/glass homogeniser and homogenised (~30 strokes). The cell suspension was transferred to eppendorfs and centrifuged for 5 minutes at 15,000rpm at 4°C. The supernatant was discarded and the cell pellet was then resuspended in 1ml ice-cold homogenisation buffer (~50-100μg protein). The suspension was then re-homogenised before being aliquoted into 10 x 100μl volumes and stored at -20°C. The membrane preparation was either assayed for radioligand binding activity (section 3.2.1.2.15) or used for immunoblotting (Chapter 2, section 2.4.3 to 2.4.7). Determination of the protein concentration was as described in Chapter 2, section 2.4.2.

3.2.1.2.15 [³H]CP-101,606 Radioligand Binding Assays

[³H]CP-101,606 radioligand competition binding assays were performed using a rapid filtration assay (Hawkins *et al.*, 1999). [³H]CP-101,606, specific activity = 29.6Ci/mmol, was stored at -20°C, and was kindly supplied by Dr. Menniti, Pfizer, Groton, USA. Well-washed HEK 293 cell homogenates as prepared in section 3.2.1.2.14 (100μg protein) (100μl) were incubated, in triplicate for 2 hours on ice, with 20μl [³H]CP-101,606 [1nM] in 60μl Tris buffer (2.3.13) and with either 20μl of buffer or unlabelled Ro 25,6981 [10μM], to a final volume of 200μl. Specific binding was defined using 20μl of ifenprodil dissolved in DMSO (100μM). Stocks of unlabelled Ro 25,6981 were dissolved in DMSO with serial dilutions made in 50mM Tris buffer (2.3.13). The binding assay was carried out using polypropylene tubes. The assay was terminated by rapid filtration through Whatman GF/B filters pre-soaked in ice-cold 10mM sodium phosphate buffer pH 7.4 for at least 15

minutes. Filters were washed (3x3ml) using ice-cold 10mM sodium phosphate buffer (pH 7.4), using a Brandell cell harvester. The filters were placed in minivials and Ecoscint Scintillation fluid (1ml/vial) was added. These were incubated for 24 hours at room temperature and bound radioactivity was quantified using a Beckmann LS 500 CE scintillation spectrophotometer with a counting time of 4 minutes per vial.

3.2.1.2.16 Data Analysis for Competition Curve Binding Assays

Results from the displacement studies were analysed by non-linear least square regression using GraphPad Prism for a two-site binding model. The displacement results were analysed by a sigmoidal dose response curve with a variable slope. The F-test was used to assess whether the one-site or the two-site competition model best fit the data ($P<0.05$ was deemed significant). The IC_{50} values for competition curves fitted to a two-site competition model were calculated from,

$$Y = \frac{A + (B-A)}{(\text{fraction } 1/1 + 10^{X-\log IC_{50}^{1}}) + (1\text{-fraction } 1/1 + 10^{X-\log IC_{50}^{2}})}$$

A and B = the minimum and maximum percentage specific binding respectively

Y = specific binding at a fixed concentration of displacing drug

X = $\log_{10}$ concentration of the displacer

IC_{50} = concentration of the displacer which inhibits 50% of the specific binding of the radioligand.

(1) and (2) = the high and low affinity sites for the one-site and two-site binding models.

3.2.1.3 Results

3.2.1.3.1 Immunoblotting analysis of HEK 293 cells transiently expressing the NR1/NR2B NMDA receptor.

In these experiments, the NR1/NR2B subtype of NMDA receptor was transfected into HEK 293 cells using the calcium phosphate precipitation method. Expression of the NR2B subtype receptor was assayed by immunoblotting (Chapter 2, section 2.3.4-2.3.7) with three different in-house generated anti-NMDA receptor antibodies, anti-NR1, anti-NR2A and anti-NR2B. Figure 3.2.1.1 shows the scanned image of the resulting film. All three anti-NMDA receptor antibodies detected a band in the adult rat brain preparation, demonstrating the presence of all three subunits NR1 (105kDa), NR2A (~180kDa) and NR2B (180kDa) in native brain tissue. However, bands were only visible demonstrating the presence of NR1 and NR2B subunits in the transfected cell homogenates. No NR2A was detected by the anti-NR2A antibody in the transfected material. This confirms that the transfection was successful and only receptors expressing NR1 and NR2B subunits are present. This analysis does not confirm however the composition of these subunits within the receptors being expressed.

Figure 3.2.1.1 Immunoblots demonstrating the expression of the NR1/NR2B NMDA receptor in HEK 293 cells.

Membranes were prepared from HEK 293 cells transfected with NR1/NR2B receptors. Expression of the NMDA receptor subtype was analysed by immunoblotting using 7.5% SDS-PAGE under reducing conditions with 50μg of protein applied per gel lane (see Chapter 2, section 2.4.3 to 2.4.7).

In-house Generated Antibodies:

Anti-NR1: Bleed 1, Stock [492μg/ml], used at [1μg/ml]

Anti-NR2A: Bleed 1, Stock [905μg/ml, used at [1μg/ml]

Anti-NR2B: Bleed 1, Stock [163μg/ml], used at [1μg/ml]

Lane 1   Adult rat brain prep probed with anti-NR1

Lane 2   Transfected HEK 293 cell homogenates probed with anti-NR1

Lane 3   Adult rat brain prep probed with anti-NR2A

Lane 4   Transfected HEK 293 cell homogenates probed with anti-NR2A

Lane 5   Adult rat brain prep probed with anti-NR2B

Lane 6   Transfected HEK 293 cell homogenates probed with anti-NR2B

NR1/NR2B Transfected HEK cells
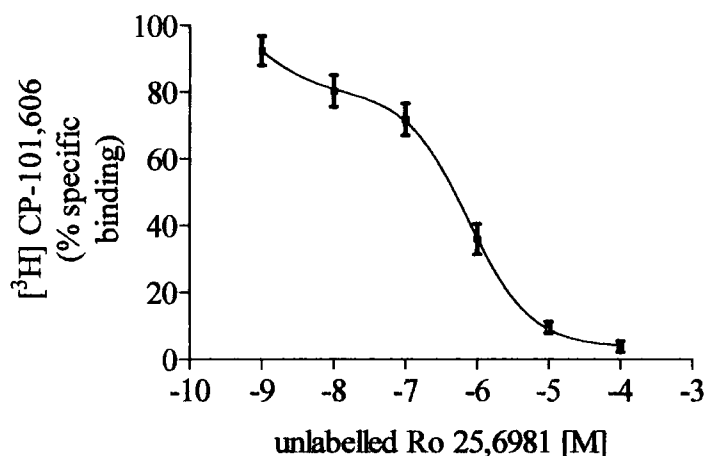
Figure 3.2.1.2 Competition curve for the inhibition of [³H]CP-101,606 radioligand binding by Ro 25,6981 to NR1/NR2B receptors expressed in HEK 293 cells. Representative curve, mean ± SD for n = 5 replicates.

	Apparent pIC₅₀		n_H
Overall	Site 1	Site 2	
6.26 ± 0.13	9.16 ± 0.45 (28%)	6.13 ± 0.15 (72%)	-0.73 ± 0.16

3.2.1.3.2 [³H]CP-101,606 competition binding to NR1/NR2B receptors expressed in HEK 293 cells by Ro 25,6981.

The effect of Ro 25,6981 on [³H]CP-101,606 binding to NR1/NR2B receptors was investigated. Figure 3.2.1.2 shows the results analysed by GraphPad Prism. Unlabelled Ro 25,6981 produced a concentration-dependent inhibition of specific [³H]CP-101,606 binding with a pseudo-Hill coefficient (n_H), which was significantly less than unity (n_H = -0.73 ± 0.16). These data fit best to a two-component competition model, comprising high and low-affinity binding sites in the ratio 28:72, indicating that Ro 25,6981 can discriminate between two binding sites in the HEK 293 cells.

3.2.1.4 Discussion

The purpose of this study was two-fold. Firstly, the successful transfection of NR1/NR2B NMDA receptors in HEK 293 cells is described, and secondly, the inhibition of [^{3}H]CP-101,606 binding by Ro 25,6981 to NR1/NR2B receptors expressed in the HEK 293 clonal cell model system. Transfection of HEK 293 cells is a well established technique and has been used previously as a heterologous expression system for different NMDA subunits within cells (Chazot *et al* 1999). Figure 3.2.1.1 shows the immunoblot analysis of the HEK 293 cells expressing the NR1/NR2B receptor. In-house generated antibodies have been used to demonstrate the presence of the NR1 (lanes 2 & 3) and NR2B (lanes 8 & 9) subunits, but the absence of NR2A (lanes 5 & 6) subunit in the transfected cells. These results demonstrate that the HEK 293 cells have been transfected successfully and are therefore viable for use in the radioligand binding study.

The radioligand binding study revealed that displacement of [^{3}H]CP-101,606 binding by Ro 25,6981 fit best to a two-site competition model indicating Ro 25,6981 can discriminate between two binding sites, one with high-affinity (pIC$_{50}$ = 9.16 ± 0.45) and one with low-affinity (pIC$_{50}$ = 6.13) in the ratio 28:72%, respectively. The high affinity binding site (Site 1) is the NR1/2B binding site, with Site 2 indicating the low affinity binding site in the cells. Ligand binding data show that other NR2B ligands behave in a similar way (unpublished data, Bradford *et al*, 2006). The levels of expression were relatively low in these experiments, hence the preponderance of a low affinity site.

Menniti *et al.* (1997) reported that racemic [^{3}H]CP-101,606 binds to a saturable site on rat forebrain membranes with a binding affinity (K_D) of 10±1 nM and a B_{max} of 1.7±0.2 pmol/mg protein. Ifenprodil, eliprodil and the polyamines spermine and spermidine all displace racemic [^{3}H]CP-101,606 from its binding site to rat forebrain membranes. Equilibrium binding was best fit by a model which assumes interaction at a single

population of sites; however, interaction with multiple sites of similar affinity cannot be excluded. No other of the tested compounds, including ligands for other glutamate, aminergic, cholinergic, opiate, or GABAergic receptors or Ca^{2+} channels, displaced racemic [^{3}H]CP-101,606 binding at pharmacologically relevant concentrations (Menniti *et al.* 1997). This study has provided evidence that another class of NR2B-selective NMDA receptor ligand, represented by Ro 25,6981 can displace [^{3}H]CP-101,606 binding to NR1/NR2B NMDA receptors expressed in HEK 293 cells. This demonstrates that CP-101,606 and Ro 25, 6981 label an overlapping binding site on the NMDA receptor.

This section of Chapter 3 has looked at the binding of NR2B antagonists to transfected receptors expressed in a clonal cell line. The next section 3.2.2 in chapter 3 describes the pharmacological characterization of a number of NR2B-selective ligands binding to native P21 and adult rat forebrain membranes. The antibodies described in this section have been used for the immunohistochemistry in section 3.2.4.

Section 3.2.2

Pharmacological profile of a range of NR2B ligands binding to P21 and adult rat brain

3.2.2.1 Introduction

The NMDAR is typically a heteromeric complex composed of two NR1 subunits, expressed throughout the adult brain, and at least two NR2 subunits, differentially expressed across the brain regions (Monyer *et al.* 1992; Kutsuwada *et al.* 1992 and Watanabe *et al.* 1992). NMDA receptors are central to remodelling of synaptic connections during postnatal development and associative learning abilities in adults. The ability to remodel neural networks is altered during postnatal development, possibly due to a change in the composition of NMDARs (Dumas, 2005). In the forebrain and cerebellum, synaptic NMDARs undergo developmental alterations that are guided, in part, by experience (Myers *et al.* 1999). Dumas (2005) describes the NMDA receptor as a molecular switch in developmental regulation of cognitive ability. As the neuronal network develops in the forebrain, synaptic NR2B-NMDARs are replaced by NR2A-NMDARs and the NR2B-NMDARs move to extra-synaptic sites. LTP and LTD are enhanced in this initial period of the switch, with synapses containing both NR2A and NR2B receptor types. NMDAR2B subunit expression then decreases and the NR2A subunit becomes dominant in the synapse, together with a reduced channel function, synaptic plasticity, and ability to switch receptor composition. In this way, a balance of plasticity and stability is achieved which is optimal for information processing and storage. The age range in this study is covered using postnatal day 21 and adult rats (3 months) to represent young and mature rodents, respectively. This early age group covers a period of development where changes in

NMDA receptor composition are likely to be associated with changes in brain development and synaptic plasticity. Any age-related NMDAR changes will not be an indication of cognitive decline involved in the normal ageing process or pathological age-related memory loss since the rats are not sufficiently mature for these changes to occur.

In this study, saturation binding of [^{3}H]Ro 25,6981 was analysed and competition binding using [^{3}H]MK-801 and [^{3}H]Ro 25,6981 were carried out with a range of NR2B-selective NMDAR antagonists to study their pharmacological profiles in P21 and adult rat brain. Saturation binding experiments involve measuring equilibrium binding of various concentrations of the radioligand to analyze the relationship between binding and ligand concentration. This determines the number of sites, Bmax, and the ligand affinity, K_D. Competitive binding experiments measure equilibrium binding of a single concentration of radioligand at various concentrations of an unlabelled competitor. This determines the affinity of the competitor for the receptor. The aim of this study was to investigate the pharmacological properties of NR2B ligands binding to native NR2B receptors in P21 and adult rat forebrain membranes, using the radiolabelled NR2B receptor antagonists [^{3}H]MK-801 and [^{3}H]Ro 25,6981 (Kindly supplied by Dr. Kemp & colleagues (Hoffmann La Roche, Switzerland)).

3.2.2.2 Methods

3.2.2.2.1 [^{3}H]MK-801 Competition Assays

[^{3}H]MK-801 competition assays were performed in the presence of 10μM L-glutamate, using a rapid filtration assay (Chazot & Stephenson, 1997a). Adult or P21 male rat forebrain membranes (section 2.4.1) (100μg protein) (100μl) were incubated with 10μM L-glutamate in 25mM sodium phosphate buffer pH 7.4, 20μl of [^{3}H]MK-801 (40nM), with either 20μl of buffer or displacing drug in the concentration range 1.0×10^{-9} to 1.0×10^{-2} M, in a final volume of 200μl for 2 hours at room temperature. All concentration points were performed in triplicate. Specific binding was defined using 100μM ketamine dissolved in 25mM sodium phosphate buffer. Bound ligand was collected by rapid filtration using a Brandel cell harvester onto glass fibre filters (GF/B) which had been pre-soaked in ice-cold 10mM sodium phosphate buffer pH 7.4 for at least 15 minutes. The filters were washed rapidly three times with ice-cold 10mM sodium phosphate buffer pH 7.4 (3 x 3ml). The filters were placed in minivials and Ecoscint Scintillation fluid (1ml/vial) was added. These were incubated for 24 hours at room temperature and radioactivity was quantified using a Beckmann LS 500 CE scintillation spectrophotometer with a counting time of 4 minutes per vial. Stocks of histamine and spermidine were dissolved in 25mM sodium phosphate pH 7.4 buffer and all subsequent dilutions were made in 25mM sodium phosphate pH 7.4 buffer. All competition binding assays were carried out using polypropylene tubes.

3.2.2.2.2 [^{3}H]Ro 25,6981 Saturation Binding Assays

For [^{3}H]Ro 25,6981 saturation experiments, adult or P21 male rat forebrain membranes (section 2.4.1) (100μg protein) (100μl) were incubated in 50mM Tris-HCL containing 5mM EDTA and 5mM EGTA, pH 7.4 (section 2.3.13) in the presence of a range of

concentrations of [^{3}H]Ro 25,6981 from 0.5nM to 40nM (20µl) to a final volume of 200µl. All concentration points were performed in triplicate. The incubation was performed in polypropylene tubes for 90 minutes at 4°C. Specific binding was defined using 100µM ifenprodil. The assay was terminated by rapid filtration as described in section 3.2.2.2.1.

3.2.2.2.3 [^{3}H]Ro 25,6981 Competition Assays

[^{3}H]Ro 25,6981 competition assays were performed by a rapid filtration assay (Hawkins *et al.* 1999). Adult or P21 male rat forebrain membranes (section 2.4.1) (100µg protein) (100µl) in 50mM Tris-HCL buffer pH 7.4 containing 5mM EGTA and 5mM EDTA were incubated with 1nM [^{3}H]Ro 25,6981 (20µl), with either 20µl of buffer or displacing drug in the concentration range 1.0×10^{-9} to 1.0×10^{-2} M, to a final volume of 200µl for 90 minutes at 4°C. All concentration points were performed in triplicate. Specific binding was defined using 100µM Ifenprodil dissolved in DMSO. Bound ligand was collected by rapid filtration using a Brandel cell harvester onto glass fibre filters (GF/B) which had been pre-soaked in ice-cold 10mM sodium phosphate buffer pH 7.4 for at least 15 minutes. The filters were washed rapidly three times with ice-cold 10mM sodium phosphate buffer pH 7.4 (3 x 3ml). The filters were placed in minivials and Ecoscint Scintillation fluid (1ml/vial) was added. These were incubated for 24 hours at room temperature and radioactivity was quantified using a Beckmann LS 500 CE scintillation spectrophotometer with a counting time of 4 minutes per vial. Stocks of Ro 25,6981, CP-101,606, and ifenprodil were dissolved in DMSO, histamine and spermidine were dissolved in 50mM Tris-HCL pH 7.4 buffer (2.3.13), and haloperidol was dissolved in absolute ethanol. All subsequent dilutions were made in 50mM Tris-HCL pH 7.4 buffer (2.3.13). All competition binding assays were carried out using polypropylene tubes.

3.2.2.2.4 Saturation Data Analysis for Radioligand Binding

Results from saturation studies were analysed by non-linear least square regression using GraphPad Prism. The saturation data were analysed by either the one-site or two-site binding hyperbola. The F-test was used to assess whether the one-site or the two-site model fit the data best ($P<0.05$ was deemed significant). The KD values for saturation curves fitted to a one-site hyperbola were calculated from the following equation,

$$Y = \frac{B_{max} \, X}{K_D + X}$$

Where: Y = specific bound [^{3}H] radioligand, X = concentration of [^{3}H] radioligand, Bmax = maximum number of binding sites.

Saturation data was fitted to the line by linear regression using GraphPad Prism for the Rosenthal transformations,

$$F(x) = ax + b$$

Where: $F(x)$ = specific bound [^{3}H] radioligand/ free [^{3}H] radioligand, a = slope – (1/K_D), x = specific bound [^{3}H] radioligand, b = x-axis intercept (B_{max}/K_D).

3.2.2.2.5 Competition Curve Data Analysis for Radioligand Binding

Results from the displacement studies were analysed by non-linear least square regression using GraphPad Prism for both a one-site and a two-site binding model. The displacement results were analysed by a sigmoidal dose response curve with a variable slope. The F-test was used to assess whether the one-site or the two-site competition model best fit the data ($P<0.05$ was deemed significant). The IC_{50} values for competition curves fitted to a one-site competition model were calculated from the following equation, Where:

$$Y = \frac{A + (B-A)}{1 + 10^{(X-\log IC50)}}$$

A and B = the minimum and maximum percentage specific binding respectively. Y = specific binding at a fixed concentration of displacing drug. X = $\log_{10}$ concentration of the displacer. IC_{50} = concentration of the displacer which inhibits 50% of the specific binding of the radioligand.

The IC_{50} values for competition curves fitted to a two-site competition model were calculated from,

$$Y = \frac{A + (B-A)}{(\text{fraction } 1/1 + 10^{X-\log IC501}) + (1\text{-fraction } 1/1 + 10^{X-\log IC502})}$$

Where: A, B, X and Y are as above, (1) and (2) = the high and low affinity sites for the one-site and two-site binding models.

3.2.2.3 Results

3.2.2.3.1 [^{3}H]MK-801 Competition binding to P21 and adult rat forebrain membranes by Spermidine

P21 and adult male rat forebrain membranes were prepared as described in Chapter 2, section 2.4.1. Competition binding assays were performed by incubating the membrane preparations (100μg) with [^{3}H]MK-801 and a concentration range of the displacing drug spermidine (see section 3.2.2.2.1). Specific binding was defined using 100μM ketamine. Results were analysed using non-linear least square regression analysis. Competition results were fit to a sigmoidal model with a variable slope, the F-test was used to asses whether the one-site or two-site competition model best fit the data (P<0.05 was deemed significant). Analysis of the P21 data gave an apparent pIC_{50} 3.29 ± 0.56. Analysis of the adult data gave an apparent pIC_{50} 2.42 ± 0.66.

3.2.2.3.2 [^{3}H]MK-801 Competition binding to P21 and adult rat forebrain membranes by Histamine

The effect of Histamine on [^{3}H]MK-801 binding to P21 and adult rat forebrain membranes was investigated. Figure 3.2.2.2 shows the results analysed by GraphPad Prism. In the P21 data histamine produced a concentration-dependent stimulation of specific [^{3}H]MK-801 binding with an apparent overall pIC_{50} = 3.7 ± 0.5. The adult data showed that histamine had no effect on the binding of [^{3}H]MK-801with pIC_{50} < 2.

3.2.2.3.3 [^{3}H]Ro 25,6981 Saturation binding to P21 and adult rat forebrain membranes

P21 and adult male rat forebrain membranes were prepared (Chapter 2, section 2.4.1) and assayed for [^{3}H]Ro 25,6981 binding activity at 0.5 to 40nM, the specific binding was defined using 100μM ifenprodil. Figure 3.2.2.3 shows the resulting saturation curves

produced in GraphPad Prism (version 4). Specific binding of $[^3H]Ro$ 25,6981 to P21 rat forebrain membranes was saturable and best fit to a one-site binding hyperbola compared to a two-site model. Analysis of the saturation binding curve using non-linear least square regression revealed that $[^3H]Ro$ 25,6981 bound to a single class of sites with a K_D of 9.5 $\pm$ 3.6 nM and a B_{max} of 2593 $\pm$ 453 fmol/mg protein. Specific binding of $[^3H]Ro$ 25,6981 to adult rat forebrain membranes was also saturable and best fit to a one-site binding hyperbola compared to a two-site model. Analysis of the saturation binding curve using non-linear least square regression revealed that $[^3H]Ro$ 25,6981 bound to a single class of sites with a K_D of 11.9 $\pm$ 4.2 nM and a B_{max} of 683 $\pm$ 111 fmol/mg protein.

3.2.2.3.4 $[^3H]Ro$ 25,6981 Competition binding to adult rat forebrain membranes by Spermidine

The effect of spermidine on $[^3H]Ro$ 25,6981 binding to adult rat forebrain membranes was investigated. Figure 3.2.2.4 shows the results. Spermidine produced a concentration-dependent inhibition of specific $[^3H]Ro$ 25,6981 binding with a pseudo-Hill coefficient (n_H) -1.45 $\pm$ 0.44. The data were best fit to one-site competition model with an apparent overall pIC_{50} = 2.34 $\pm$ 0.15 (100%). Spermidine (10mM) was used in $[^3H]Ro$ 25,6981 and $[^3H]CP$-101,606 ligand autoradiographical studies to define specific binding (see sections 3.1 and 3.2.3).

3.2.2.3.5 $[^3H]Ro$ 25,6981 Competition binding to P21 and adult rat forebrain membranes by Histamine

Competition binding assays were performed by incubating P21 and adult rat forebrain membranes (100μg) with $[^3H]Ro$ 25,6981 and a range of concentrations of the histamine. Specific binding was defined using 100μM Ifenprodil. Results were analysed using non-linear least square regression analysis and were fitted to a sigmoidal model with variable

slope. In both P21 and adult experiments, histamine had no effect on [^{3}H]Ro 25,6981 binding. There was an apparent overall pIC$_{50}$ < 2 for both P21 and adult membrane preparations.

3.2.2.3.6 [^{3}H]Ro 25,6981 Competition binding to P21 and adult rat forebrain membranes by Ifenprodil

The effect of Ifenprodil on [^{3}H]Ro 25,6981 binding to P21 and adult rat forebrain membranes was investigated. Figure 3.2.2.6 shows the results. For the P21 data, Ifenprodil produced a concentration-dependent inhibition of specific [^{3}H]Ro 25,6981 binding with a pseudo-Hill coefficient (n$_H$) -0.87 ± 0.20. The data were best fit to one-site competition model with an apparent overall pIC$_{50}$ = 5.06 ± 0.12 (100%). For the adult data, Ifenprodil produced a concentration-dependant inhibition of specific [^{3}H]Ro 25,6981 binding with a pseudo-Hill coefficient (n$_H$) -0.65 ± 0.23, which was significantly less than unity. The data were best fit to two-site competition model, comprising high- and low-affinity binding sites in the ratio 37:63 (high:low %, SD±5). Site 1 apparent pIC$_{50}$ = 6.59, site 2 apparent pIC$_{50}$ = 5.00.

3.2.2.3.7 [^{3}H]Ro 25,6981 Competition binding to P21 and adult rat forebrain membranes by Haloperidol

The effect of Haloperidol on [^{3}H]Ro 25,6981 binding to P21 and adult rat forebrain membranes was investigated. Figure 3.2.2.7 shows the results. For the P21 data, haloperidol produced a concentration-dependent inhibition of specific [^{3}H]Ro 25,6981 binding with a pseudo-Hill coefficient (n$_H$) -0.33 ± 0.12, which was significantly less than unity. The data were best fit to two-site competition model, comprising high- and low-affinity binding sites in the ratio 56:44 (high:low %, SD±13). Site 1 apparent pIC$_{50}$ = 6.22, site 2 apparent pIC$_{50}$ = 3.92. For the adult data, haloperidol produced a concentration-

dependent inhibition of specific [^{3}H]Ro 25,6981 binding with a pseudo-Hill coefficient (n_H) -0.77 ± 0.24. The data were best fit to one-site competition model with an apparent overall pIC_{50} = 4.00 ± 0.53 (100%).

3.2.2.3.8 [^{3}H]Ro 25,6981 Competition binding to P21 and adult rat forebrain membranes by Ro 25,6981

The effect of Ro 25,6981 on [^{3}H]Ro 25,6981 binding to P21 and adult rat forebrain membranes was investigated. Figure 3.2.2.8 shows the results. For the P21 data, Ro 25,6981 produced a concentration-dependent inhibition of specific [^{3}H]Ro 25,6981 binding with a pseudo-Hill coefficient (n_H) -0.76 ± 0.16, which was significantly less than unity. The data were best fit to two-site competition model, comprising high- and low-affinity binding sites in the ratio 79:21 (high:low %, SD±17). Site 1 apparent pIC_{50} = 6.95, site 2 apparent pIC_{50} = 5.37. For the adult data, Ro 25,6981 produced a concentration-dependant inhibition of specific [^{3}H]Ro 25,6981 binding with a pseudo-Hill coefficient (n_H) -0.99 ± 0.62. The data were best fit to one-site competition model with an apparent overall pIC_{50} = 6.29 ± 0.29 (75%).

3.2.2.3.9 [^{3}H]Ro 25,6981 Competition binding to P21 and adult rat forebrain membranes by CP-101,606

The effect of CP-101,606 on [^{3}H]Ro 25,6981 binding to P21 and adult rat forebrain membranes was investigated. Figure 3.2.2.9 shows the results. For the P21 data, CP-101,606 produced a concentration-dependent inhibition of specific [^{3}H]Ro 25,6981 binding with a pseudo-Hill coefficient (n_H) -0.99 ± 0.56. The data were best fit to one-site competition model with an apparent overall pIC_{50} = 6.80 ± 0.26 (80%). For the adult data,

CP-101,606 produced a concentration-dependent inhibition of specific [^{3}H]Ro 25,6981 binding with a pseudo-Hill coefficient (n_H) -0.77 ± 0.20, which was significantly less than unity. The data were best fit to two-site competition model, comprising high- and low-affinity binding sites in the ratio 73:27 (high:low %, SD±34). Site 1 apparent pIC_{50} = 6.64, site 2 apparent pIC_{50} = 5.34.
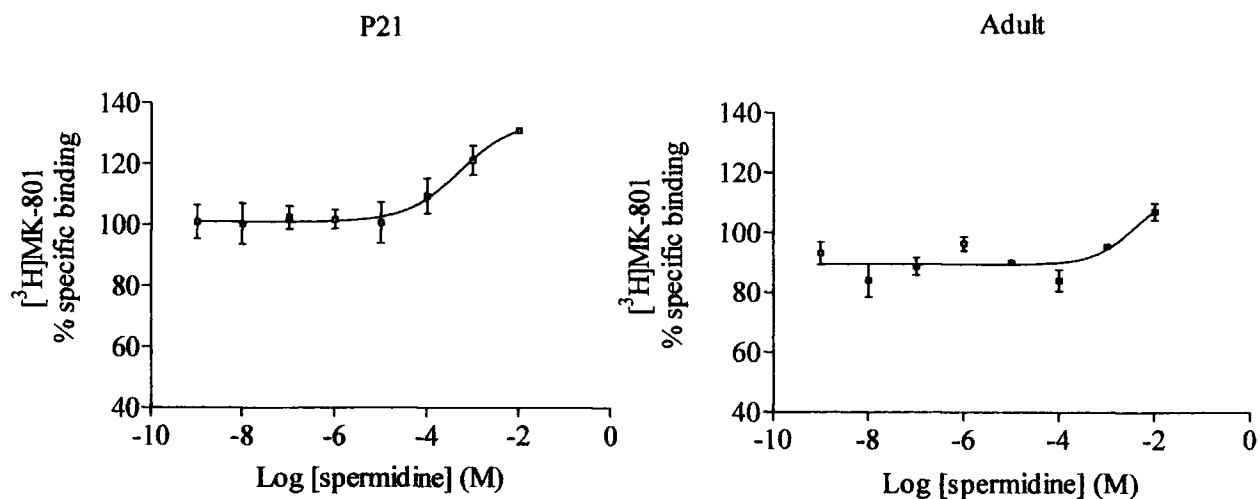
Figure 3.2.2.1 (A,B) Competition curves for the stimulation of [^{3}H]MK-801 radioligand binding by Spermidine, to (A) P21 and (B) Adult rat forebrain membranes. Mean values ± SD for at least n = 3 separate experiments.

	Apparent pIC$_{50}$ Overall
P21	3.29 ± 0.56
Adult	2.42 ± 0.66

Table 3.2.2.1 Summary of the apparent pIC$_{50}$ for [^{3}H]MK-801 binding using Spermidine in P21 and Adult membrane preparations.
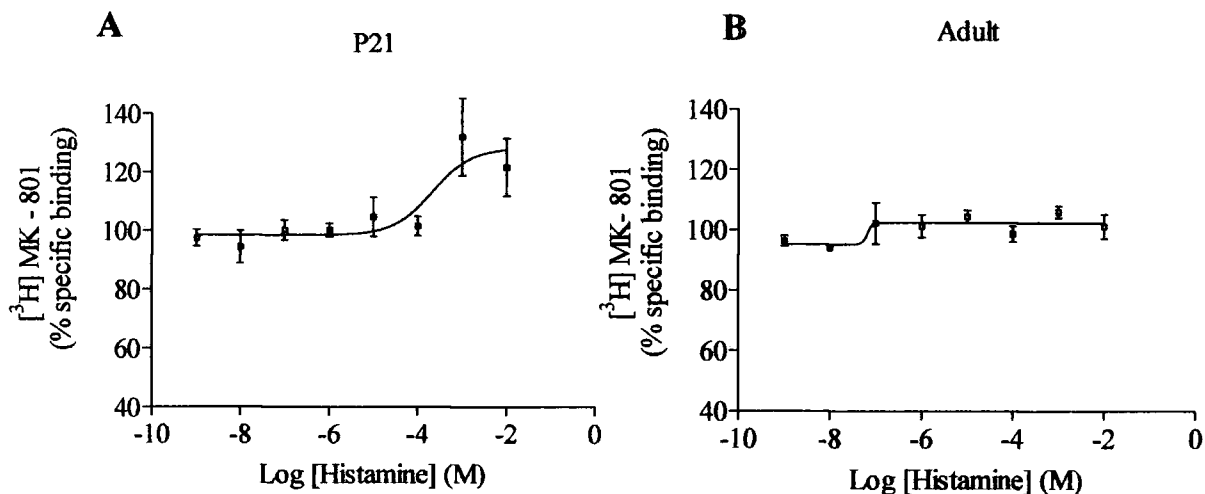
Figure 3.2.2.2 (A,B) Competition curves for the stimulation of [^{3}H]MK-801 radioligand binding by Histamine, to (A) P21 and (B) Adult rat forebrain membranes. Mean values ± SD for at least n = 3 separate experiments.

	Apparent pIC$_{50}$ Overall
P21	3.7 ± 0.5
Adult	< 2

Table 3.2.2.2 Summary of the apparent pIC$_{50}$ for [^{3}H]MK-801 binding using Histamine in P21 and Adult membrane preparations.
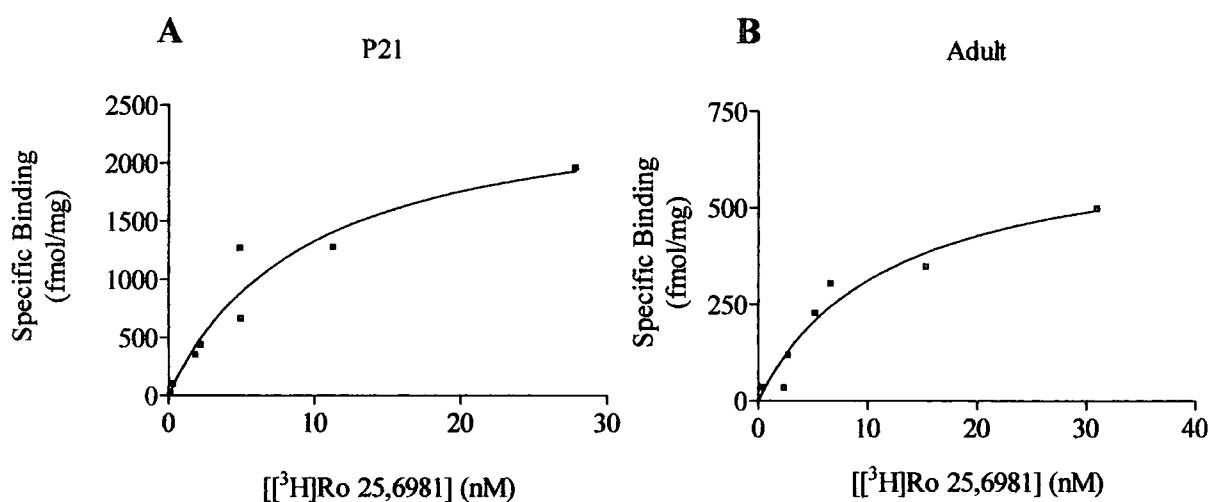
Figure 3.2.2.3 (A,B) [^{3}H]Ro 25,6981 Saturation Binding Curves. [^{3}H]Ro 25,6981specific binding using (A) P21 and (B) Adult rat forebrain membranes. Representative curves, mean ± SD for n = 3 replicates.

	P21	Adult
B_{max} (fmol/mg)	2593 ± 453	683 ± 111
K_D (nM)	9.5 ± 3.6	11.9 ± 4.2

Table 3.2.2.3 B_{max} and K_D data for [^{3}H]Ro 25,6981 Saturation Curves
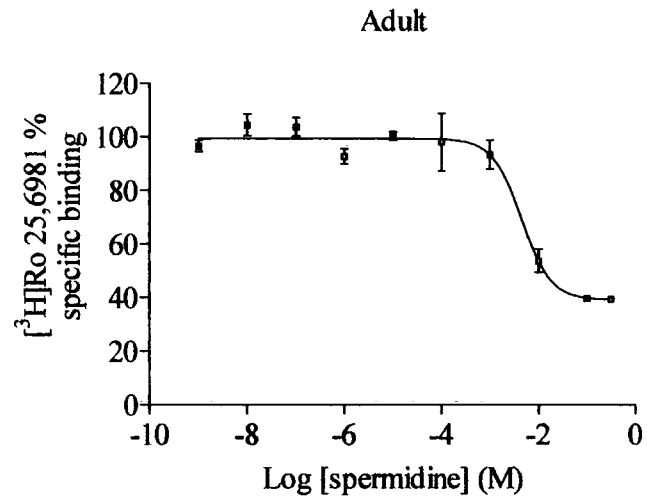
Adult

Figure 3.2.2.4 Competition curves for the inhibition of [^{3}H]Ro 25,6981 radioligand binding by Spermidine, to Adult rat forebrain membranes. Mean values ± SD for at least n = 3 separate experiments.

	Apparent pIC$_{50}$ Overall	n$_H$
Adult	2.34 ± 0.15	-1.45 ± 0.44

111
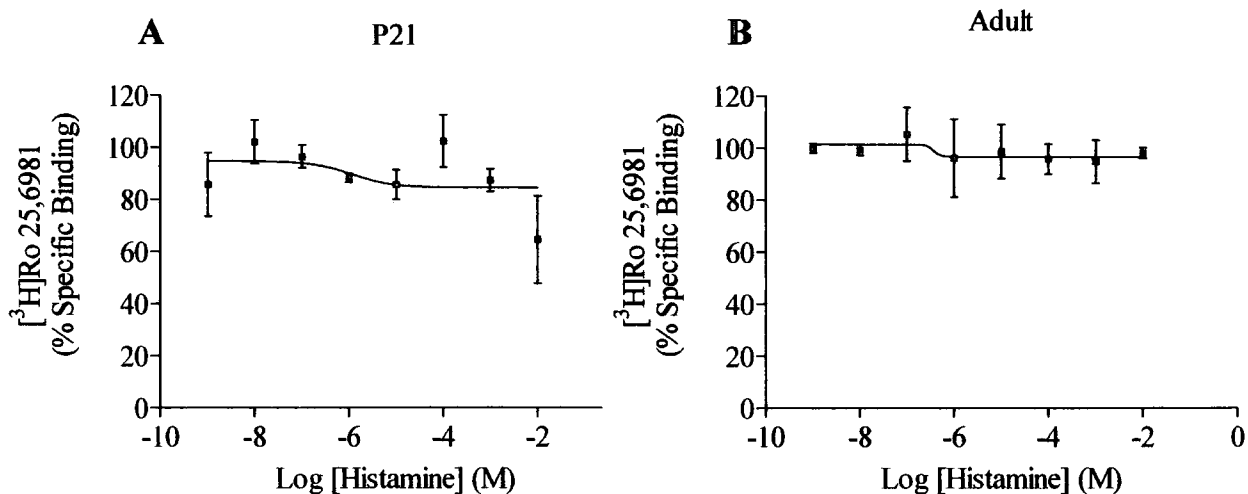
Figure 3.2.2.5 (A,B) Competition curves for the inhibition of [³H]Ro 25,6981 radioligand binding by Histamine, to (A) P21 and (B) Adult rat forebrain membranes. Mean values ± SD for at least n = 3 separate experiments.

	Apparent pIC_{50} Overall
P21	< 2
Adult	< 2

Table 3.2.2.5 Summary of the apparent pIC_{50} for [³H]Ro 25,6981 binding using Histamine in P21 and adult membrane preparations
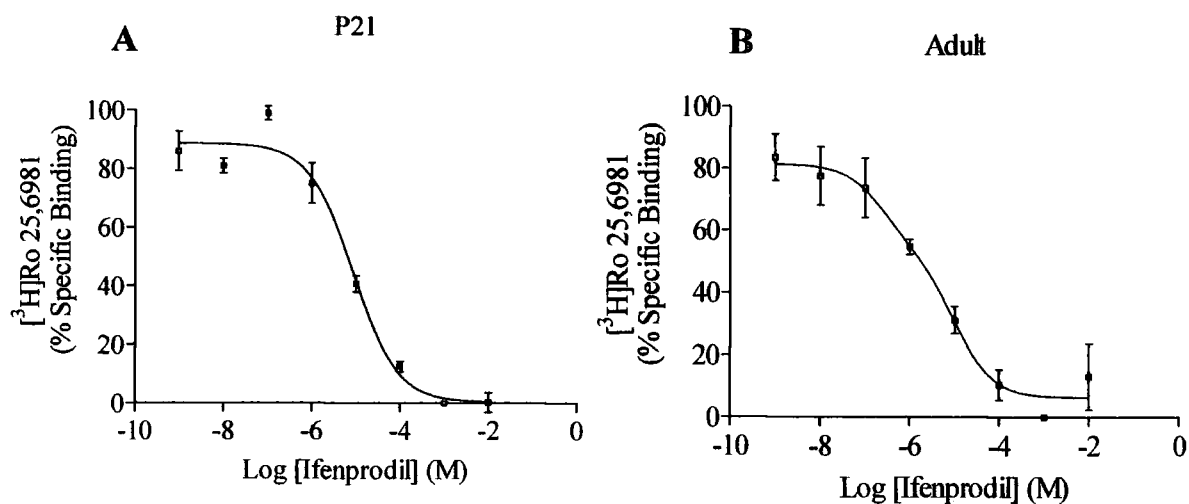
Figure 3.2.2.6 (A,B) Competition curves for the inhibition of [^{3}H]Ro 25,6981 radioligand binding by Ifenprodil, to (A) P21 and (B) Adult rat forebrain membranes. Mean values ± SD for at least n = 3 separate experiments.

	Apparent pIC$_{50}$			n$_H$
	Overall	Site 1	Site 2	
P21	5.06 ± 0.12	-	5.06 (100%)	-0.87 ± 0.20
Adult	5.52 ± 0.20	6.59 (37 ± 5%)	5.00 (63 ± 5%)	-0.65 ± 0.23

Table 3.2.2.6 Summary of the apparent pIC$_{50}$ and n$_H$ for [^{3}H]Ro 25,6981 binding using Ifenprodil in P21 and Adult membrane preparations.

113
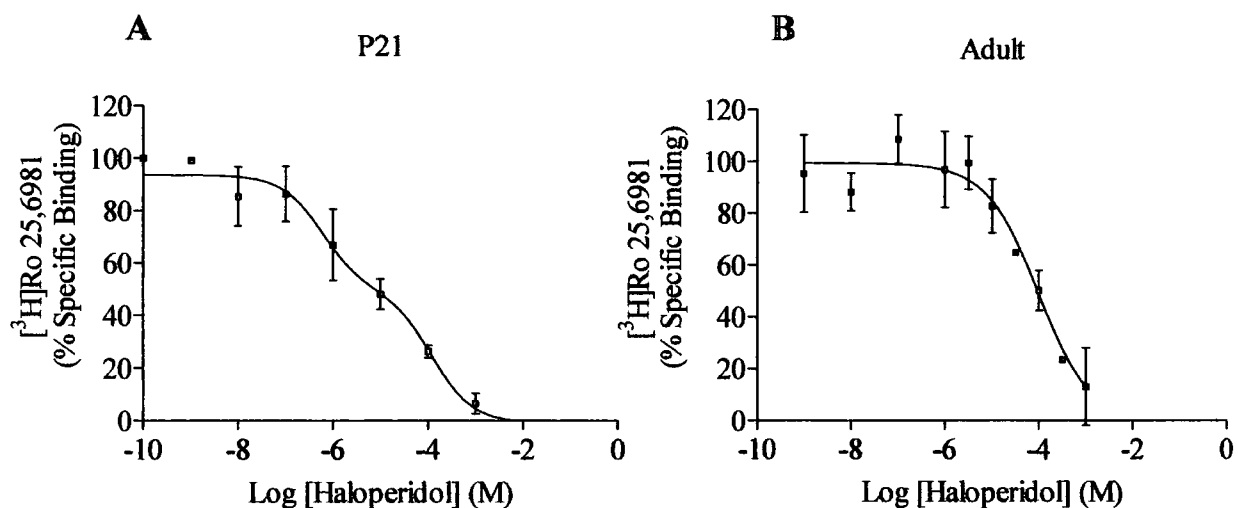
Figure 3.2.2.7 (A,B) Competition curves for the inhibition of [^{3}H]Ro 25,6981 radioligand binding by Haloperidol, to (A) P21 and (B) Adult rat forebrain membranes. Mean values ± SD for at least n = 3 separate experiments.

	Apparent pIC$_{50}$			n_H
	Overall	Site 1	Site 2	
P21	4.74 ± 0.55	6.22 (56 ± 13%)	3.92 (44 ± 13%)	-0.33 ± 0.12
Adult	4.00 ± 0.53	-	4.00 (100%)	-0.77 ± 0.24

Table 3.2.2.7 Summary of the apparent pIC$_{50}$ and n_H for [^{3}H]Ro 25,6981 binding using Haloperidol in P21 and Adult membrane preparations.
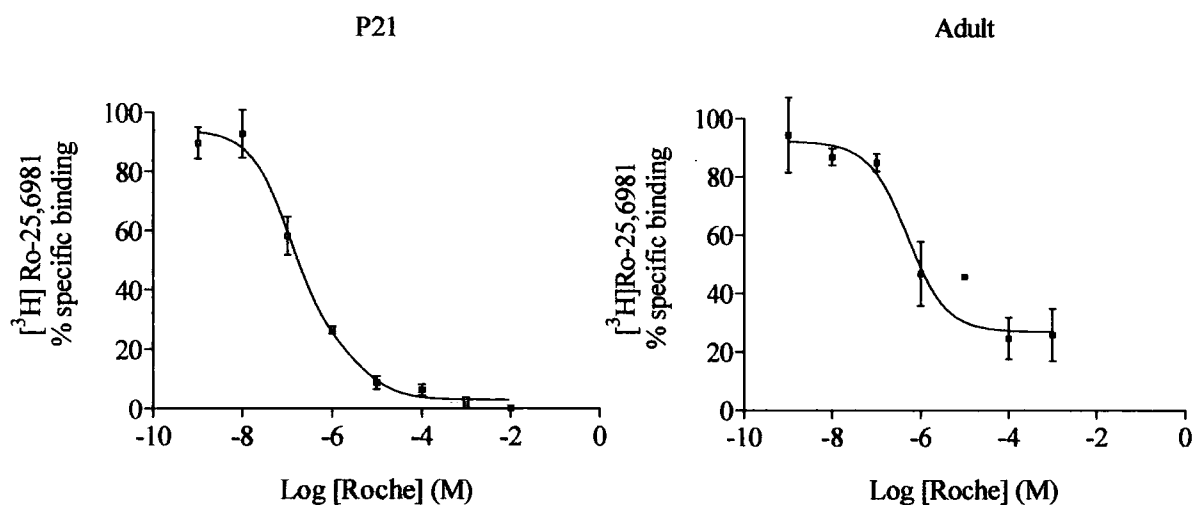
Figure 3.2.2.8 (A,B) Competition curves for the inhibition of [^{3}H]Ro 25,6981 radioligand binding by Ro 25,6981, to (A) P21 and (B) Adult rat forebrain membranes. Mean values ± SD for at least n = 3 separate experiments.

	Apparent pIC$_{50}$			n$_H$
	Overall	Site 1	Site 2	
P21	6.70 ± 0.13	6.95 (79 ± 17%)	5.37 (21 ± 17%)	-0.76 ± 0.16
Adult	6.29 ± 0.29	6.29 (75%)	< 3 (25%)	-0.99 ± 0.62

Table 3.2.2.8 Summary of the apparent pIC$_{50}$ and n$_H$ for [^{3}H]Ro 25,6981 binding using Ro 25,6981 in P21 and Adult membrane preparations.
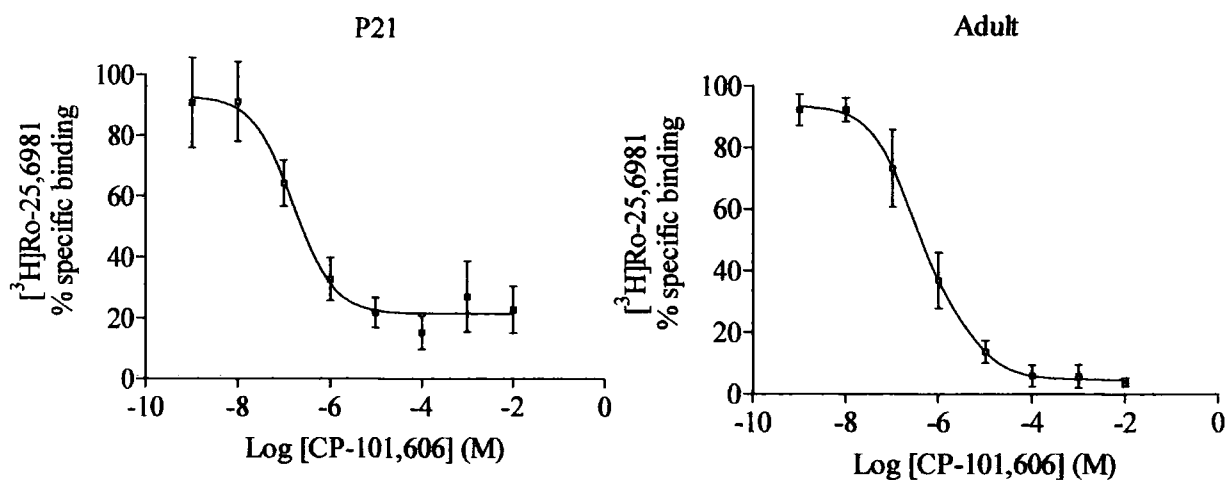
Figure 3.2.2.9 (A,B) Competition curves for the inhibition of [^{3}H]Ro 25,6981 radioligand binding by CP-101,606, to (A) P21 and (B) Adult rat forebrain membranes. Mean values ± SD for at least n = 3 separate experiments.

	Apparent pIC$_{50}$			n$_H$
	Overall	Site 1	Site 2	
P21	6.80 ± 0.26	6.80 (80%)	< 2 (20%)	-0.99 ± (0.56)
Adult	6.33 ± 0.17	6.64 (73 ± 34%)	5.34 (27 ± 34%)	-0.77 ± 0.20

Table 3.2.2.9 Summary of the apparent pIC$_{50}$ and n$_H$ for [^{3}H]Ro 25,6981 binding using CP-101,606 in P21 and Adult membrane preparations.
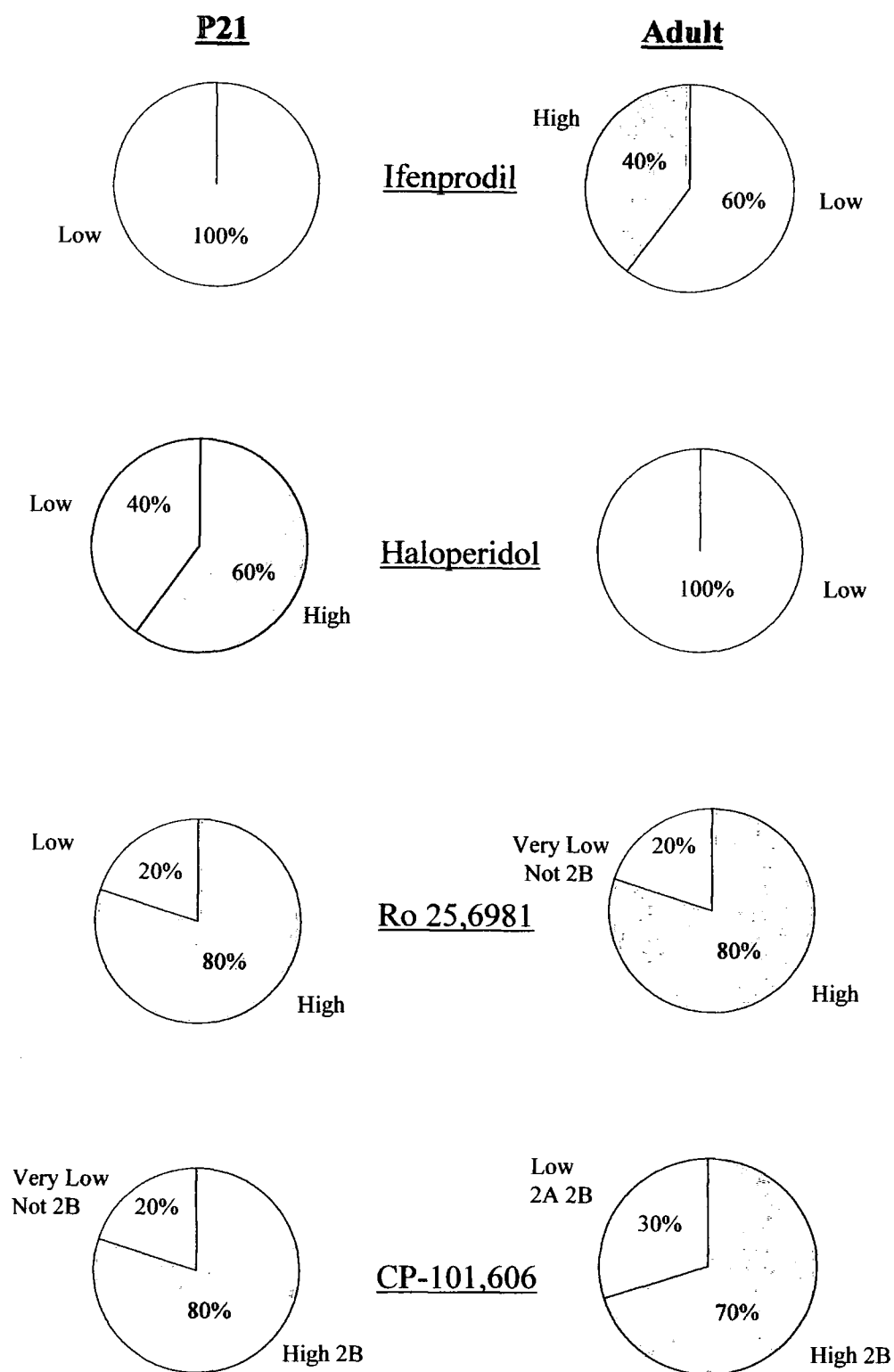
Figure 3.2.2.10 Relative Percentages of High- and Low-affinity binding sites in P21 and adult rat forebrain membranes using NR2B ligands Ifenprodil, Haloperidol, Ro 25,6981 and CP-101,606.

117

3.2.2.4 Discussion

This study describes the pharmacological characterisation of NR2B ligands binding to native NR2B receptors in P21 and adult rat forebrain membranes using the radiolabelled NR2B antagonists [^{3}H]Ro 25,6981 and [^{3}H]MK-801.

3.2.2.4.1 [^{3}H]MK-801 Competition binding

Figures 3.2.2.1 and 3.2.2.2 show competition curves for the stimulation of [^{3}H]MK-801 binding by spermidine and histamine respectively using P21 and adult rat forebrain membranes. MK-801 is an open-channel blocker NMDA antagonist. Figure 3.2.2.1 shows there is a difference in level of binding affinity and stimulation by spermidine in P21 and adult brain. The stimulation is more pronounced in the P21 than the adult rat brain. This is consistent with the hypothesis that the level of NR2B expression is higher in P21 than the adult rat brain. Figure 3.2.2.2 shows that histamine behaves in a very similar way to spermidine. Histamine stimulated [^{3}H]MK-801 binding in the P21 rat brain but had no affect on the adult rat brain binding levels. This would suggest a greater expression of NR2B-containing receptors in the P21 than the adult rat brain. Both spermidine and histamine bind to other distinct binding sites than the MK-801 binding site in the adult brain, since they produced a positive modulation of MK-801 binding. Histamine has numerous functions in the brain and has been shown to modulate responses of NMDA receptors on hippocampal neurons by a mechanism that does not involve classical histamine receptors (Williams, 1994). Studies by Williams (1994) showed that histamine potentiated responses to NMDA at heteromeric NR1/NR2 receptors containing the NR1 subunit together with the NR2B subunit but not the NR2A or NR2C subunit. The results

suggested that histamine acts directly at a novel recognition site on some subtypes of NMDA receptors to increase their activity.

3.2.2.4.2 [^{3}H]Ro 25,6981 Saturation Binding

The saturation data for [^{3}H]Ro 25,6981 binding is shown in Figure 3.2.2.3 for P21 and adult rat brain. Specific binding of [^{3}H]Ro 25,6981 to P21 rat forebrain membranes was saturable and best fit to a one-site binding hyperbola. Analysis of the saturation binding curve revealed that [^{3}H]Ro 25,6981 bound to a single class of sites with a K_D of 9.5 ± 3.6 nM and a B_{max} of 2593 ± 453 fmol/mg protein. Specific binding of [^{3}H]Ro 25,6981 to adult rat forebrain membranes was also saturable and best fit to a one-site binding hyperbola. Analysis of the saturation binding curve revealed that [^{3}H]Ro 25,6981 bound to a single class of sites with a K_D of 11.9 ± 4.2 nM and a B_{max} of 683 ± 111 fmol/mg protein. The specific binding of [^{3}H]MK801 to adult rat brain membranes was investigated by Chazot et al (1993) and showed that [^{3}H]MK-801 binding had a B_{max} = 1820 fmol/mg. The Bmax for [^{3}H]Ro 25,6981 binding represents 38% of the [^{3}H]MK-801 binding, suggesting that there is a 38% NR2B population of NMDA receptors in the adult rat forebrain, this correlates to work by Chazot et al (1997). The data shows that there are higher levels of NR2B-containing receptors in the P21 rat brain than the adult indicated by the higher B_{max} value, although the affinities were very similar, with K_D values at 9.5 and 11.9nM, respectively. Hawkins et al (1999) performed saturation experiments for the binding of [^{3}H]Ro 25,6981 to NR1-1a/NR2B receptors expressed in HEK 293 cells. Analysis of the data revealed a single binding site with a K_D = 10.5 ± 1.7, which is similar to the findings in this section.

3.2.2.4.3 [³H]Ro 25,6981 Competition Binding

Figure 3.2.2.4 shows the inhibition of [³H]Ro 25,6981 binding by Spermidine in the adult

rat brain. The apparent $pIC_{50} = 2.34 \pm 0.15$, and there is an incomplete inhibition of [³H]Ro

25,6981 binding, with ~40% of the binding not displaced by Spermidine. This suggests

that there may be binding occurring at another site which is not being displaced by the

Spermidine. 10mM Spermidine was used in subsequent autoradiography studies to define

specific binding. Figure 3.2.2.5 shows that histamine had no affect on [³H]Ro 25,6981

binding in both P21 and adult rat forebrain membranes. The apparent pIC_{50} for both ages

was < 2, and no inhibition or stimulation of binding was seen. These results suggest that

histamine binds to a distinct binding site in the two ages studied, and that this site is distinct

from the Spermidine binding site shown in Figure 3.2.2.4.

The affect of Ifenprodil, Haloperidol, Ro 25,6981 and CP-101,606 on [³H]Ro 25,6981

binding are shown in Figures 3.2.2.6 to 3.2.2.9 respectively and the results are summarised

in Figure 3.2.2.10. Mutel *et al* (1998) demonstrated that inhibition of [³H]Ro 25,6981

binding to rat brain membranes using different compounds. The Ki (µM) values for

Ifenprodil were 0.02 ± 0.004, and for Haloperidol were 0.6 ± 0.2. Menniti *et al* (1997)

reported that racemic [³H]CP-101,606 binds to a saturable site on rat forebrain membranes

with a binding affinity $K_D = 10 \pm 1$ nM. The effect of Ifenprodil on [³H]Ro 25,6981 binding

to P21 and adult rat forebrain membranes is shown in Figure 3.2.2.6. For the P21 data,

Ifenprodil produced a concentration-dependent inhibition of specific [³H]Ro 25,6981

binding with an apparent overall $pIC_{50} = 5.06 \pm 0.12$ (100%). For the adult data, Ifenprodil

produced a concentration-dependent inhibition of specific [³H]Ro 25,6981 binding, best fit

to a two-site competition model, comprising high- and low-affinity binding sites in the ratio

37:63 (high:low %, SD±5). Site 1 apparent $pIC_{50} = 6.59$, site 2 apparent $pIC_{50} = 5.00$. The

data shows that there is an additional high-affinity binding site in the adult rat brain. Compared to the one binding site in the P21 rat brain, there is another population of receptors to which Ifenprodil is binding with high affinity in the adult brain, as well as the low affinity binding site displayed in the P21 rat brain. Figure 3.2.2.10 shows the relative percentages of high- and low-affinity binding sites in P21 and adult rat forebrain membranes using the NR2B selective compounds stated. The mean percentages are shown in each diagram, and have been approximated to give a representative value, allowing for a degree of error within the radioligand binding experiments and analyses.

Figure 3.2.2.7 shows the effect of Haloperidol on [^{3}H]Ro 25,6981 binding to P21 and adult rat forebrain membranes. For the P21 data, Haloperidol produced a concentration-dependent inhibition of specific [^{3}H]Ro 25,6981 binding best fit to a two-site competition model, comprising high- and low-affinity binding sites in the ratio 56:44 (high:low %, SD±13). Site 1 apparent pIC_{50} = 6.22, site 2 apparent pIC_{50} = 3.92. For the adult data, Haloperidol produced a concentration-dependent inhibition of specific [^{3}H]Ro 25,6981 binding best fit to a one-site competition model with an apparent overall pIC_{50} = 4.00 ± 0.53 (100%). These results are represented in Figure 3.2.2.10, where for the P21 data, Haloperidol fully displaced the [^{3}H]Ro 25,6981 binding from the high (60%) and low (40%) affinity binding sites. For the adult data, one low affinity binding site was seen and the [^{3}H]Ro 25,6981 was also fully displaced by Haloperidol.

Figure 3.2.2.8 shows the effect of Ro 25,6981 on [^{3}H]Ro 25,6981 binding to P21 and adult rat forebrain membranes. For the P21 data, Ro 25,6981 produced a concentration-dependent inhibition of specific [^{3}H]Ro 25,6981 binding best fit to a two-site competition model, comprising high- and low-affinity binding sites in the ratio 79:21 (high:low %, SD±17). Site 1 apparent pIC_{50} = 6.95, site 2 apparent pIC_{50} = 5.37. For the adult data, Ro

25,6981 produced a concentration-dependent inhibition of specific [^{3}H]Ro 25,6981 binding best fit to a one-site competition model with an apparent overall pIC_{50} = 6.29 ± 0.29 (100%). These results are represented in Figure 3.2.2.10, where for the P21 data, Ro 25,6981 fully displaced the [^{3}H]Ro 25,6981 binding from the high (80%) and low (20%) affinity binding sites. For the adult data, one high-affinity binding site (80%) was seen and the [^{3}H]Ro 25,6981 was not fully displaced by Ro 25,6981. Approximately 20% of the binding was not displaced. These results taken together would suggest that there may be three potential Ro 25,6981 binding sites in the rat brain. A high affinity site as seen in the P21 (80%) and adult (80%), (average pIC_{50} = 6.5), an intermediate-affinity site as seen in the P21 (20%), (pIC_{50} = 5.4), and a very low-affinity site seen in the adult (20%)(pIC_{50}< 3). The very low-affinity site may represent a population of non-NMDA receptors bound by [^{3}H]Ro 25,6981 and which cannot be displaced by Ro 25,6981.

Figure 3.2.2.9 shows the effect of CP-101,606 on [^{3}H]Ro 25,6981 binding to P21 and adult rat forebrain membranes. For the P21 data, CP-101,606 produced a concentration-dependent inhibition of specific [^{3}H]Ro 25,6981 binding best fit to a one-site competition model, with an apparent overall pIC_{50} = 6.80 ± 0.26 (80%). For the adult data, Ro 25,6981 produced a concentration-dependent inhibition of specific [^{3}H]Ro 25,6981 binding best fit to two-site competition model, comprising high- and low-affinity binding sites in the ratio 73:27 (high:low %, SD ± 34). Site 1 apparent pIC_{50} = 6.64 (73%), site 2 apparent pIC_{50} = 5.34 (27%). These results are represented in Figure 3.2.2.10, where for the P21 data, CP-101,606 did not fully displaced the [^{3}H]Ro 25,6981 binding. Approximately 20% of the binding was not displaced. There may be another binding site distinct from the NR2B site where [^{3}H]Ro 25,6981 is bound and cannot be displaced by CP-101,606. For the adult data, CP-101,606 fully displaced the [^{3}H]Ro 25,6981 binding from the high (73%) and low (27%)

122

affinity binding sites. These results would suggest that, as with the previous Ro 25,6981 binding data, there may be three potential CP-101,606 binding sites in the rat brain. A high affinity site as seen in the P21 (80%) and adult (73%), (average pIC_{50} = 6.8), an intermediate-affinity site as seen in the adult (27%), (pIC_{50} = 5.3), and a very low-affinity site seen in the P21 (20%)(pIC_{50}<2). The very low-affinity site may represent a population of non-NMDA receptors bound by [^{3}H]Ro 25,6981 and which cannot be displaced by CP-101,606.

In Figure 3.2.2.10, the Ro 25,6981 data is very similar between the two ages studied. In both P21 and adult, all the NR2B containing receptors are labelled. There are subtle differences in the pharmacology of the other ligands used. CP-101,606 reveals an additional intermediate-affinity binding site to the high–affinity site in the adult rat brain, with the P21 rat brain showing high- and very low-affinity binding sites. CP-101,606 behaves in a distinct way to Ifenprodil, where binding in the two ages for one ligand is the reverse of that seen in the other. That is, in the adult, the majority of binding for CP-101,606 is at a high-affinity site (70%) with the minority at a low-affinity site (30%). Ifenprodil data for the adult shows the majority of binding is at a low-affinity (60%) site and the minority at a high-affinity (40%) site. The mean percentages are similar and suggest that in the adult rat forebrain, these ligands are labelling distinct populations of NR2B-containing receptors.

The Ro 25,6981 and CP-101,606 data suggest there are three binding sites for these ligands in the rat brain. Both the ligands are able to displace bound [^{3}H]Ro 25,6981 from the high- and intermediate-affinity sites in the P21 and adult rat forebrain membranes, although the low-affinity sites may be another population of non-NMDA receptors, or NMDA receptor binding sites which are insensitive to the Ro 25,6981 and CP-101,606 ligands. As previously described (section 3.2.2.1), the NMDA receptor can act as a molecular switch in developmental regulation of cognitive ability. Hebbian rules for synaptic plasticity (Hebb,

1949) are well accepted and thought to guide cortical network formation during the experience-sensitive critical period and evidence suggests NMDA properties conform to mediate this plasticity (Dumas, 2005). The critical period when somatosensory maps can be altered by activity or experience occurs during the first week after birth in rats. Dumas (2005) describes how the neuronal network develops in the forebrain, with synaptic NR2B-NMDARs replaced by NR2A-NMDARs and the NR2B-NMDARs moving to extra-synaptic sites. LTP and LTD are enhanced in this initial period of the switch, with synapses containing both NR2A and NR2B receptor types. NMDAR subunit expression then decreases and the NR2A subunit become dominant in the synapse, together with a reduced channel function, synaptic plasticity, and ability to switch receptor composition. In this way, a balance of plasticity and stability is achieved which is optimal for information processing and storage. The CP-101,606 data, shown in Figure 3.2.2.9, also suggest that a switch in the composition of NMDA receptors may be occurring between P21 and adult rat brain. The P21 data shows a high affinity binding site (80%) and a very low affinity (20%) non-NMDA binding site, whereas the adult data reveals a high and low affinity NMDA receptor binding site. The low affinity site may represent a population of NMDA receptors that contain a different subunit composition to that of the high affinity site, possibly NR1/2A/2B. This would demonstrate a switch in proportion of NR2A to NR2B subunit populations in the P21 compared to adult rat forebrain. The Ro 25,6981 data , see Figure 3.2.2.8, is similar between the two ages, with both P21 and adult showing approximately 80% of binding occurring at a high affinity binding site. The adult Ro 25,6981 binding and the P21 CP-101,606 binding both have approximately 20% of the total [^{3}H]Ro 25,6981 binding not displaced, suggesting that 20% of Ro 25,6981 and CP-101,606 binding is labelling a non-NMDA receptor population, perhaps a σ site (Chaffey and Chazot, unpublished). The other 80% in both cases show the NMDA receptor binding to NR2B-

124

containing receptor populations. There is evidence for switches in subunit composition in the hippocampus. *In situ* hybridization assays for NMDAR subunit mRNA in the hippocampus show that, in general, NR1 and NR2A expression levels increase from birth to the third postnatal week (Monyer *et al.*, 1994, Zhong *et al.*, 1995) in parallel with NR1 and NR2A protein levels (Wenzel *et al.*, 1997). Beyond P21, NR1 and NR2A expression decreases slightly to reach adult levels by P35. Analysis of NR2B subunit levels in hippocampal tissue revealed high levels at birth and a slight increase to P21 (Wenzel *et al.*, 1997). The results from this section provide further evidence for heterogeneity in NR2B subunit containing receptors, and that the composition of the receptor can affect the pharmacological properties, shown here by the differences in binding between the NR2B-selective ligands. There is evidence for different populations of NR2B receptors in the P21 and adult rat forebrain membranes, and they display different affinities for ligands.

The next section, 3.2.3, of Chapter 3, uses the radioligands [^{3}H]Ro 25,6981 and [^{3}H]CP-101,606 in autoradiographical studies of P21 and adult rat brain. This will reveal the distribution and abundance of NR2B-containing NMDA receptors in the brain for both age groups.

Chapter 3

Section 3.2.3

Ligand Autoradiographical comparison of Ro 25,6981 and CP-101,606 in Juvenile (P21) and Adult rat brain: Focus on cognitive centres.

3.2.3.1 Introduction

The NR2B receptors are known to play an important role in learning and memory and to be involved in neuron cell death accompanying cerebral ischemia, seizures, and Alzheimer's disease (Kito et al.,1990). Nicolas & Carter (1994) demonstrated the autoradiographical distribution and characteristics of NMDAR2B receptors in the rat brain via the ifenprodil binding site. High-affinity [^{3}H]ifenprodil sites, were concentrated in the cortex, hippocampus, striatum, and thalamus with little or no labelling of hindbrain or cerebellar regions. This distribution matches that of NMDAR2B mRNA, supporting data showing that ifenprodil has a preferential action at NMDA receptors containing this subunit. CP-101,606, an NMDA receptor antagonist, (see 1.13) is structurally similar to ifenprodil, and has been shown by Menniti et al (1997) to potently and efficaciously protect hippocampal neurons from glutamate toxicity but was less effective for cerebellar granule neurons. Their preliminary autoradiography results indicate that the CP-101,606 binding site is localized in forebrain, most notably in hippocampus and the outer layers of cortex. The functional selectivity for hippocampal neurons, forebrain localization of binding sites, and structural relation to ifenprodil suggest that CP-101,606 is an NMDA antagonist highly selective for NR2B subunit containing receptors. Mutel et al (1998) studied the in vitro binding

properties of [³H]Ro 25-6981 in rat brain, and showed the overall distribution of [³H]Ro 25-6981 binding sites correlated well with that of NR2B (but not NR2A) transcripts, revealed by *in situ* hybridization histochemistry. Therefore CP-101,606 and Ro 25,6981, two potent and selective antagonists of NMDA receptors containing NR2B subunits, are the ligands of choice for this study.

The literature does not indicate conclusively either way what effect ageing may have on the expression of NMDA receptors in the rodent brain. The NMDA receptor complex in rat brain was studied by Kito *et al* (1990) using *in vitro* autoradiography with [³H]-CPP and [³H]-glycine. Both [³H]-glycine and [³H]-CPP binding sites were most abundant in the hippocampus and cerebral cortex, and they showed a similar distribution pattern throughout the brain. [³H]-glycine binding sites greatly decreased in the hippocampus and cerebral cortex, in aged brain, although [³H]-CPP binding sites were well preserved in these brain areas. Neither ligand binding sites changed in the mid-brain and cerebellum regions in the aged brain. These results suggest that NMDA receptors are primarily affected in the aging process. Clark *et al* (1992) used *in vitro* autoradiography of hippocampal excitatory amino acid binding to study age and memory performance in young and aged Fischer 344 rats. Significant differences were observed between the young and old rats in the levels of N-methyl-D-aspartate, CPP, kainate, and AMPA binding in subregions of the hippocampus. There was an age-related decline in hippocampal glutamate receptors, although no relationship was observed between the density or distribution of receptors and performance in the memory task in the aged rats. These studies were unable to distinguish NMDA receptor subtypes.

As previously described in section 3.1, the technique of autoradiography has been used for over 50 years and is an extremely useful method of detecting the presence and distribution of receptors in tissue sections. It has been used here to map the binding of [³H]Ro 25,6981

127

and [^{3}H]CP-101,606 in juvenile (P21, post natal day 21) and adult rat brain sections. Both these ligands label N-methyl-D-aspartate (NMDA) receptors containing the NR2B subunit. The aim of this study was two-part, firstly to assess the differences in NMDAR2B distribution patterns in the various brain regions, labelled by each of the radioligands. Secondly, the effects of age upon the binding was investigated, using postnatal day 21 and adult rats (3 months) to represent young and mature rodents, respectively. Since the NR2B subunit has been implicated in having a role in learning and memory, and is involved in synaptic plasticity of the developing brain, it is therefore predicted that as memory and cognitive ability decrease with age, so too would the expression of the NR2B subunit within the brain. It is expected that binding levels of the two ligands would decrease in the adult tissue when compared to the P21 tissue. P21 ligand binding levels would be expected to be higher due to the predicted high NR2B-containing NMDA receptor expression at the early developmental stages of the rodent brain, when there is increased synaptic plasticity and memory formation. Using the Ro 25,6981 and CP-101,6096 ligands will enable a comparison to be made between the expression of the two distinct NR2B subtype populations for both P21 and adult rat brain sections. The method used in this study was that essentially described by Mutel *et al.* (1998), with some modifications made, and is described in (3.1.2.2). Autoradiography was carried out on slide-mounted either P21 or adult rat brain sections, prepared as described in (3.1.2.1) using the radiolabelled ligands [^{3}H]CP-101,606 and [^{3}H]Ro 25,6981. Spermidine was used to define specific binding of the radioligand (Hawkins *et al.* 1999).

3.2.3.2 Methods

3.2.3.2.1 Perfusion and Sectioning of Rat Brain

The perfusion was performed by Dr C.L. Thompson. A P21 or adult male wild-type Sprague-Dawley rat brain was prepared as described in section 3.1.2.1.

3.2.3.2.2 NMDA R2B Receptor Autoradiography

The autoradiographical method used was that essentially described by Mutel *et al.* (1998), with some modifications made. See section 3.1.2.2.

3.2.3.2.3 [^{3}H]Ro 25,6981 and [^{3}H]CP-101,606

See section 3.1.2.3

3.2.3.2.4 Image analysis

See section 3.1.2.4

3.2.3.2.5 Statistical Analysis

See section 3.1.2.5

Outer Frontal Cortex

Striatum

Inner Frontal Cortex

Thalamus

Entorhinal Cortex

Hippocampal Formation

Cerebellum

The Hippocampal Formation

CA2

Pyramidal Cells (CA2)

CA 3

CA1

SO   SR

Polymorph Layer

Granule Layer

Dentate Gyrus

SO = Stratum Oriens
SR = Stratum Radiatum
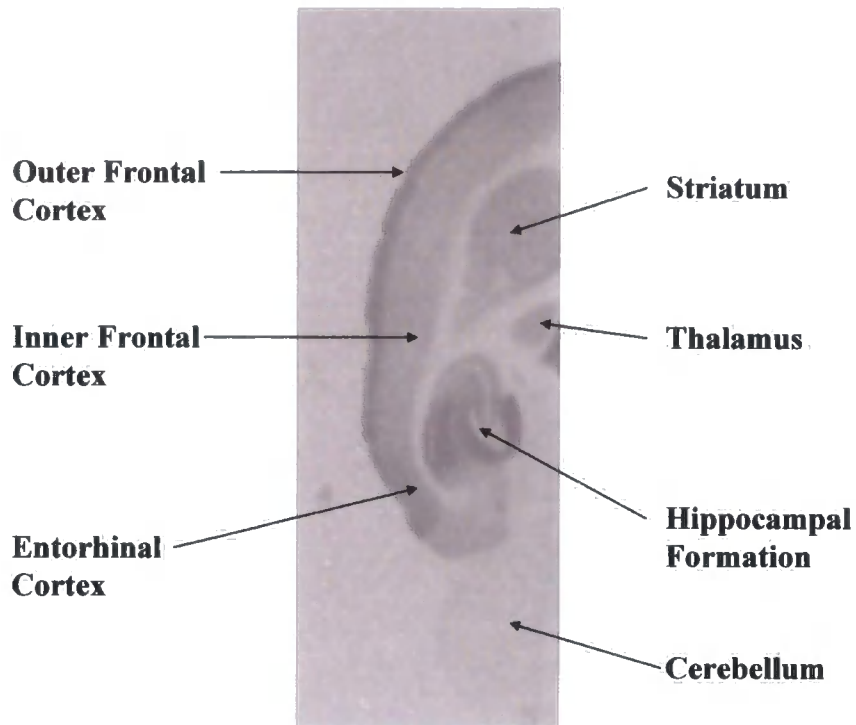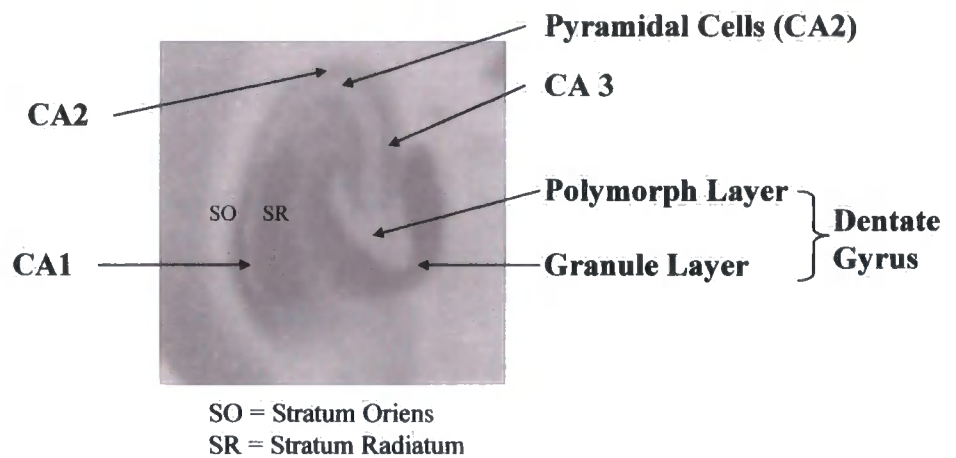
Figure 3.2.3.1 **Example of an adult rat brain labelled with [^{3}H]Ro 25,6981 showing the areas analysed. CA1 SO, CA1 SR, CA2 SO, CA2 SR, CA3 SO, CA3 SR (Lucidum), DG Poly (Dentate Gyrus Polymorph layer), DG gran (Dentate Gyrus granule layer), PC (CA2 Stratum Pyramidale cells), ent cx (Entorhinal cortex), In F cx (Inner frontal cortex), Out F cx (Outer Frontal cortex), Thal (Thalamus), Stria (Striatum) and Cereb (Cerebellum).**

130

[³H]Ro 25,6981   **[³H]CP-101,606**

Total

Adult

Non-Specific

Total

P21
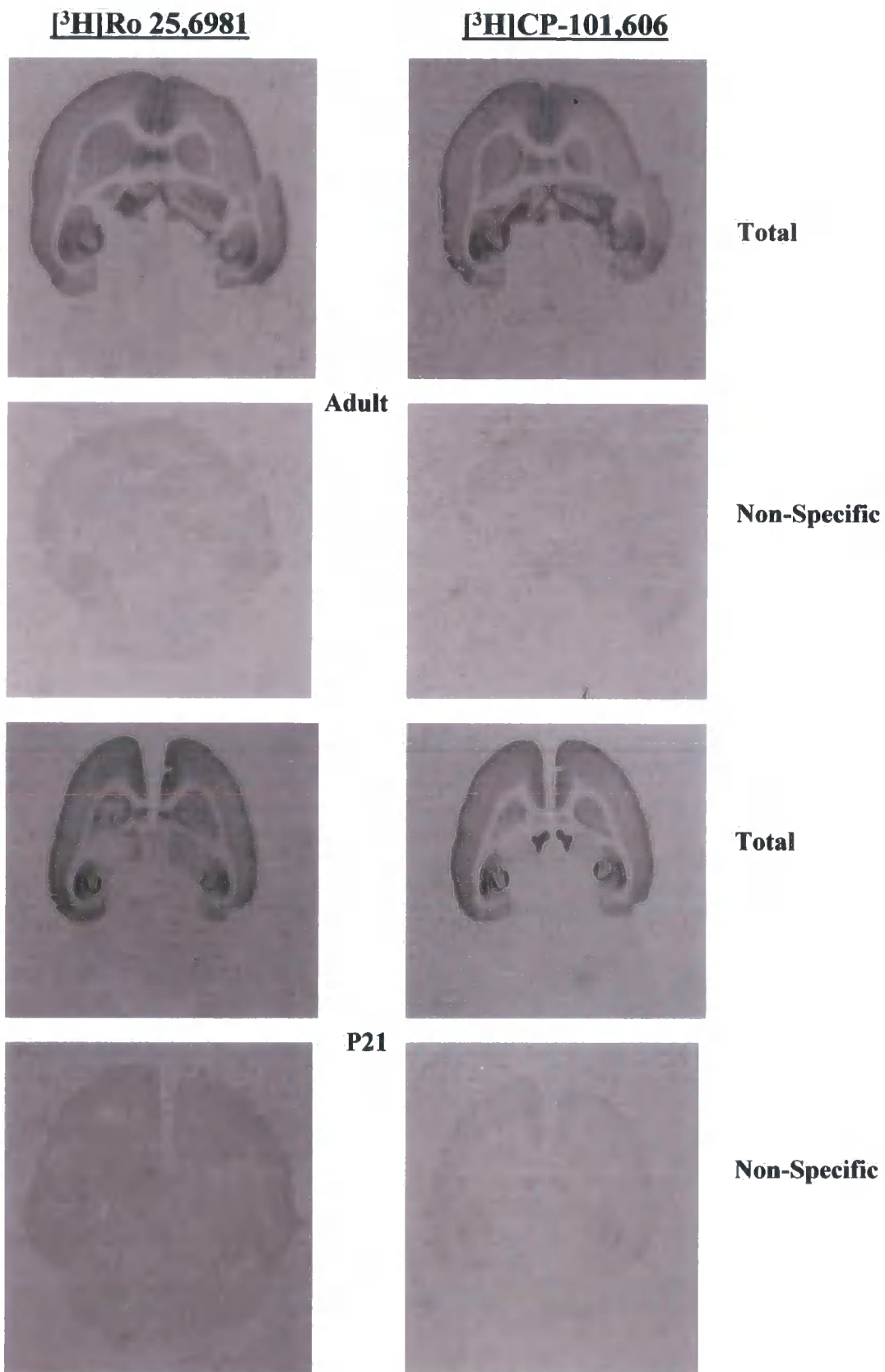
Non-Specific

Figure 3.2.3.1(a) [³H]Ro 25,6981 and [³H]CP-101,606 Total binding and
Non-Specific binding in Adult and P21 rat brain sections.   131

[³H]Ro 25,6981   **[³H]CP-101,606**
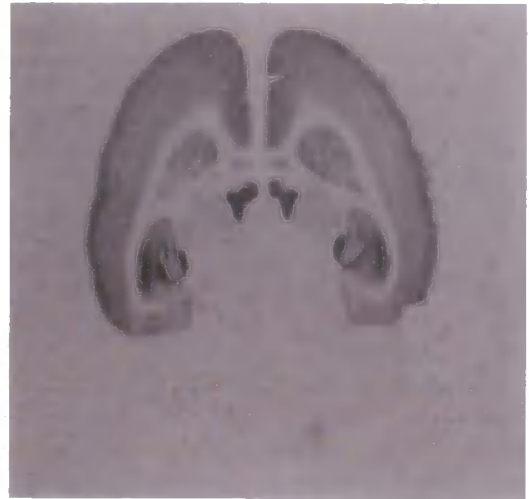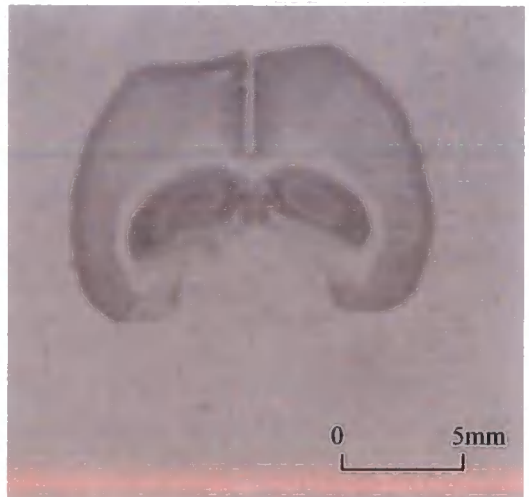
Figure 3.2.3.2 Autoradiography of P21 Rat brain slices. (A,C) [³H]Ro 25,6981 labelled receptors and (B,D) [³H]CP-101,606 labelled receptors. Specific binding defined using 10mM spermidine.

[³H]Ro 25,6981

[³H]CP-101,606

A

B

C

D

0 5mm
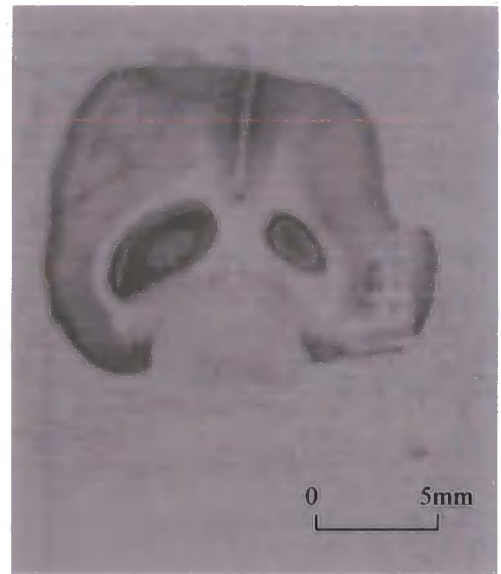
Figure 3.2.3.3 Autoradiography of Adult Rat brain slices. (A,C) [³H]Ro 25,6981 labelled receptors and (B,D) [³H]CP-101,606 labelled receptors. Specific binding defined using 10mM spermidine.

133

3.2.3.3 Results

3.2.3.3.1 Results (Figure 3.2.3.1-3.2.3.3)

The results in this section follow the same format as for section 3.1. The first four figures

(Figure 3.2.3.1-3) are scanned images of the resulting films showing a qualitative analysis

of the binding data. These are followed in Figure 3.2.3.4-10 by a quantitative analysis of

the binding levels in each tissue. Figure 3.2.3.1 is a representative example of an adult rat

brain section showing the typical pattern of radioligand binding seen in the brain areas

analysed, in this case [^{3}H]Ro 25,6981 has been used. The darker areas indicate those which

have been labelled by the radioligand, the greater the intensity, the higher the binding

density in that tissue. The brain sections are cut horizontally as described in 3.2.3.2.1 with

the areas labelled being identified using "The Rat Brain in Stereotaxic Coordinates" by G.

Paxinos and C. Watson, Academic Press, 4th Edition (1998). There is clear labelling seen in

the hippocampal formation, which has been divided into the following sections for analysis,

CA1 SO (stratum oriens), CA1 SR (stratum radiatum), CA2 SO, CA2 SR, CA3 SO, CA3

SR, DG Poly (Dentate Gyrus Polymorph layer), DG gran (Dentate Gyrus granule layer),

PC (CA2 striatum pyramidale cells). The pyramidal cell bodies and polymorph layer of the

dentate gyrus show very little binding, suggesting the receptors containing the NR2B

subunits are located on the neuronal projections which are seen labelled in the SO, SR and

granule layer. The frontal cortex is also well labelled, and has been divided into two; the

outer frontal cortical laminae in many of the sections, clearly shows a higher binding level

than that seen in the inner frontal cortical laminae. The entorhinal cortex, striatum,

thalamus are also well labelled. The cerebellum shows very low binding levels. Figure

3.2.3.1(a) shows representative examples of P21 and adult rat brain sections labelled with

Ro 25,6981 and CP-101,606, showing total and non-specific binding levels. There is very

low binding in the non-specific sections. Figure 3.2.3.2 and 3.2.3.3 show scanned images of the resulting films showing representative examples of both [^{3}H]Ro 25,6981 (left hand side) and [^{3}H]CP-101,606 (right hand side) binding in P21 rat brain and adult rat brain sections respectively. A similar distribution pattern of binding was seen across the tissue for both [^{3}H]Ro 25,6981 and [^{3}H]CP-101,606 ligands and between P21 and adult sections. In the P21 sections, there was a noticeably higher binding level of [^{3}H]Ro 25,6981 overall than the [^{3}H]CP-101,606 ligand binding levels. This difference was also apparent in the adult sections, but to a much lesser extent. In each of the examples shown, ligand binding was seen in the frontal and entorhinal cortex, striatum, thalamus, hipppocampal formation and appeared to be just above background in the cerebellum. Non-specific binding was defined using 10mM spermidine. As described in section 3.2.3.2.4, the specific value is calculated by subtracting mean non-specific binding from mean total binding.

3.2.3.3.2 Results (Figure 3.2.3.4-3.2.3.7). Refer to legends below each figure.

135
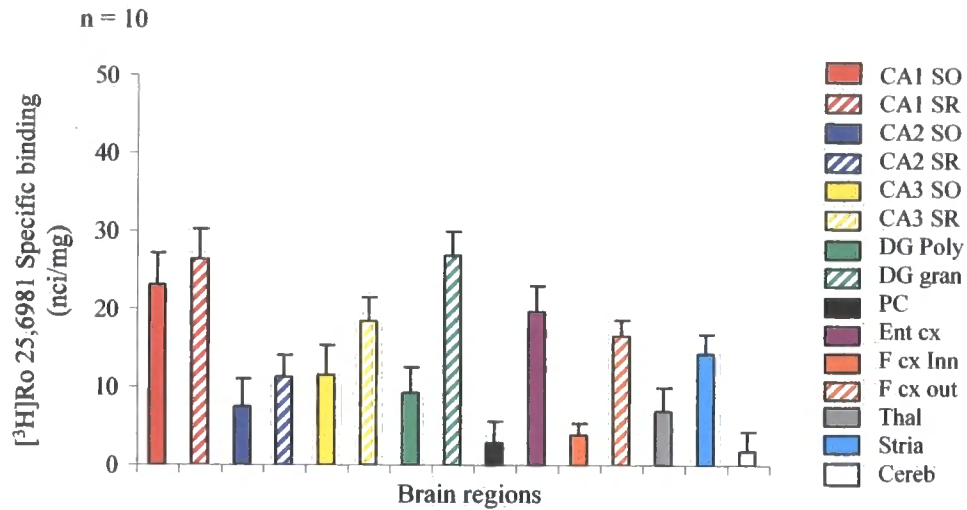
Figure 3.2.3.4 Graph showing the differences in [³H]Ro 25,6981 specific binding (nci/mg) densities (mean ± SD for n = 10 determinations) for Adult Rat brain.

Adult rat brain sections prepared as described in section 3.2.3.2.1 were assayed for radiolabelled Ro 25,6981 binding by autoradiography (3.2.3.2.2). As shown in figure 3.2.3.4, there were high levels of [³H]Ro 25,6981 binding in the CA1 SO, CA1 SR, CA3 SR, DG Gran, Ent CX and F CX Outer compared to the other regions analysed. The striatum showed similar binding levels when compared to F CX Outer. The lower levels of binding were seen in the regions CA2 SO, PC, F CX Inner, thalamus and very low binding in the cerebellum. There is variation in the levels of [³H]Ro 25,6981 binding seen between the different brain regions analysed. Binding levels ranged from the highest level in the CA1 SR to the lowest in the cerebellum.

n = 10
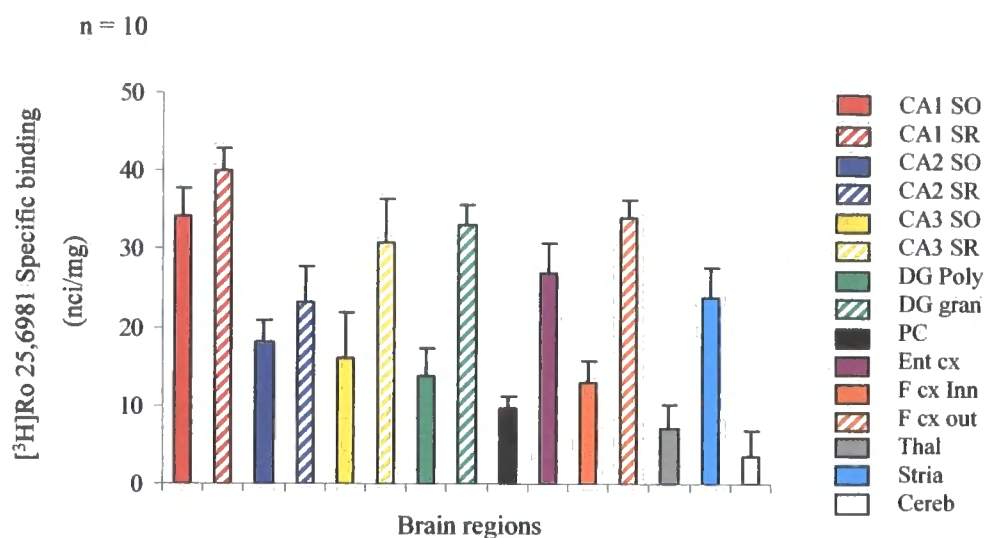
Figure 3.2.3.5 Graph showing the differences in [³H]Ro 25,6981 specific binding (nci/mg) densities (mean ± SD for n = 10 determinations) for P21 Rat brain.

P21 rat brain sections prepared as described in section 3.2.3.2.1 were assayed for radiolabelled Ro 25,6981 binding by autoradiography (3.2.3.2.2). As shown in figure 3.2.3.5, there were higher levels of [³H]Ro 25,6981 binding in the CA1 SO, CA1 SR, CA2 SR, CA3 SR, DG Gran, Ent CX, F CX Outer and Striatum than in the other regions analysed. There were lower levels of binding seen in the CA2 SO, CA3 SO, DG Poly, PC, F CX Inner, thalamus and cerebellum than in the regions mentioned above. There is variation in the levels of [³H]Ro 25,6981 binding seen between the different brain regions analysed. Binding levels ranged from the highest level in the CA1 SR to the lowest in the cerebellum.

137
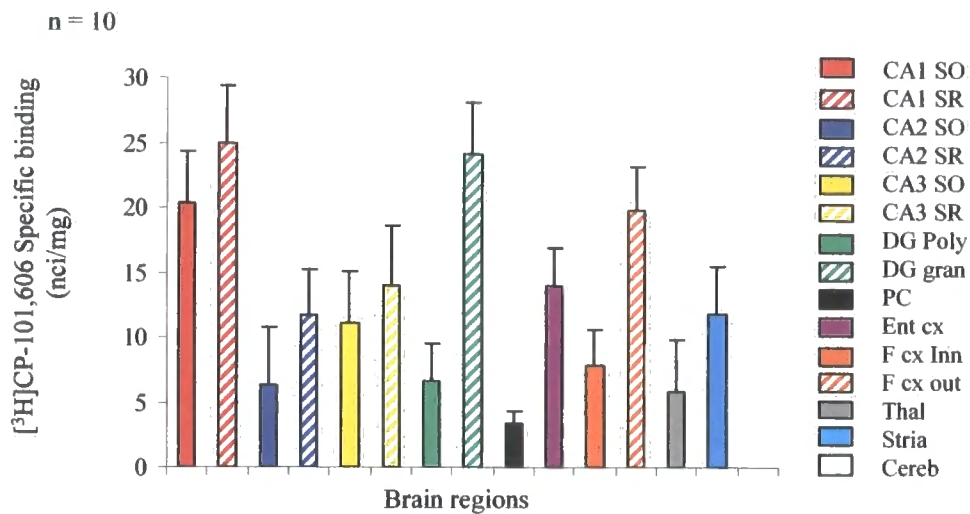
Figure 3.2.3.6 Graph showing the differences in $[^3H]$CP-101,606 specific binding (nci/mg) densities (mean $\pm$ SD for n = 10 determinations) for Adult Rat brain.

Adult rat brain sections prepared as described in section 3.2.3.2.1 were assayed for radiolabelled CP-101,606 binding by autoradiography (3.2.3.2.2). As shown in figure 3.2.3.6, there were higher levels of $[^3H]$CP 101,606 binding in the CA1 SO, CA1 SR, DG Gran and F CX Outer than in the other regions analysed. The lowest binding levels were seen in the CA2 SO, DG Poly, PC, F CX Inner and thalamus regions. The cerebellum binding levels were equal to background. There is variation in the levels of $[^3H]$CP-101,606 binding seen between the different brain regions analysed. Binding levels ranged from the highest level in the CA1 SR to the lowest in the pyramidal cell layer.

138
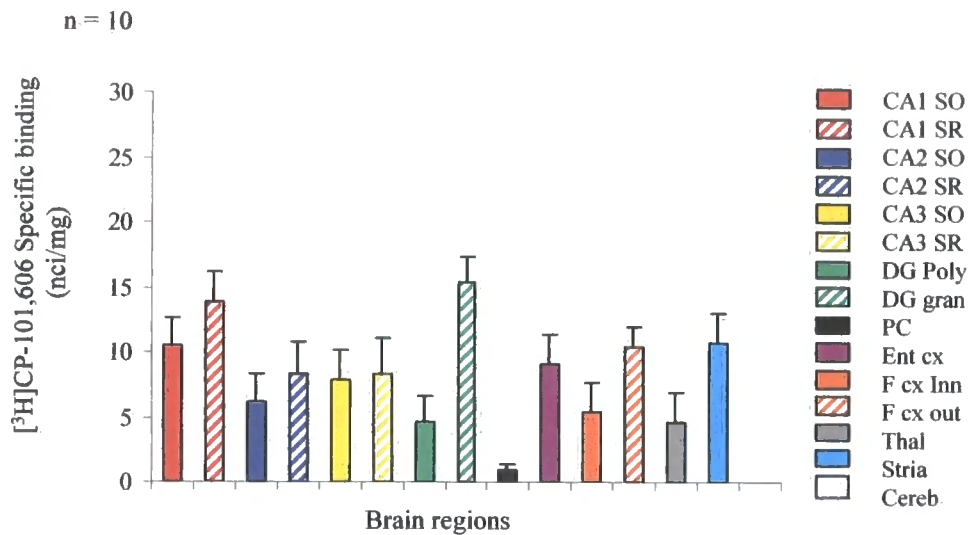
Figure 3.2.3.7 Graph showing the differences in [^{3}H]CP-101,606 specific binding (nci/mg) densities (mean ± SD for n = 10 determinations) for P21 Rat brain.

P21 rat brain sections prepared as described in section 3.2.3.2.1 were assayed for radiolabelled CP-101,606 binding by autoradiography (3.2.3.2.2). As shown in figure 3.2.3.7, there were higher levels of [^{3}H]CP 101,606 binding in the CA1 SR and DG Gran than in the other regions analysed. The lowest levels of binding were seen in the DG Poly, Pyramidal cells, F CX Inner and the thalamus, with binding levels in the cerebellum equal to background. There is variation in the levels of [^{3}H]CP-101,606 binding seen between the different brain regions analysed. Binding levels ranged from the highest level in the DG Gran to the lowest in the pyramidal cell layer.

3.2.3.3.3 Results (Figure 3.2.3.8 (A-O)).

The standard curves generated from each autoradiogram tritium standard scale were used to convert optical density values (dots per inch (dpi)) units to concentration of radioligand bound to the tissue (nci/mg of tissue protein). The same data as previously described (see figures 3.2.3.4-7) were further analysed to show mean specific binding levels ($\pm$ SD for n = 10 determinations) for both [^{3}H]Ro 25,6981 and [$^3$H]CP-101,606 in P21 and adult brain sections in each brain region defined. Several interesting observations are apparent from the results. Firstly, when comparing binding levels of the [^{3}H]Ro 25,6981 ligand between P21 and adult brain sections, the P21 binding levels were significantly higher (p< 0.02) in all the areas analysed with the exception of the CA3 SO (p = 0.1), thalamus (p = 0.94) and the cerebellum (p = 0.27). The thalamus and cerebellum were two regions which showed very low levels of binding in both P21 and adult tissue (see figures 3.2.3.4-5) with the cerebellum only just above background intensity in both cases. Secondly, when comparing binding levels of the [^{3}H]CP-101,606 ligand between P21 and adult brain sections, there were no significant differences between the two ages except in the CA1 SO (p = 0.02), CA1 SR (p = 0.05), F CX Outer (p = 0.02) and striatum (p = 0.05). The CA1, F CX Outer and striatum were areas where the highest levels of [^{3}H]CP-101,606 binding were observed in both P21 and adult sections (see figures 3.2.3.6-7). Thirdly, when comparing binding levels of the [^{3}H]Ro 25,6981 and [^{3}H]CP-101,606 in the adult tissue there were no significant differences between the two ligands except in the CA3 SR (p = 0.05), Ent CX (p = 0.004) and the F CX Inner (p = 0.001). [^{3}H]Ro 25,6981 binding was significantly higher in the adult CA3 SR and the Ent CX, where as the [^{3}H]CP-101,606 binding was significantly higher in the adult F CX Inner. Fourthly, when comparing binding levels of the [^{3}H]Ro 25,6981 and [^{3}H]CP-101,606 in the P21 tissue, there were

140

significantly higher levels of [^{3}H]Ro 25,6981 binding in all the regions analysed ($p = <0.005$), with the exception of the CA3 SO ($p = 0.11$) and the thalamus ($p = 0.96$).
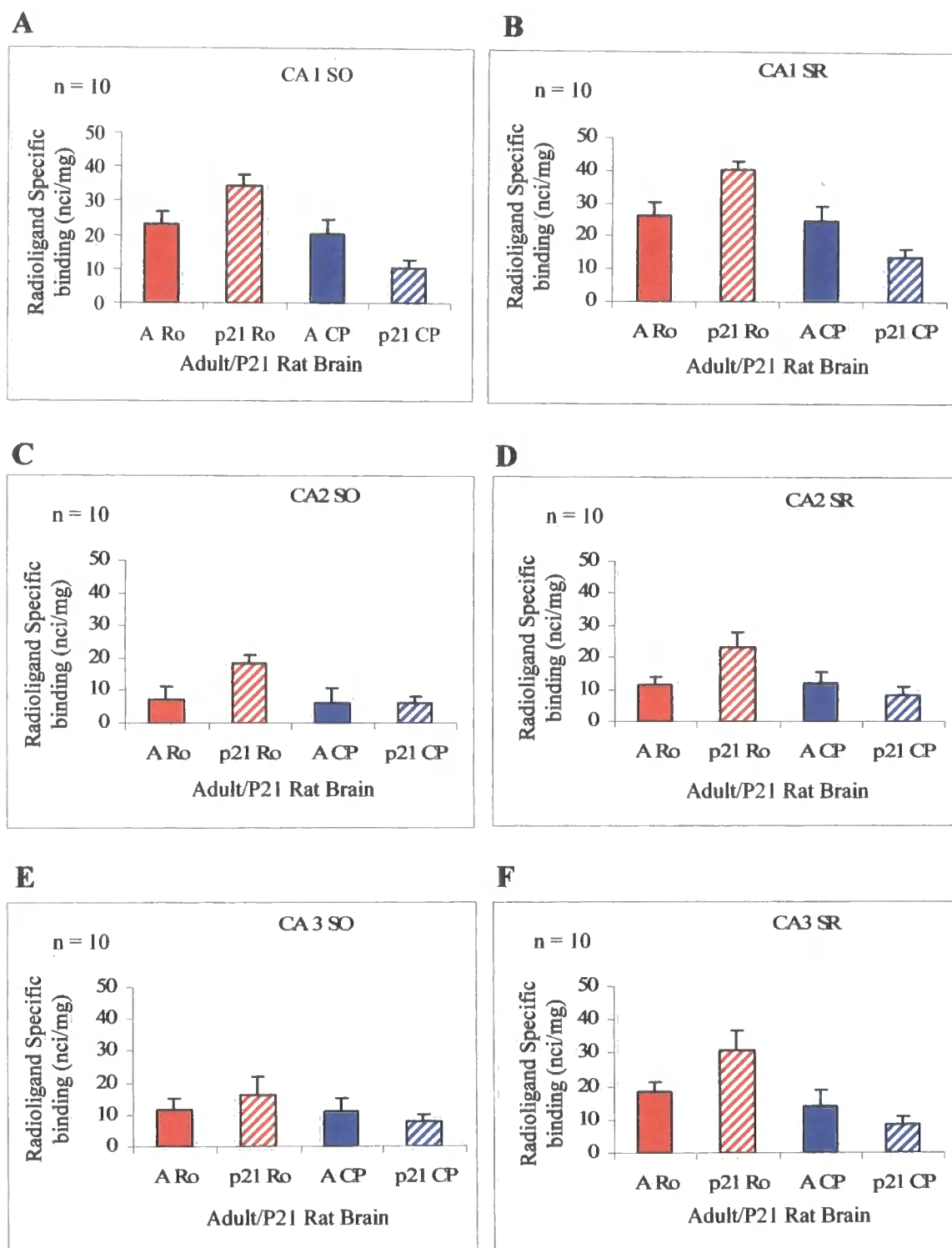
Figure 3.2.3.8 (A-F) Mean average specific binding (nci/mg) ± SD of [³H]Ro 25,6981 and [³H]CP-101,606 for Adult and P21 rat in (A) CA1 SO (B) CA1 SR (C) CA2 SO (D) CA2 SR (E) CA3 SO and (F) CA3 SR. (SO = stratum oriens, SR = stratum radiatum, A = adult, Ro = Ro 25,6981, CP = CP 101,606)

142
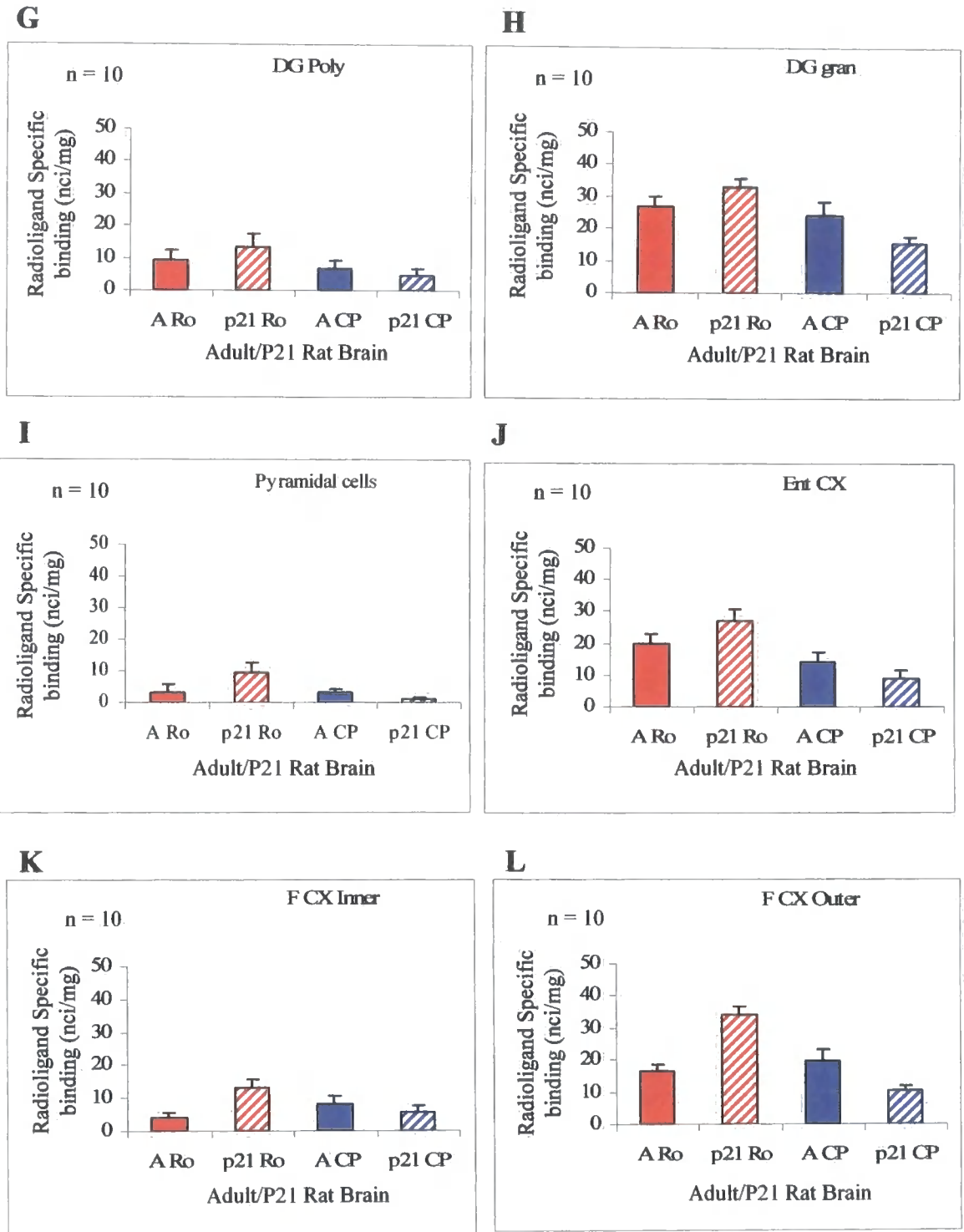
Figure 3.2.3.8 (G-L) Mean average specific binding (nci/mg) ± SD of [³H]Ro 25,6981 and [³H]CP-101,606 for Adult and P21 rat in (G) DG Polymorph (H) DG Granule (I) Pyramidal cells (J) Entorhinal cortex (K) Frontal Cortex Inner and (L) Frontal Cortex Outer. (DG = dentate gyrus layers, A = adult, Ro = Ro 25,6981, CP = CP 101,606)

143

M
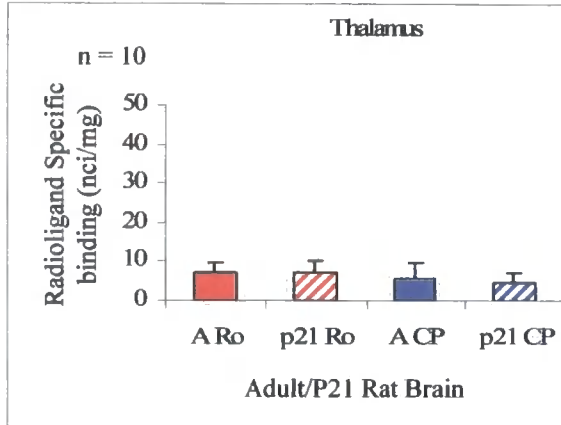
N
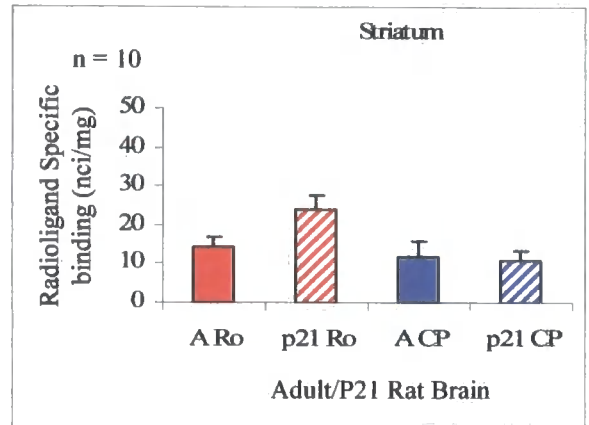
O
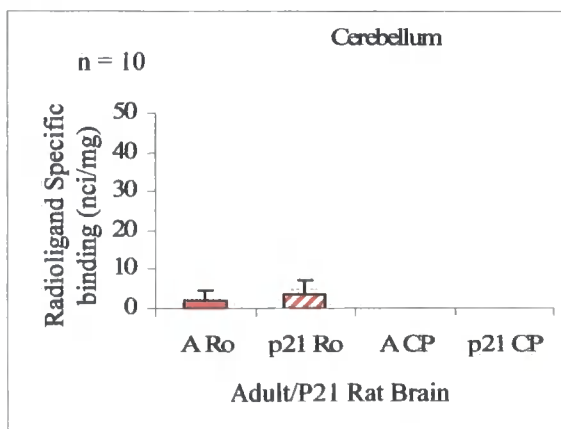
Figure 3.2.3.8 (M-O) Mean average specific binding (nci/mg) ± SD of [³H]Ro 25,6981 and [³H]CP-101,606 for Adult and P21 rat in (M) Thalamus (N) Striatum (O) Cerebellum. (A = adult, Ro = Ro 25,6981, CP = CP 101,606)

3.2.3.4 Discussion

The work in this section builds on existing studies on the NR2B-selective ligands Ro 25,6981 and CP-101,606. Their ability to bind to distinct NR2B receptor subtypes and the distribution pattern of binding in the mouse brain have already been discussed. This section demonstrates the abundance and distribution of ligand binding found in the rat brain. One of the main findings from this study has been that there are higher levels of $[^3H]$Ro 25,6981 binding in P21 rat brain tissue than in adult tissue, suggesting a higher expression of NR2B-containing NMDA receptors in the P21 tissue. The exceptions to this were seen in the CA3 SO, thalamus and striatum where binding levels were very similar between the two ages. Knowing the suggested implication of the NR2B subunit in learning, memory and cognitive function, this finding may suggest there is a decrease in cognitive performance in early adulthood, which is reflected in a decline in NR2B expression. The hippocampus, located inside the temporal lobe of the brain, and part of the limbic system, plays an important role in memory and spatial navigation. The hippocampus has been implicated in the normal operation of learning and memory in humans since the discovery that bilateral surgical removal of the medial temporal lobes results in profound amnesia (Scoville & Milner, 1957). Their paper concluded that the degree of memory loss appeared to depend on the extent of hippocampal removal. Memory loss was caused by the medial temporal lobe excision, but early memories and technical skills ability remained intact. There was no deterioration in personality or general intelligence, and no complex perceptual disturbance such as is seen after a more complete bilateral temporal lobectomy. Therefore the anterior hippocampus and hippocampal gyrus, either separately or together, are critically concerned in the retention of current

experience. Animals with lesions of the hippocampus show marked impairments in memory tasks (Jarrard, 1978; McNaughton *et al.*, 1989 and Morris *et al.*, 1982) clearly implicating the hippocampus in age-related spatial memory deficits in rats. It is also known that in Alzheimer's disease, the human hippocampus is one of the first brain regions to suffer damage; memory problems and disorientation are amongst the first symptoms. The study of the hippocampus of the rat has provided important information concerning the function of this structure in humans. The general patterns of cell connections are remarkably conserved throughout the evolution of mammals. The neural circuits of the hippocampus of human and rodent are fundamentally the same, and both species show age-related alterations in spatial memory. In this study, the hippocampal formation, which includes the dentate gyrus and the sub fields CA1, CA2 and CA3, has been subdivided for analysis. The CA1 and CA3 fields make up the hippocampus proper, with the CA2 representing only a very small portion of the hippocampus. The entorhinal cortex is considered the main source of input to the hippocampus along the perforant pathway. The main output pathways of the hippocampus arise from the CA1 field and the subiculum. Region CA1 receives input from the CA3 subfield. It is widely accepted that each of these regions has a unique functional role in the information processing of the hippocampus, but to date the specific contribution of each region is poorly understood.

Figure 3.2.3.9

Figure 3.2.3.9 Drawing of the neural circuitry of the rodent hippocampus. S. Ramón y Cajal, 1911

The anatomist Giulio Cesare Aranzi (circa 1564) first used the term hippocampus to describe the cerebral organ because of its visual resemblance to a seahorse. This organ was initially connected with the sense of smell, rather than with its known function in memory acquisition. The Russian Vladimir Bekhterev noted the role of the hippocampus in memory around 1900, based on observations of a patient with profound memory disturbances. Psychologists and neuroscientists agree that the hippocampus has an essential role in the formation of new memories.

The second observation from this study has been the similar binding levels of $[^3H]$CP-101,606 in the P21 and adult rat brain sections. The exceptions to this were the CA1, outer regions of the frontal cortex and the striatum, where in each case, there were significantly higher binding levels of $[^3H]$CP-101,606 in the adult than in the P21 tissue. This is the reverse of what was seen with the Ro 25,6982 ligand. Previous studies (Chazot *et al.*, 2002a) provided evidence for two distinct classes of NR2B-directed NMDA receptor antagonists. These suggest that Ro-25,6981 binds with high affinity irrespective whether another NR2 subunit type is present, and a second class which is affected significantly by the presence of another NR2 subunit type within the receptor complex, exemplified by CP-101,606. If CP-101,606 binds to NMDA receptors which only contain the NR2B subunit, then our results would suggest an

147

increase in the expression of these receptors with increasing age, since there are higher binding levels in the adult tissue than in the P21. The results show that Ro 25,6981 binding decreases with age, and therefore, if the NR2B subunit population remains constant or is increasing with age (suggested by the CP-101,606 results) then perhaps another NR2 subunit population is decreasing in compensation for this alteration.

This leads to a third interesting observation from this study that there are no significant differences in the binding levels of the two ligands when looking at the adult tissue. In the majority of regions analysed, there were no significant differences between ligands despite the higher Ro 25,6981 binding levels observed in the P21 tissue. The exceptions to this were seen in the CA3 SR and Ent CX, where a higher Ro 25,6981 binding level was seen, and the inner layer of the frontal cortex, where in contrast, a higher level of CP-101,606 binding was seen. This higher binding level observed with the CP-101,606 ligand may possibly be due to the ligand binding to the NMDA receptor and/or another distinct receptor. If both ligands show similar binding levels in aged brain tissue, and yet label distinct subunit populations, this would suggest a change occurring with age in the expression of certain NR2 subunits, see Figure 3.2.3.10. The fourth main observation from these data is that there is significantly higher binding levels of Ro 25,6981 than CP-101,606 in P21 rat brain tissue. The only exceptions to this were the CA3 SO and the thalamus where binding levels were very similar. The majority of brain regions analysed showed a higher binding of Ro 25,6981 than CP-101,606 at P21, and an identical binding level of the two ligands in the adult Chapter 3, section 3.1 describes the abundance and distribution of the NR2B receptor population in the adult mouse brain. Interestingly, although the distribution pattern was similar to that seen in the rat, that is, higher levels of NR2B

148

labelling were seen in the hippocampal CA1 subfield, striatum, outer frontal and entorhinal cortex compared to cerebellum and thalamus, the study showed that there was a difference in the binding levels between the two ligands used. [^{3}H]Ro 25,6981 binding was higher than [^{3}H]CP-101,606 in the majority of brain regions analysed. These data suggest a species difference in the NR2B receptor populations in the adult brain tissue. The adult rat brain shows similar binding levels between the two ligands, and the adult mouse brain shows a higher [^{3}H]Ro 25,6981 binding level. This may be due to a difference in the receptor subtype populations that are present within the tissues.

Autoradiographical experiments performed by Kito *et al.* (1990) in the rat brain showed that glycine and L-glutamate binding sites were most abundant in the hippocampus and cerebral cortex. Glycine binding sites were severely decreased in the hippocampus and cerebral cortex, in aged brain, although L-glutamate binding sites were well preserved in these brain areas. In the mid-brain regions and cerebellum, neither glycine nor L-glutamate binding sites changed in the aged brain. The NR2B subunit has been implicated in the induction of LTP at hippocampal synapses and is involved in learning and memory. Aged rats are known to have deficits in LTP, learning and memory, and results show that aged rats also have significantly lower levels of NR2B mRNA and protein compared to young rats. It was also noted that no changes were seen in either the mRNA or the protein levels of the NR2A subunit (Clayton & Browning 2001). Conversely, work by Tang *et al.* (1999) has shown that over-expression of the NR2B subunit in the forebrains of transgenic mice leads to enhanced activation of NMDA receptors, and that these mice exhibit superior ability in learning and memory in various behavioural tasks. This suggests that NR2B is critical in gating the age-dependent threshold for plasticity and memory

formation. Neural plasticity is most pronounced during development, and the function of the NMDA receptor is variable during development. Expression of the NR2A and NR2B subunits was examined in the mouse somatosensory cortex and thalamus from postnatal day 2 (P2) to P15 using reverse transcription-PCR, *in situ* hybridization histochemistry, and immunocytochemistry. At both cortical and thalamic synapses, a quantitative switch in the dominant synaptic subunit from NR2B to NR2A was accompanied by a similar change in the cellular expression of NR2A but not of NR2B. Displacement of NR2B subunits from synapses was not accompanied by an increase in an extrasynaptic pool of this subunit. Thus, the switch in synaptic NR2 subunit predominance does not occur by changes in expression or displacement from synapses and may reflect the formation of new synapses from which NR2B is lacking (Liu *et al.* 2004b). Dumas (2005) describes the NMDA receptor as a molecular switch in developmental regulation of cognitive ability. As the neuronal network develops in the forebrain, synaptic NR2B-NMDARs are replaced by NR2A-NMDARs and the NR2B-NMDARs move to extra-synaptic sites. LTP and LTD are enhanced in this initial period of the switch, with synapses containing both NR2A and NR2B receptor types. NMDAR subunit expression then decreases and the NR2A subunit become dominant in the synapse, together with a reduced channel function, synaptic plasticity, and ability to switch receptor composition. A balance of plasticity and stability is achieved which is optimal for information processing and storage.

Distribution studies in the rat brain by Laurie *et al.* (1997) showed NR2B was primarily in the forebrain. NR2B and NR2D were abundant at birth and declined with age, especially in cerebellum. The mouse, rabbit, frog and human brain were also analysed and showed the NR2 subunit sizes (~170 kDa) were similar to those of the corresponding rat subunits and were similarly distributed. Their results showed that

the NR2 subunits are similarly expressed in a variety of species. The results from this section agree with these findings and show that the NR2B subunit is similarly distributed in the mouse (section 3.1) and rat brain.

The Ro 25,6981 data from this study complements recent findings and supports the hypothesis that age-related alterations in the expression of the NR2B subunit might underlie deficits in LTP and learning and memory in older animals. The CP-101,606 data however has not shown a decrease in binding level with age, rather that binding remains at a similar level or is increased in the adult tissue. These are interesting observations since they suggest a possible switch in a certain NR2B subtype population with age. As the overall NR2B subtype population (NR1/2B/2A, or 2B/2C and 2B/2D) decreases with age (shown by the Ro 25,6981 binding), the NR2B subtype population (NR1/2B) increases with age (shown by the CP-101,606 binding). This was the case for the majority of brain regions analysed. The exception to this was the striatum where Ro 25,6981 binding decreased with age but CP-101,606 binding remained at a similar level for both P21 and adult. If the NR1/2B subtype is increasing with age, yet the overall NR2B subtype population is decreasing with age, there may be compensatory decreases of another NR2B receptor subtype. (see Figure 3.2.3.10 below).

Overall decrease in [^{3}H]Ro 25,6981 binding with age (NR2B subtype population containing NR1/2B, NR1/2A/2B, NR1/2C/2B, NR1/2D/2B)

Increase in [^{3}H]CP-101,606 binding with age (NR2B subtype population containing NR1/2B)
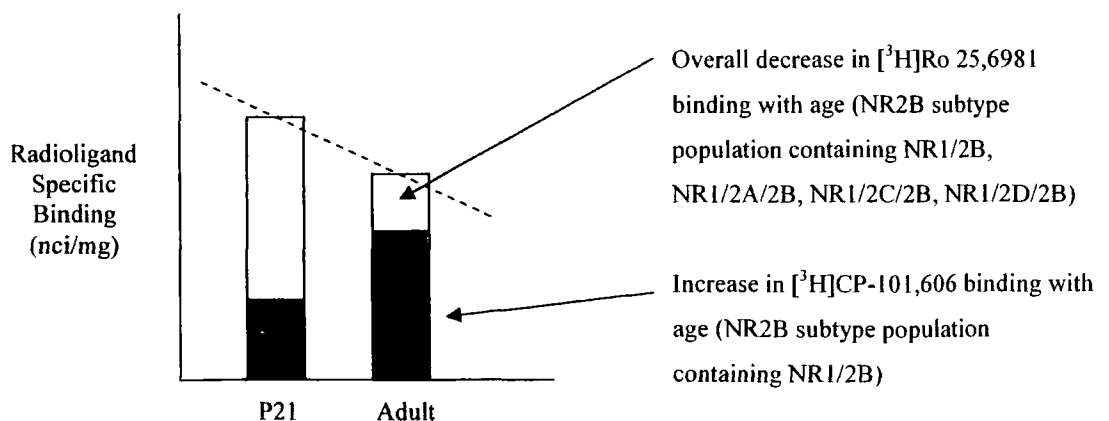
Figure 3.2.3.10 Specific binding levels of NMDA R2B subtype populations in P21 and adult rat brain (HYPOTHESIS).

151

The experiments in this section are a continuation of the work done by Menniti *et al.*

(1997) and Mutel *et al.* (1998), and have shown similar findings in overall distribution.

The autoradiographical method, used by Mutel *et al.* (1998), and slightly adapted for

use in this present study, have also produced supportive findings. Mutel *et al.* reported

that higher densities of [^{3}H]Ro25,6981 binding sites in the rat brain were seen in

several layers of the cortex, the hippocampus, dentate gyrus and caudate putamen

(striatum). Moderate densities were seen in the globus pallidus, thalamus and spinal

cord, with the lowest densities seen in the cerebellum, pons and medulla. It was also

revealed by *in situ* hybridisation histochemistry that overall, the distribution of [^{3}H]Ro

25,6981 binding sites correlated well with that of the NR2B mRNA, but was not the

case for NR2A mRNA. Figure 3.2.3.4 and 3.2.3.5 in this section show [^{3}H]Ro 25,6981

specific binding in P21 and adult rat brain respectively, and show the higher densities

are generally found in the entorhinal and outer frontal cortex, and the CA1, CA3 SR

and dentate gyrus granule cell layer of the hippocampus. Moderate binding densities

were seen in the CA2 and striatum, with the lowest densities seen in the cerebellum,

thalamus, inner frontal cortical areas and the pyramidal cell layer of the

Hippocampus. The distribution pattern of [^{3}H]CP-101,606 binding was also studied using

autoradiography and Menniti *et al.* (1997) reported the highest densities of CP-

101,606 sites were seen in the hippocampus and cortex. Within the hippocampus,

binding is most dense in the CA1 stratum radiatum and the dentate gyrus. The cortex

also showed the highest binding levels in the outer layers compared to the inner

layers. Moderate binding was seen in the striatum and the lower levels were seen in

the thalamus and cerebellum. Figure 3.2.3.6 and 3.2.3.7 show [^{3}H]CP-101,606 specific

binding in P21 and adult rat brain respectively and suggest that our findings are very similar. The highest CP-101,606 binding levels were observed in the CA1, granule layer of the dentate gyrus and the outer layer of the frontal cortex. Moderate binding levels were seen in the entorhinal cortex and the striatum, with the lowest levels seen in the thalamus, inner cortical regions, cerebellum and the pyramidal cell layers of the hippocampus. This is the case for both P21 and adult tissue labelled by the CP-101,606 ligand.

This study has provided an extensive collection of evidence to support the theory that these two ligands are labelling distinct populations of NR2B receptors. Furthermore, there is an age-dependent decline in overall NR2B subtypes between 3 weeks and 3 months of age in rats. This section provides the first evidence for a switch in NR2B subtype during this period of ageing. This section has covered the earlier period of ageing with changes in NR2B expression possibly being related to changes in synaptic plasticity and development. The later period of ageing is studied in humans and is described in Chapter 4. In the human study, the affects of old age and pathological changes on cognitive ability and levels of NR2B-containing receptors are analysed.

Chapter 3

Section 3.2.4

Expression of the NR2B subunit protein in P21 and adult rat brain:

3.2.4.1. Introduction

For many years antibodies have been widely used in biochemical techniques as selective probes to study the structure and function of important biological macromolecules. Their unique structure and function makes them useful research tools since they can be very antigen specific. Immunohistochemistry (IHC) (3.2.4.2.4) is a method of detecting the presence of specific proteins or antigens in cells or tissue sections, using labelled antibodies as specific reagents through antigen-antibody interactions that are visualized by a marker such as an enzyme. The antibodies can be polyclonal or monoclonal in origin, the monoclonal ones being more specific in nature. Polyclonal antibodies are a mixture of different antibodies with varying affinities towards different epitopes on the antigen. Immunohistochemistry is commonly used for the diagnosis of various cancers; however the technique is also widely used to understand the distribution and localization of biomarkers in different parts of a tissue. Since it involves specific antigen-antibody reactions, it has advantages over traditionally used staining techniques that identify only a limited number of proteins, enzymes and tissue structures. In this study, IHC will be used to map the distribution of the NR2B subunit of the NMDA receptors in rodent brain sections. The method involves an unlabelled primary antibody binding to a specific antigen in the tissue. This antibody-antigen complex is then bound by a secondary antibody. The secondary antibody must correspond to the IgG of the animal species in which the primary antibody

has been raised. This is a relatively sensitive method due to signal amplification through several secondary antibody reactions with different antigenic sites on the primary antibody. The secondary antibody is then labelled with an enzyme such as peroxidase (Nakane & Pierce 1967). In the presence of a substrate and chromagen, the enzyme forms a coloured precipitate demonstrating the sites of antibody-antigen binding in a semi-quantifiable manner. Correct tissue preparation is vital to ensure the preservation of tissue architecture and cell morphology, therefore, prompt and adequate fixation is essential to maximize the antibody binding capability. In this study the tissue has been fixed by transcardial perfusion using 4% paraformaldehyde, a technique known to give superior results, particularly in neuronal tissue. The development by Shi *et al.* in 1991 of Antigen Retrieval (AR) techniques has further enhanced the use of fixatives for IHC and has therefore been incorporated into the protocol. A high-temperature heating method that breaks the protein cross-links formed by the fixing process is used to uncover the antigenic sites in the tissue sections that have been masked by fixation. This step was therefore carried out in the study. Generation of peptide-directed polyclonal antibodies involves the selection and production of a short antigenic amino acid sequence corresponding to a specific portion of the receptor. These regions are available in the native state for antibody binding since they are usually hydrophilic and found on the protein surface. As synthetic peptides are small in size they require coupling to a carrier protein of another species than the immunised animal; in this study, thyroglobulin is used. The conjugation strategy is designed to mimic that of the natural protein therefore, N-terminal sequences would be coupled through the C-terminus and vice versa. Antibody generation is described in (3.2.4.2.1). Chazot *et al.* (1992) successfully employed this technique to raise specific antibody probes for NMDA receptor subunits. NMDA receptor subunit-specific antibodies were used by Thompson *et al* (2002) to map the distribution of NR1, 2A, 2B and 2D subunits in adult mouse hippocampal

formation. Previous immunohistochemical studies have demonstrated the presence and distribution of NMDA receptor subunits in the rat brain. The subunits appear to display distinct but over-lapping expression patterns in the brain during different stages of development, which in turn may be related to their various functions (Takai *et al*. 2003b). In the present study the in-house produced and purified NMDAR subunit-specific antibodies anti-NR2B receptor antibodies were used as immunological probes to study the cellular distribution of native NR2B subunits in P21 and adult rat brain.

3.2.4.2 Methods

3.2.4.2.1 Antibody generation and characterisation

Peptide-directed anti-NMDA receptor subunit-specific antibodies were generated to investigate the cellular distribution of NR2B subunits in rodent tissue. The anti-NR2B (46-60) antibodies were generated and characterised as previously described (Chazot & Stephenson, 1997a; Hawkins *et al*, 1999). Briefly, the peptide corresponding to the amino acids 46-60 (DEVAIKDAHEKDDFCys) of the rat NR2B subunit was conjugated to thyroglobulin by the Cys coupled method. The resultant conjugate was used to generate polyclonal antibodies in rabbits. The rabbits were inoculated with peptide-carrier protein conjugate emulsified with complete Freund's adjuvant. Blood collected at one month intervals after subsequent immunisations, was allowed to clot contract. The serum, separated from cellular material by centrifugation, was stored at -20°C. The method, as described by Chazot *et al*. (1997a), couples the NR2B peptide 46-60 cys to thyroglobulin by the *m*-maleimidobenzoic acid N-hydroxysuccinimide ester coupling method to cross-link the peptide to the carrier protein. The use of a peptide-carrier protein conjugate necessitates the affinity purification of the anti-peptide antibodies from the resultant antiserum to remove the anti-carrier protein antibodies that can potentially cause high non-specific binding. The peptide affinity columns are synthesised to mimic the coupling between the peptide and carrier protein.

3.2.4.2.2 Peptide Affinity Purification of Antibodies:

For the purification of anti-peptide polyclonal antibodies a Sepharose column (1 ml) linked to the appropriate peptide was equilibrated with 100mls of TBS (section 2.3.12). Immune serum (4ml) was applied to the column using a Pasteur pipette and incubated for 2 h at room temperature or overnight at 4°C with gentle shaking. Unbound immune serum was allowed to pass through the column under gravity flow and discarded. The column was washed with 100mls of TBS and the bound antibody was eluted from the column with 50mM glycine/HCl pH 2.3 (10ml). The purified antibody fractions (1 ml) were collected in eppendorfs containing 1 M Tris (20 µl) to give a final pH 7.4. The O.D. at $\lambda = 280$nM of the antibody fractions was determined and the concentration of the antibodies was calculated using the Beer Lambert law,

$$C = \frac{A}{\epsilon L}$$

Where;

C, is the concentration of antibody

A, is the absorbance of the antibody at $\lambda = 280$nM

ϵ, is the molar extinction coefficient

L, is the path length

The yields of purified antibodies were in the range 0.2-0.6 mg protein/ml. The antibody-containing fractions were pooled and dialysed against (500ml) TBS overnight at 4°C. The affinity column was regenerated with 100mls of TBS and stored with (10ml) TBS

containing 0.025% (w/v) sodium azide at 4°C until further use. After dialysis the concentration of the purified antibody was recalculated by measuring the O.D. at λ = 280nM. The purified antibodies were then stored with the addition of 0.025% (w/v) sodium azide at 4°C until use.

3.2.4.2.3 Perfusion Fixation and Sectioning of Rat Brain

The perfusion fixation was performed by Dr C.L. Thompson. An adult wild-type Sprague-Dawley rat was deeply anaesthetised using Pentobarbitol, and assessed by failed nictating reflex and pressure-induced retraction of hind limb. The anaesthetised rodent was then pinned out with its ventral surface uppermost. The ribcage was exposed and retracted, and a 25 gauge microlance was inserted into the left ventricle through which ice-cold 0.1M sodium phosphate buffer pH 7.4 containing 0.1% (w/v) sodium nitrate was perfused via a peristaltic pump, and the right atrium was cut. The rodent was exsanguinated in this manner for 5 minutes. The perfusate was then exchanged for freshly prepared, ice-cold fixative (4% paraformaldehyde in 0.1M NaPO buffer, pH 7.4) for 20 minutes, after which the brains were dissected out and immersed in fixative (4% paraformaldehyde in 0.1M NaPO buffer pH 7.4) overnight at 4°C. The brains were then cryoprotected by sucrose infiltration. The fixed PBS (section 2.3.11) washed brains were transferred into 10% (w/v) sucrose in PBS, for 48 hours prior to sectioning. The sucrose infiltrated brains were frozen in isopentane over liquid nitrogen for 1 minute at −70°C, and then horizontally sectioned (25µm) on a cryostat (-24°C). The sections were stored at 4°C in PBS, containing 0.02% (w/v) sodium azide until use.

3.2.4.2.4 Immunohistochemistry using Vectastain ABC Kit

This method uses the Vectastain ABC kit as a means of detecting the bound antibody and also to amplify the signal. The kit uses the biotin-avidin-peroxidase system. Free floating sections (25μm) of P21 or adult rat brain were prepared as described in section 3.4.2.2 and were initially incubated for 10 minutes at room temperature in 50mM TBS containing 10% (w/v) methanol and 3% (v/v) hydrogen peroxide, to quench endogenous peroxidase activity. Slices were then incubated in 50mM TBS containing 0.2% (w/v) glycine and 0.2% (v.v) Tween-20 for 15 minutes at room temperature, to mop-up any unreacted aldehyde groups from the fixative. Sections were then incubated in 50mM Tris buffer containing 0.2% Triton-X-100 detergant before being placed in 50mM Na Citrate buffer pH 8.4 for 30 minutes at room temperature. The sections remained in the Na Citrate buffer and the 24 well-plate was placed in a waterbath at 80°C for 30 minutes. A repeat of the wash with Triton-X-100 was then carried out for 15 minutes. Non-specific antibody binding sites on the fixed tissue were blocked by incubating with 50mM TBS containing 2% (v/v) goat serum and 0.2% Tween-20 for 1 hour at room temperature. Samples were placed on the shaker. After blockade of the non-specific antibody binding sites, sections were incubated with affinity purified antibodies at working concentrations of 0.5-2μg/ml, for 2 hours at room temperature, or overnight at 4°C with gentle shaking. After incubation with the primary antibody, sections were washed (3 x 1ml) with 50mM TBS containing 1% (v/v) goat serum for 5 minutes. Sections were then incubated with Vectastain anti-rabbit biotinylated secondary antibody (50μl/5ml TBS containing 1% (v/v) goat serum) for 20 minutes at room temperature with gentle shaking. Unbound biotinylated secondary antibody was removed and the sections were washed (3 x 1ml) with 50mM TBS containing 1% (v/v) goat serum for 5 minutes. The sections were then incubated for 5 minutes at room temperature with Vectastain ABC reagent, which was prepared 10 minutes prior to

application to the section (100μl of Vectastain A mixed with 5mls 50mM TBS then 100μl of Vectastain B was added and gently mixed).After incubation with Vectastain ABC reagent the sections were washed (5 x1ml) with 50mM TBS. Sections were then incubated in the dark with horseradish peroxidase substrate diaminobenzadine (DAB) (10mg) dissolved in 10ml TBS, and 6μl of 30% (v/v) hydrogen peroxidase, until optimal staining was achieved (5-20 minutes). Once optimal staining was achieved the substrate was discarded and sections were washed (2 x 1ml) with distilled water. Sections were mounted on microscope slides using (300μl) DPX mountant.

3.2.4.2.5 Toluidine Blue staining of Brain Sections.

Slide-mounted brain sections processed for autoradiographic studies were stained using 0.02% (w/v) toluidine blue. Briefly, frozen sections were thawed for one hour at room temperature. Sections were then hydrated by incubation in decreasing concentrations of ethanol, for five minutes each at room temperature (100%, 90%, 70% and 50%). Following a three minute incubation in deionised water, sections were incubated for 10 minutes in toluidine blue stain at room temperature. Excess stain was rinsed by immersing in deionised water and sections were allowed to dry at room temperature over night. Sections were coverslipped using DPX mountant.

3.2.4.2.6 Photographing of Brain Sections

Rodent brain slices were photographed using a Nikon Coolpix 950 digital camera attached to a Nikon Elipse E400 microscope. The aperture (F 4.1) and shutter speed (1/30) were fixed. Images in Figure 3.2.4.1 were scanned using the Dell All-In-One Scanning system.

161

3.2.4.3 Results

### 3.2.4.3.1 Figure 3.2.4.1 Immunoblotting analysis using anti-NMDA antibodies

Adult rat brain preparation (Chapter 2, section 2.4.1) were probed with the anti-NR2B antibody generated in this study, as well as in-house generated anti-NR2A and anti-NR1 antibodies. Immunoblotting was carried out using 7.5% SDS-PAGE under reducing conditions with 50μg of protein applied per gel lane (see Chapter 2, section 2.4.3-2.4.7). Figure 3.2.4.1 shows the scanned image of the resulting film. All three anti-NMDA receptor antibodies detected a band in the adult rat brain preparation, demonstrating the presence of all three subunits NR1 (105kDa), NR2A (~180kDa) and NR2B (180kDa) in native brain tissue (Figure 3.2.4.1). The anti-NR1 and anti-NR2B antibodies detected bands in the transfected cell homogenates, demonstrating the presence of NR1 and NR2B subunits, and indicating the selectivity of the antibody produced (Figure 3.2.1.1). This analysis provides evidence that the antibodies have been generated successfully, that they identify the correct NMDA subunits and they can be used in further experiments. In this study, the antibodies were used to probe P21 and adult rat brain sections using immunohistochemical techniques.

3.2.4.3.2 Figure 3.2.4.2 DAB and Toluidine Blue stained sections

This study involved using whole horizontally cut P21 and adult rat brain sections. Sections were cryostat cut at 25μm to maintain the integrity of the sections during the experiment, and were subjected to an antigen retrieval technique (Shi *et al*, 1991) to ensure maximal antigen-antibody interaction (see 3.2.4.2.4). Figure 3.2.4.2 (A and C) show P21 and adult rat brain sections respectively, stained with DAB. The P21 section is visibly darker than the

adult, suggesting a greater presence of NR2B subunits, which has resulted in a higher level of antibody binding and therefore more intense DAB staining. Both the P21 and adult sections show more intense staining in the hippocampal region and outer layers of the cortex. Figure 3.2.4.2 (B and D) show P21 and adult rat brain sections respectively, stained with Toluidine Blue. These sections have the cerebellum present and clearly show staining in this area, as well as defining the cortical regions and striatum. These images reveal an overall pattern of DAB staining in the sections analysed. The next set of Figures (Figures 3.2.4.3 to 3.2.4.6) show more detailed digital pictures of the sections taken at x100 and x200 magnification. See Appendix One for anti-NR2D immunohistochemistry data.

Anti-NMDA antibodies
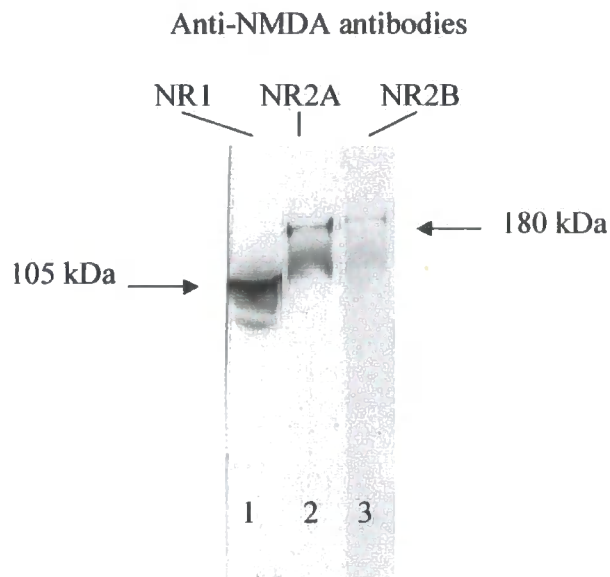
Figure 3.2.4.1 Immunoblots of native rat brain preparation probed with anti-NR1, anti-NR2A and anti-NR2B antibodies.

Lane 1   Adult rat brain prep probed with anti-NR1

Lane 2   Adult rat brain prep probed with anti-NR2A

Lane 3   Adult rat brain prep probed with anti-NR2B

The In-house generated antibodies were:

Anti-NR1: Bleed 1, Stock [492µg/ml], used at [1µg/ml]

Anti-NR2A: Bleed 1, Stock [905µg/ml, used at [1µg/ml]

Anti-NR2B: Bleed 1, Stock [163µg/ml], used at [1µg/ml].

A

P21 NR2B

B

P21 Rat

C

Adult NR2B

D
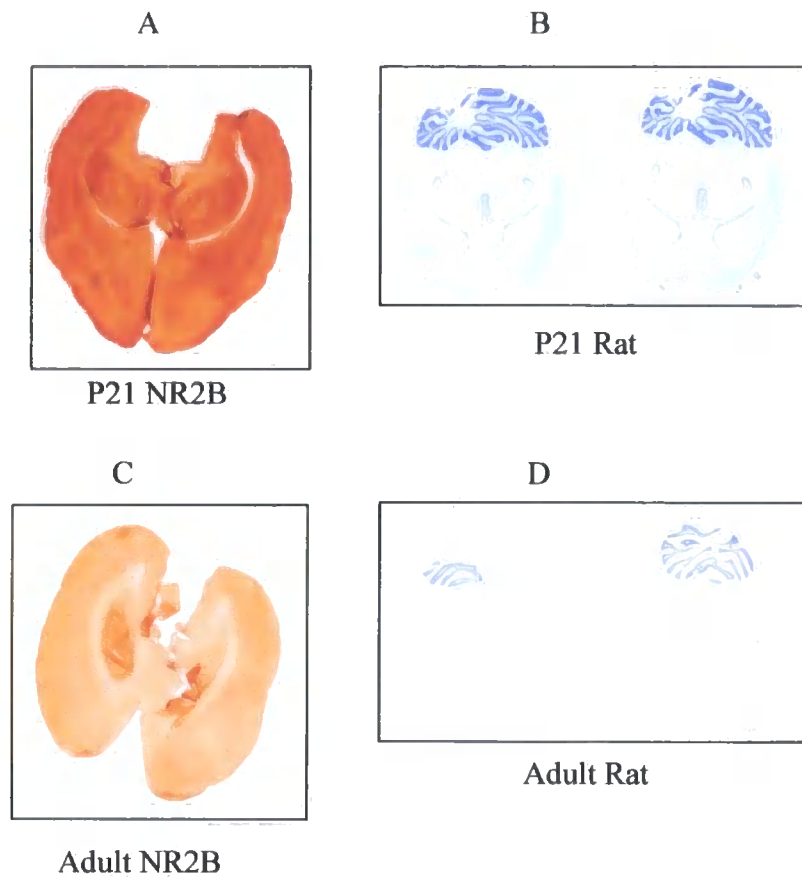
Adult Rat

Figure 3.2.4.2 **Immunohistochemical images of Rat brain sections stained with DAB (A) P21 NR2B (C) Adult NR2B and rat brain sections stained with Toluidine blue (B) P21 and (D) Adult rat.**

3.2.4.3.3 Figure 3.2.4.3 Immunohistochemical staining of P21 Hippocampal Formation

Previous immunoblotting (see Figure 3.2.4.1 and Figure 3.2.1.1.) demonstrated that the anti-NR2B antibody was correctly labelling the NR2B subunit population in rat brain tissue. Preliminary experiments were performed to define the optimal working concentration of the anti-NR2B antibody for immunohistochemical localisation studies of P21 and adult rat brain sections. Antibody concentrations of 2, 1 and 0.5µg/ml were used and sections were incubated in DAB stain for time periods ranging from 5-20 minutes. Optimal staining was obtained when [1µg/ml] antibody was used and DAB staining was for 20 minutes in the dark. Figure 3.2.4.3 shows the staining seen in the CA1, CA2 and dentate gyrus of the hippocampal formation in P21 rat brain tissue. Anti-NR2B immunoreactivity was observed in the stratum oriens and stratum radiatum of the CA1 and CA2 regions, indicating the presence of NR2B subunits along the neurone projections from the pyramidal cell bodies. The staining was of similar moderate intensity in both these regions. The layer of pyramidal cell bodies is clearly visible due to its lack of immunoreactivity and staining. The area of negative immunoreactivity in the dentate gyrus is also visible, although is more diffuse in distribution, with the pyramidal cell body layer in the CA1 and CA2 being quite a compact and distinct band.

3.2.4.3.4 Figure 3.2.4.4 Immunohistochemical staining of adult Hippocampal Formation

Adult rat brain sections were probed for the presence of NR2B subunits using the anti-NR2B antibody [1µg/ml], as for the P21 sections. Figure 3.2.4.4 shows the staining seen in the CA1, CA2 and dentate gyrus of the hippocampal formation in adult rat brain tissue. Anti-NR2B immunoreactivity was observed in the stratum oriens and stratum radiatum of

the CA1 and CA2 regions, again indicating the presence of NR2B subunits on the neurone projections. The overall intensity of the staining was less than that seen in the P21 CA1 and CA2 regions, and the stratum oriens appears to be more intensely stained than the stratum radiatum in the adult sections, something which was not observed in the P21 sections. The differences in overall staining intensity between the P21 and adult tissue suggest that there is a greater expression of NR2B subunits in the P21 rat sections. The layer of pyramidal cell bodies is clearly visible due to its lack of immunoreactivity and staining. The area of negative immunoreactivity in the CA1, CA2 and dentate gyrus is more diffuse in distribution than seen in the P21 sections.

2B P21 CA1
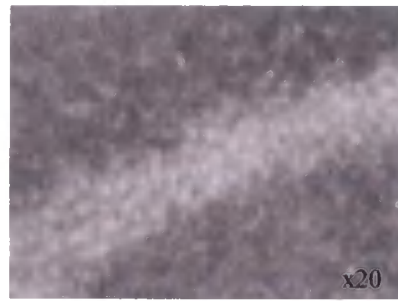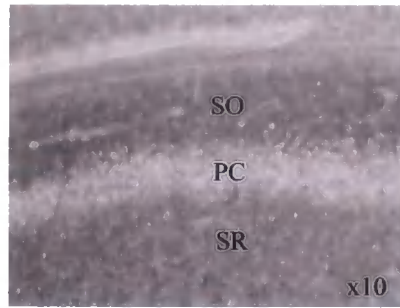
2B P21 CA2

2B P21 Dentate Gyrus

Figure 3.2.4.3 Immunohistochemical staining of P21 rat Hippocampal Formation using anti-NR2B antibody. SO = Stratum Oriens, PC = Pyramidal cells, SR = Stratum Radiatum.
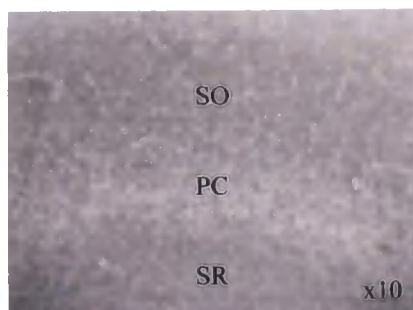
168

2B Adult CA1

2B Adult CA2
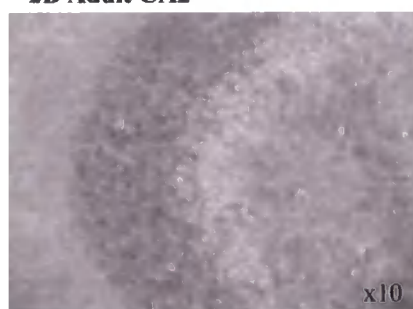

2B Adult Dentate Gyrus

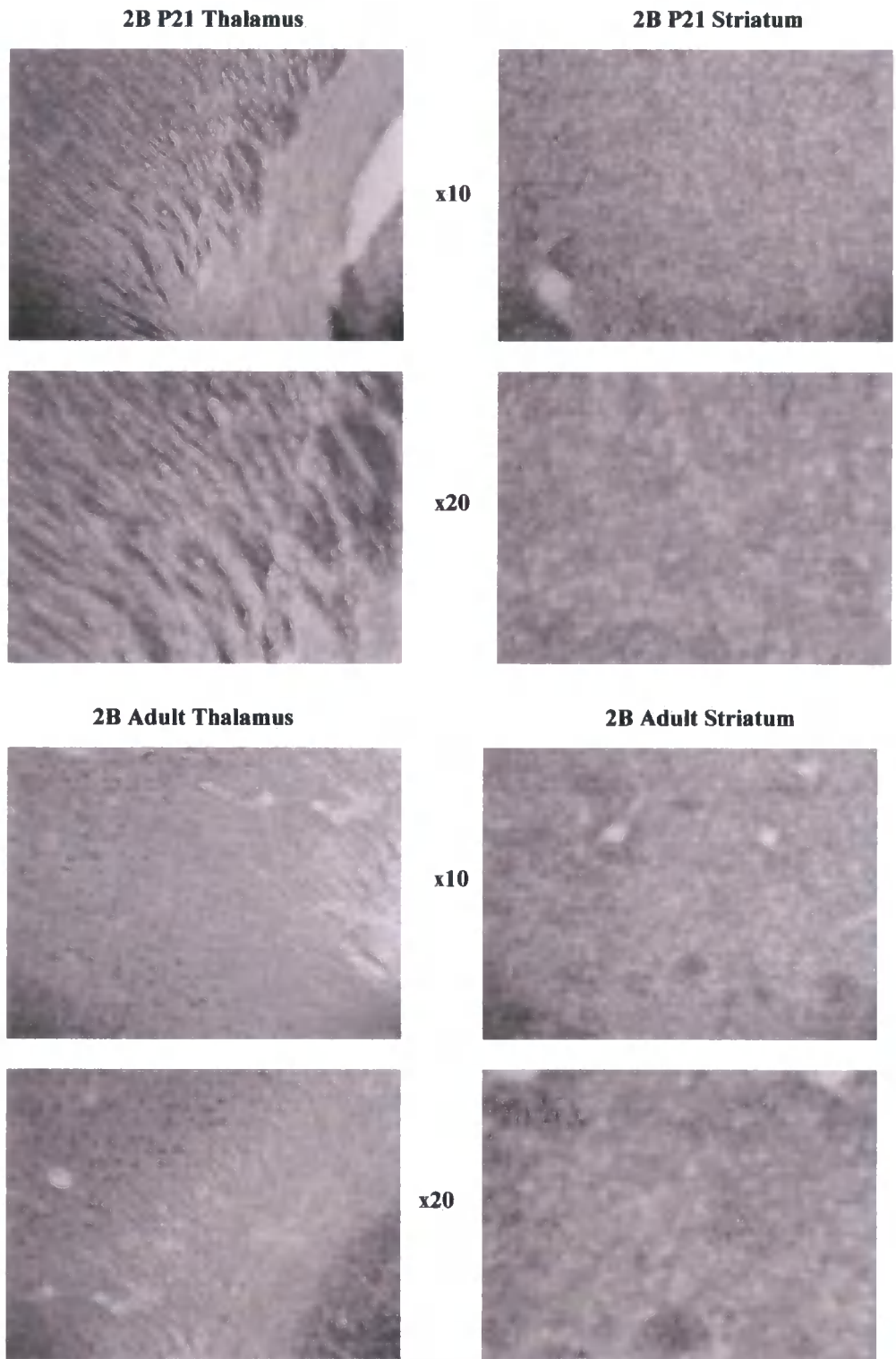<u>Figure 3.2.4.4</u> Immunohistochemical staining of Adult rat Hippocampal Formation using anti-NR2B antibody.

SO = Stratum Oriens, PC = Pyramidal cells, SR = Stratum Radiatum.

3.2.4.3.5 Figure 3.2.4.5 Immunohistochemical staining of P21 and adult Thalamus and Striatum

Anti-NR2B staining was observed in both P21 and adult thalamus and striatum. Immunopositive staining was more intense in the P21 section than the adult for both these regions, although was more pronounced in the P21 thalamic tissue, suggesting a greater NR2B expression. Striatal neurones also showed prominent punctuate staining of the cell bodies distributed throughout the tissue.

3.2.4.3.6 Figure 3.2.4.6 Immunohistochemical staining of P21 and adult Frontal and Entorhinal Cortex

The frontal and entorhinal cortex of both P21 and adult rat brain sections showed immunopositive staining for NR2B expression. In the frontal cortex, cortical layers I, II, III, IV and V are clearly visible, each having a distinct cell morphology and difference in staining intensity, ranging from most intense staining in layers I and II, to the least intense staining in layer III, with punctuate staining in layer V. There was very little difference in overall staining between P21 and adult frontal cortex, with the exception of the very outer layer I, which was more highly stained in the P21 section. The entorhinal cortex showed a similar pattern and intensity of staining to that of the frontal cortex for both P21 and adult brain sections. Cortical layers I to V were clearly visible, with the most intense staining seen in layer I and II. There were no observable differences in staining intensity between P21 and adult rat brain sections.

2B P21 Thalamus   **2B P21 Striatum**

2B Adult Thalamus   **2B Adult Striatum**

Figure 3.2.4.5 Immunohistochemical staining of P21 and Adult rat Thalamus and Striatum using anti-NR2B antibody.

171

2B P21 Frontal Cortex　　　　　　　　**2B P21 Entorhinal Cortex**

2B Adult Frontal Cortex　　　　　　　**2B Adult Entorhinal Cortex**
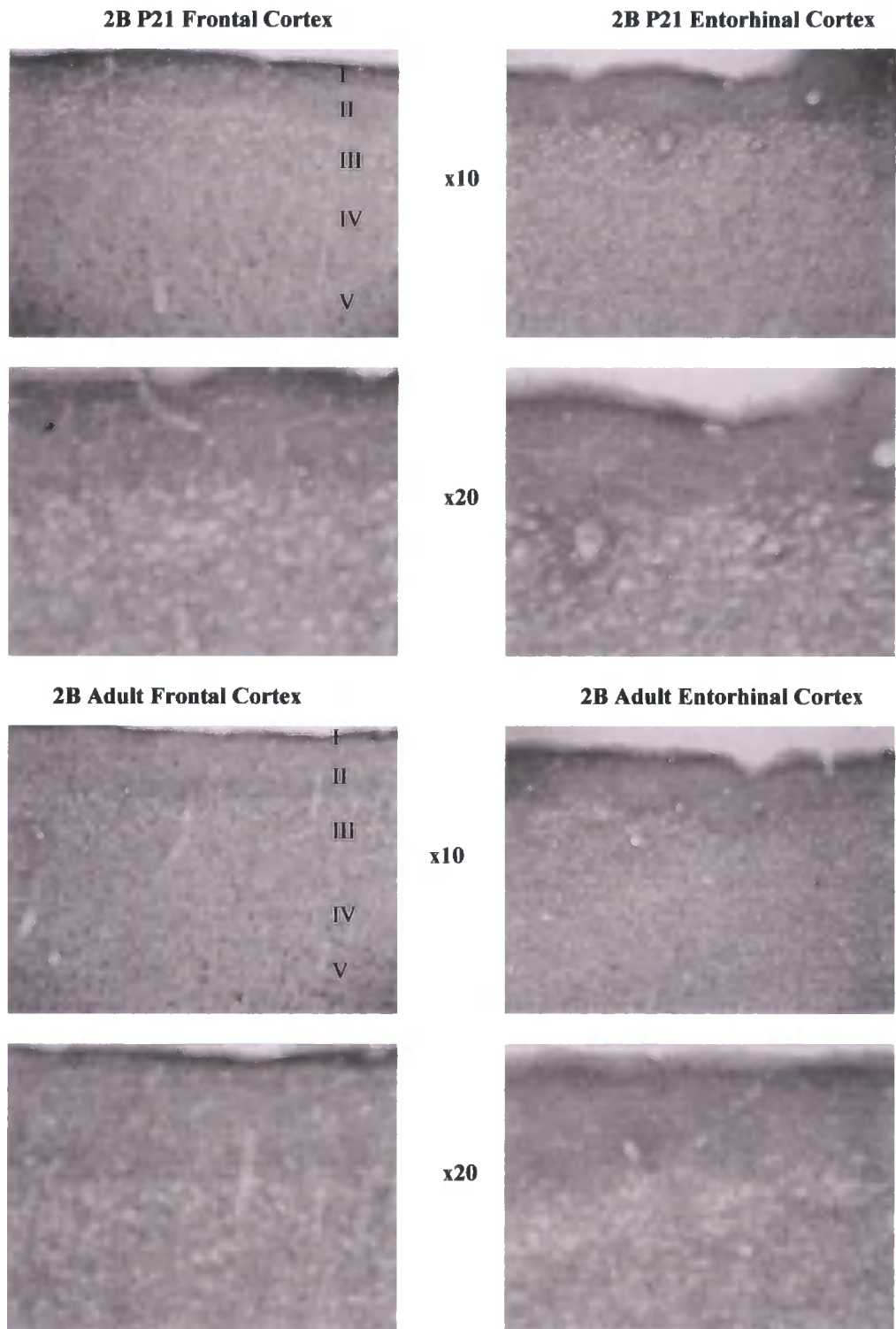
Figure 3.2.4.6 **Immunohistochemical staining of P21 and Adult rat Frontal and Entorhinal Cortex using anti-NR2B antibody.**

172

3.2.4.4 Discussion

This semi-quantitative study has revealed the distribution and abundance of the NMDAR-2B subunit protein in P21 and adult rat brain sections. Sections were prepared and assayed identically and the results are shown in Figures 3.2.4.1 to 3.2.4.6. The main difference seen between the two ages was the apparent higher staining intensity observed in the P21 hippocampal formation, thalamus and outer cortical layers, compared to the adult sections. This suggests a greater expression of NR2B protein in the P21 than the adult. Autoradiography results (see Chapter 3, section 3.2.3) comparing the distribution and abundance of NR2B-containing receptors between P21 and adult rat brain sections also revealed that, using the $[^3H]$Ro 25,6981 ligand, a higher binding level, and therefore presence of NR2B receptors, was present in the P21 rat brain compared to adult. These results taken together support the theory that NR2B is widely expressed in the brain from the early stages of development, but decreases with age, as NR2B receptors are replaced by NR2A receptors at synaptic sites (Dumas 2005). The ages used in this study range from 3 weeks to 3 months, and cover the early adult developmental period. The differences in NR2B expression between these two ages show developmental changes which may reflect alterations in synaptic plasticity of the neurones at this critical and sensitive developmental time point. Saturation experiments (Chapter 3, section 3.2.2) of the $[^3H]$Ro 25,6981 ligand for both P21 and adult tissue showed a greater number of NR2B binding sites in the P21 than the adult rat brain (P21 B_{max} (fmol/mg) 2593 compared to adult B_{max} (fmol/mg) 683), and so suggest a greater expression of NR2B protein. Although immunohistochemical studies show only the presence of the protein, and not the presence of functional receptors, there does appear to be a trend for both protein and receptor expression to be greater in the P21 than adult rat brain. Immunohistochemical studies by Takai *et al.* (2003b)

demonstrated the presence and distribution of NMDA receptor subunits in the rat brain. The subunits appear to display distinct but over-lapping expression patterns in the brain during different stages of development, which in turn may be related to their various functions. NR1, NR2A and NR2B are the major NMDA receptor subunits expressed during development and can be present in different combinations in different subpopulations of striatal neurons. Expression patterns of the NR1, NR2A and NR2C subunits were very similar, each increasing from embryonal day 18 (E18) to postnatal day 14 (P14), however, mild NR2B expression was observed in the hippocampus and cerebral cortex of E20, moderate expression was seen in these regions in P1 and P4, but negative to minimal expression was seen from P7 to P14 (Takai *et al* 2003b). Using immunohistochemical methods, Krebs *et al*. (2003) detected the presence of the NR2B subunit in neurons but not astrocytes in the CA1 and subicular regions of the rat hippocampus. However, after ischemia-induced neuronal death in these regions, double immunohistochemical labelling revealed that NR2B subunits co-localized with the astrocyte marker glial fibrillary acid protein and with NR1 subunits that are required for functional NMDA receptors. Lau *et al*. (2003) investigated the patterns of gene expression of NMDARs in the rat neostriatum during postnatal development. Reverse transcriptase-polymerase chain reactions (RT-PCR) indicated that levels of NR1, NR2A and NR2D mRNAs reached peak levels between postnatal days (PND) 7 and 14. The levels of NR2B and NR2C mRNAs were low at PND 1 and their levels increased at PND 7 and remained high in adults. Immunoreactivity profiles of the various subunits indicate that there are differential patterns of expression of NR mRNAs and immunoreactivity in the neostriatum during different stages of postnatal development. A quantitative analysis of endogenous mRNA levels of NR1, NR2A, NR2B, NR2C, NR2D and NR3A in the rat brain was carried out by Goebel & Poosch (1999). Results showed that there was a spatio-temporal level of expression throughout the brain

174

for each of the receptor subunits with some regions showing a strong preference for a particular subunit. The level of mRNA expression for NR1 greatly exceeded that of the other subunits combined. The relative proportions of the other subunits (NR2A-D and NR3A) varied widely, suggesting that NMDA receptor composition is unique to each region of the brain.

Previous studies by Wang *et al.* (1995) described the distribution of the NR2A and NR2B subunits in the rat brain using antibody detection. High levels of NR2A were located in the hippocampus and cerebral cortex, intermediate levels in striatum, olfactory tubercle, mid-brain, olfactory bulb, and cerebellum, and low levels in the pons-medulla. High levels of NR2B were expressed in the olfactory tubercle, hippocampus, olfactory bulb, and cerebral cortex. Intermediate levels were expressed in striatum and mid-brain, and low levels were detected in the pons-medulla. No signal for NR2B was found in the cerebellum. Thompson *et al.* (2000) found NR2B immunoreactivity in the cell bodies of pyramidal neurons, granule cells, hilar cells of the dentate gyrus and apical dendrites of the CA subfields. The present study showed a lack of NR2B immunostaining in the cell bodies of the pyramidal cells, but did however show staining of the CA subfields. Anti-NR2B subunit-specific immunostaining was prominent in Purkinje cell bodies and dendrites but absent from the granule cell layer in the adult mammalian cerebellum (Thompson *et al.* 2000). The hippocampus was also the focus of study for Watanabe *et al.* (1993). They produced affinity-purified antibodies against NR2A, NR2B and NR1 NMDAR subunits and determined their distributions in the mouse hippocampus. All three subunits were detected at the highest level in the strata oriens and radiatum of the CA1 subfield, and high levels were also seen in most other neuropil layers of the CA1 and CA3 subfields and of the dentate gyrus. However, the stratum lucidum, a mossy fibre-recipient layer of the CA3

subfield, contained low levels of the NR2A and NR1 subunits and almost excluded the NR2B subunit.

Babb *et al.* (2005) demonstrated that NR1 and NR2B receptor proteins are differentially expressed during pre- and postnatal development in the rat cortex. Developmental changes in NR1 and NR2B expression were consistent with those of mRNA. NR2B mRNA was expressed in the embryonic rat cortex and increased prenatally, reaching a maximum by the day of birth and remained roughly constant into adulthood. The results from the present study showed similar levels of NR2B immunoreactivity in the cortical regions for both P21 and adult rat brain sections. This is consistent with the findings of Babb *et al* (2005), Watanabe *et al.* (1992) and Sheng *et al.* (1994).

Immunohistochemical analyses have demonstrated that NMDA receptor subunits are differentially expressed during development, suggesting that the subunit composition of the NMDA receptor is altered during development (Watanabe *et al.*, 1992, Monyer *et al.*, 1994., Sheng *et al.*, 1994., Zhong *et al.*, 1995). The results from this section as well as the findings from the autoradiography experiments from previous sections, have provided further evidence for a change in subunit expression in the rat brain occurring over the age range P21 to adult.

In summary, chapter 3 has shown the pharmacological profile of [^{3}H]CP-101,606 binding to recombinant NR1/NR2B receptors, as well as a range of NR2B ligands binding to native P21 and adult rat brain. Expression of the NR2B protein in P21 and adult rat brain is described in 3.2.4. Autoradiographical studies have shown the abundance and distribution of the NR2B receptor population in mouse, P21 and adult rat brain, and this technique will be used in chapter 4 to demonstrate the abundance and distribution of the NR2B receptor in normal and diseased human brain, across the age range 62-92 years.